THESE

Présentée à

L'Université des Sciences et Technologies de Lille

Pour obtenir le titre de

DOCTEUR EN CHIMIE

Spécialité : Sciences de la Matière, du Rayonnement et de l'Environnement

Par

Samadhan LOMATE

Développement de catalyseurs performants pour l'oxydation sélective d'éthanol en oxyde d'éthylène

Soutenance le 28 Septembre 2015 devant la commission d'examen :

Rapporteurs :

Dr. Jean-Marc MILLET, Directeur de recherche CNRS, IRCE, Lyon (France)

Prof. Bernard NIEUWENHUYS, Professeur, Leiden University, Leiden (Pays-Bas)

Examinateurs :

Dr. Oliver FRANKE, CLARIANT (Allemagne)

Prof. Anne-Cécile ROGER, University de Strasbourg, Strasbourg (France)

Dr. Axel LOFBERG, Chargé de recherche CNRS, Lille (France)

Directeur :

Prof. Sébastien PAUL, Ecole Centrale de Lille

Co-directeur :

Dr. Jean- Sébastien GIRARDON, Université de Lille 1

THESIS

Persented at

Université des Sciences et Technologies de Lille

For obtaining a title of

DOCTOR IN CHEMISTRY

Spécialité : Sciences de la Matière, du Rayonnement et de l'Environnement

by

Samadhan LOMATE

Development of high performance catalysts for the selective oxidation of ethanol to ethylene oxide

Defended on the 28th September 2015

Reviewers :

Dr. Jean-Marc MILLET, CNRS Research Director, IRCE, Lyon (France)

Prof. Bernard NIEUWENHUYS, Professsor, Leiden University, Leiden (Netherlands)

Examiners :

Dr. Oliver FRANKE, CLARIANT (Germany)

Prof. Anne-Cécile ROGER, University of Strasbourg, Strasbourg (France)

Dr. Axel LOFBERG, CNRS Researcher, Lille (France)

Director :

Prof. Sébastien PAUL, Ecole Centrale de Lille

Co-director :

Dr. Jean- Sébastien GIRARDON, Université de Lille 1

Acknowledgement

First of all, I would like to express my immense and sincere gratitude to my research supervisor Prof. Sébastien PAUL and co-supervisor Dr. Jean- Sébastien GIRARDON for their constant support and guidance throughout my research work. My heartfelt thanks for their valuable time in bringing this output and shaping this thesis in the perfect manner.

I could not find enough words to thank the efforts and input rendered by Dr. Benjamin KATRYNIOK and Dr. Marcia ARAQUE MARIN to bring this thesis to this stage. The enthusiasm and interest he paid to resolve any problem is an inspiration for me. Many many thank to them for their efforts to teach so many scientific things, which can be seen as an output in this thesis.

I owe my deepest gratitude to Prof. Franck DUMEIGNIL, who introduced me to the research in France by giving an opportunity in this prestigious laboratory. Also, I would like to express my whole hearted thanks for his useful advices and care during my difficult situations.

My sincere thanks to Olivier GARDOLL, Dr. Joelle THURIOT-ROUKOS, Gérard CAMBIEN, Johann JEZEQUEL, Martine TRENTESAUX, Zohra Gueroui and Dr. KANG for their valuable help in characterization and technical support.

I owe my gratitude towards *Unité de Catalyse et Chimie du Solide* (UCCS, UMR 8181) of *Université des Sciences Technologies de Lille* (USTL) and *Ecole Centrale de Lille* (EC Lille) for providing a scientific environment and experimental platform.

I am grateful to CLARIANT for the financial support during my thesis as well as Dr. Olaf WACHSEN, Dr. Vanessa BACHER, Dr. Oliver FRANKE and Dr. Normen SZESNI for their kind attention.

I am also thankful to Dr. Jean-Marc MILLET and Prof. Bernard NIEUWENHUYS for accepting the role of Referees for my thesis as well as Dr. Axel LOFBERG and Dr. Oliver FRANKE and Prof. Anne-Cécile ROGER for examining the thesis.

I also acknowledge the homely environment provided by my colleagues and friends in EC Lille, Dr. Jorge Beiramar, Dr. Fangli Jing, Dr. Svetlana Heyte, Dr. Thomas Bonnotte, Dr. Ajay Ghalwadkar, David Melendez, Mengnan Lu, Xiaofeng Yi, Mengdie Cai, Dr. Vijayanand S., Dr. Swati Pandhare, Dr. Yoshihiro Kon, Haiqin Quan, Dr. Luan, Mengdie Cai, Tong Li, Dr. Zeineb Assaf, Gaetan Perrussel, Anouchka Kimene, Alexandrec, Dr. Robert Woicieszak, Maha Ammoury, Marine Gaillard and Soraya Zaid for their helping hands and making my stay in France more memorable.

I also would like to thank my Indian friends Dr. Pushpendra Kumar, Mohit Makkar, Mayank Jha, Anagha Ghalwadkar, Dr. Pranay Morajkar, Dr. Lishil Silvester, Narinder Singla, Debarun Dhali, Koyal, Bilquis, Priyanka and Richa for their friendly environment and support.

My deepest and special acknowledgement goes to my parents, my brother, my sisters and my wife for their love, support and encouragement which made me to come up to this level.

Samadhan LOMATE

Table of Contents

Abstract

This thesis deals with the development of a heterogeneously catalyzed process for the direct conversion of ethanol into ethylene oxide. Many catalysts consisting in gold, silver or copper nanoparticles dispersed on the surface of various supports (Al_2O_3, SiO_2, TiO_2, ZrO_2 and activated carbon) were prepared using different techniques including impregnation and co-precipitation methods. These catalysts were characterized in order to determine their structural, textural and chemical properties as well as their elemental compositions using XRD, XPS, XRF, SEM, TEM and TPR. The performance of the catalysts for the direct conversion of ethanol to ethylene oxide was determined in a vapor phase down-flow fixed-bed reactor at atmospheric pressure. Furthermore, the impact of reaction conditions (temperature, GHSV, ethanol/oxygen ratio) was also studied. It was found that the catalysts preparation and reaction conditions strongly affect the catalytic performance, which is ascribed to the fine-tuning of the redox cycle enabling the stabilization of the oxidation state of the active metal. The best results were obtained on a copper-based catalyst supported on TiO_2, which contained the anatase phase. For this catalyst it was found that the reduction of the copper species took place at a lower temperature than on the other types of supports. The best performance obtained using this catalyst was an ethanol conversion of 99% together with a selectivity in ethylene oxide of 61% at 250 °C.

Résumé

Cette thèse porte sur le développement d'un procédé catalytique pour la conversion directe d'éthanol en oxyde d'éthylène. De nombreux catalyseurs composés de nanoparticules d'or, d'argent ou de cuivre déposés à la surface de divers supports (Al_2O_3, SiO_2, TiO_2, ZrO_2 et charbon actif) ont été préparés en utilisant différentes techniques, dont l'imprégnation et la co-précipitation. Ces catalyseurs ont été caractérisés afin de déterminer leurs propriétés structurales, texturales et chimiques ainsi que leurs compositions élémentaires en utilisant les analyses DRX, XPS, XRF, MEB, MET et TPR. Les performances de ces catalyseurs pour la conversion directe d'éthanol en oxyde d'éthylène ont été déterminées dans un réacteur à lit fixe en phase vapeur sous pression atmosphérique. En outre, l'influence des conditions de réaction (température, GHSV, rapport éthanol / oxygène) a été étudié. Il a été constaté que les conditions de préparation du catalyseur et de mise en œuvre en réaction affectent de manière significative les performances catalytiques, très probablement en permettant de jouer sur le cycle redox du métal actif en catalyse et en stabilisant son état d'oxydation. Les meilleures performances ont été obtenues sur un catalyseur au cuivre sur support TiO_2 contenant une phase anatase. Pour ce catalyseur il a été observé que la réduction des nanoparticules de cuivre peut être obtenue à plus basse température que lorsque les autres supports sont employés. Les meilleures performances obtenues sur ce catalyseur sont une conversion en éthanol de 99% et une sélectivité en oxyde d'éthylène de 61% à 250 °C.

Chapter 1

Introduction

1.1 Ethylene oxide

Ethylene oxide (noted EO in the following), or oxirane, (molecular formula C_2H_4O) (Scheme 1-1) is the most simple epoxide molecule. Under standard conditions it is a colorless gas that liquefies at 10°C with sweet or etheric odor. Because of its chemical properties, mainly its high reactivity and its high miscibility with water or organic solvents, ethylene oxide is one of the most versatile intermediate of the chemical industry despite of its high toxicity [1, 2].

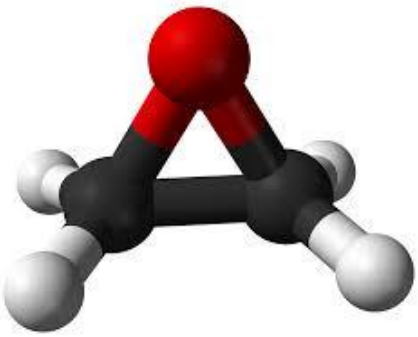

Scheme 1-1: Ethylene oxide molecule

The first synthesis of ethylene oxide was reported [3] in 1859 by the French scientist Wurtz from 2-chloroethanol (ethylene chlorohydrin). Due to an uncompetitive cost, this protocol was not employed for a long time. In 1931, Lefort succeeded in preparing ethylene oxide by direct oxidation of ethylene using a silver catalyst [4, 5]. This catalysis-based approach is still employed nowadays as industrial process for ethylene oxide production from direct oxidation of ethylene [6].

1.1.1 Applications of ethylene oxide

Ethylene oxide is currently used as a sterilizing agent, fumigant and insecticide, either alone or together with carbon dioxide [7]. In everyday life, ethylene oxide is used to sterilize drugs, hospital equipment's, reusable medical items, packaging material, food, scientific equipment's, clothing, aircrafts and other items [8, 9].

Nevertheless the main application of ethylene oxide remains its utilization as source molecule used in the manufacture of chemical derivatives such as mono-ethylene glycol, di-ethylene glycol, tri-ethylene glycol, polyethylene glycol, ethylene glycol ethers, ethanolamines and some other important chemicals (Figure 1-1).

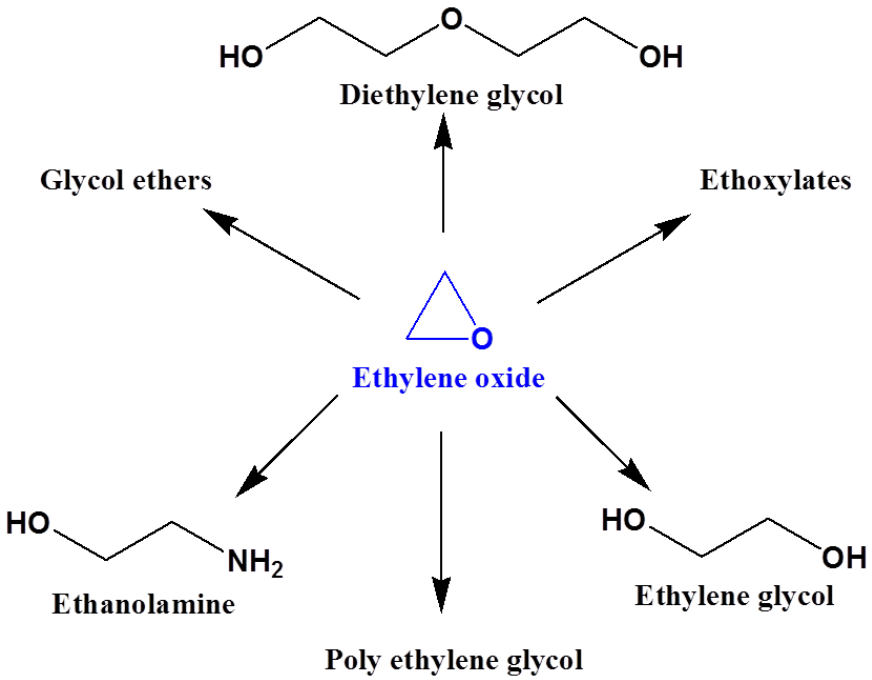

Figure 1-1: Routes for valorization of ethylene oxide

The repartition of the ethylene oxide consumption is shown in Figure 1-2 and more detailed information about each product issued from ethylene oxide are given below.

- **Ethylene glycol**

Ethylene glycol is one of the most important industrial chemicals found in many consumers products, including automotive antifreeze, hydraulic brake fluid, stamp pad ink, plastic paints and cosmetics. More than 65% of ethylene oxide production is used for synthesizing ethylene glycol. Ethylene glycol is an intermediate in the production of polyethylene terephthalate (PET) by a polymerization reaction with a nucleophile, whereby the annual consumption of mono-ethylene glycol is about 15 million metric tons [10-12].

- **Ethoxylates**

Ethoxylates are nonionic surfactants, which are incorporated in many industrial formulations. The synthesis is based on the addition of ethylene oxide to an alcohol. 13% of ethylene oxide are consumed for the synthesis of ethoxylates [14, 15].

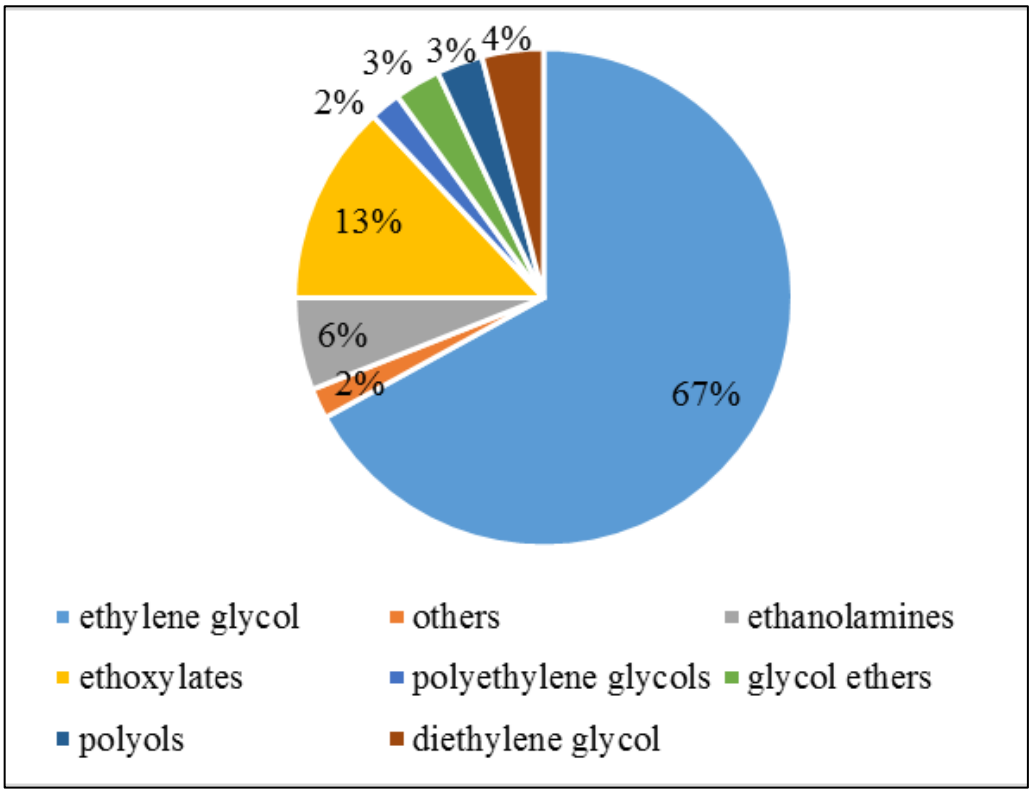

Figure 1-2: Consumption of ethylene oxide [13]

- **Glycol ether**

The production of ethylene glycol ether is performed by a reaction between ethylene oxide and alcohols (n-butanol). It is commonly used in paints and cleaner [16]. The glycol ether production consumes about 3% of the worldwide ethylene oxide.

- **Ethanolamine**

Ethanolamine is synthesized by the reaction of ethylene oxide and ammonia in an aqueous environment. Ethanolamine is widely used in surfactants, softeners, gas purification and pharmaceutical industries. Furthermore, it is used in the production of monoethanolamine (MEA) and diethanolamine (DEA). This chemistry represents 6% of the total ethanol oxide consumption [17-19].

- **Poly ethylene glycol**

The reaction of an organic acid with ethylene oxide gives the corresponding ethylene glycol monoester. This product further reacts with ethylene oxide to yield poly ethylene glycol. Ethylene glycol diesters may be obtained directly by the reaction of ethylene oxide and an acid anhydride [20-22].

Ethylene oxide is also used in the synthesis of acrylates whereby ethylene forms 2-hydroxylethyl acryl ethers [23].

1.1.2 Ethylene oxide production

Ethylene oxide has been produced commercially by two basic routes. In the first route, ethylene oxide was synthesized by the direct oxidation of ethylene chlorohydrin using potassium hydroxide as shown in Figure 1-3. This process was first commercialized in 1925 in the US. In the following, this process was introduced during First World War in Germany by Badische Anilin-und Soda Fabrik (BASF) [24]. But the chlorohydrin process was inefficient because most of the chlorine was lost as potassium chloride [25].

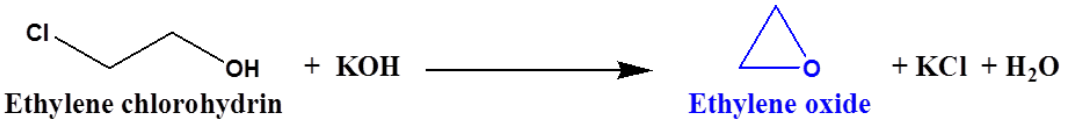

Figure 1-3: Ethylene oxide synthesis from ethylene chlorohydrin

Since this process was not economically competitive, it was quickly replaced by the direct oxidation process as dominant technology whereby till date nearly all the ethylene oxide in the world is obtained by the direct oxidation of ethylene. The corresponding reaction can be divided into two categories depending on the source of oxidizing agent i.e. air or oxygen. In 1937, Union Carbide Corp. first commercialized an air-based direct oxidation process. The first oxygen based process was commercialized by Shell Oil Co. in 1958 [26]. The main disadvantage of the direct oxidation of ethylene process is the low yield or selectivity to ethylene oxide per mole of ethylene consumed, since 20-25% of the ethylene is converted to CO_2 and water. Indeed, the operating conditions must be carefully controlled to maximize the ethylene oxide selectivity. Silver-based catalysts were found the best catalysts for the direct oxidation of ethylene into

ethylene oxide. Two reactions are possible over the silver surface: ethylene oxide formation by partial oxidation (Figure 1-4) and complete combustion by total oxidation to CO_2 and H_2O (Figure 1-5) [5].

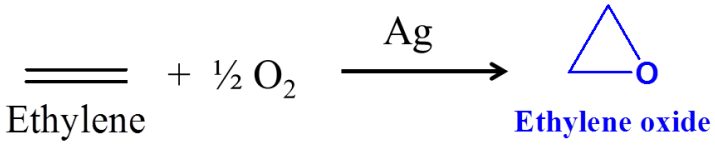

Figure 1-4: Direct oxidation of ethylene to ethylene oxide

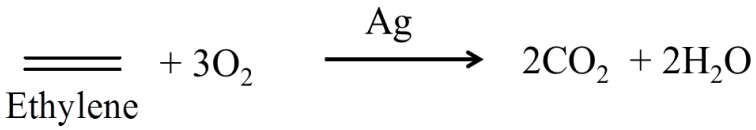

Figure 1-5: Total oxidation (combustion) of ethylene

The ethylene conversion in the commercial process is typically 10-20%. An increase in the conversion is generally accompanied by the formation of CO_2 and water from complete combustion of ethylene with oxygen.

Since the selective oxidation of ethylene is of high commercial interest, this reaction was extensively studied and numerous patents were filed, but the exact reaction mechanism was not fully understood in the beginning [27]. In fact, there was much controversy on the nature of the oxygen species responsible for the ethylene oxide formation. Different surface characterization techniques indicated that there are three types of adsorbed oxygen species on silver i.e. monoatomic, diatomic and subsurface oxygen.

The monoatomic chemisorbed oxygen was found responsible for both ethylene oxide and CO_2 formation. So, the most important factor to control is chemisorbed monoatomic oxygen. Monoatomic chemisorbed oxygen with strongly negative charge acts as a base, leading to the abstraction of hydrogen, but also promotes the complete combustion of ethylene. Intermediates of the total oxidation of ethylene are acetaldehyde, acetic acid, formic acid and oxalic acid [28]. The environment of adsorbed oxygen atom determines whether the reaction with ethylene leads to the formation of ethylene oxide or to other oxidation products [29]. If subsurface oxygen is present, it

competes with adsorbed atomic oxygen for silver electrons, reducing the negative charge on the adsorbed oxygen. The molecular structure is preserved and the formation of ethylene oxide is predominant [30]. Corresponding results were also confirmed by theoretical calculation [31].

As aforementioned, the direct oxidation of ethylene to ethylene oxide over a silver catalyst can use two different oxidizing agents: air and pure oxygen. In the latter case, due to the low per pass conversion of ethylene, a recycling loop is necessary. This leads to the accumulation of nitrogen in the process cycle, whereby a substantial purge as well as intermediate removal of carbon dioxide is required. On the contrary, the oxygen-based process facilitates the recycling of unconverted ethylene [26, 32] but the capital cost of a such a process is much higher than the one based on air due to the necessity to install a unit of cryogenic separation of air. The general reaction conditions for air and oxygen-based process are summarized in the Table 1-1.

Table 1-1: General reaction conditions for ethylene to ethylene oxide reaction [25, 33, 34]

Parameters	Air oxidation	Oxygen oxidation
Ethylene, mol.%	2–10	20–35
Oxygen, mol.%	4–8	4–8
Carbon dioxide, mol.%	5–10	5–10
Ethane, mol.%	0–1	0–1
Temperature, °C	220–277	220–235
Pressure, MPa	1–3	2–3
Space velocity, h^{-1}	2000–4500	2000–4500
Pressure drop, kPa	41–152	41–152
Conversion, %	20–65	8–12
Selectivity (mol. basis, %)	63–75	75–82

At present, most of the ethylene oxide is produced by the oxygen-based process but whatever the process, it is conveniently divided into three main sections: reaction zone, ethylene oxide recovery and ethylene oxide purification (Figure 1-6). The tubular reactor is generally surrounded by water or coolant in order to remove the heat of the exothermal oxidation reactions and allow precise temperature control. If organic heat transfer media are employed, the extracted

energy is used to generate steam in secondary cycles, which can then be used to pre-heat the inlet flows.

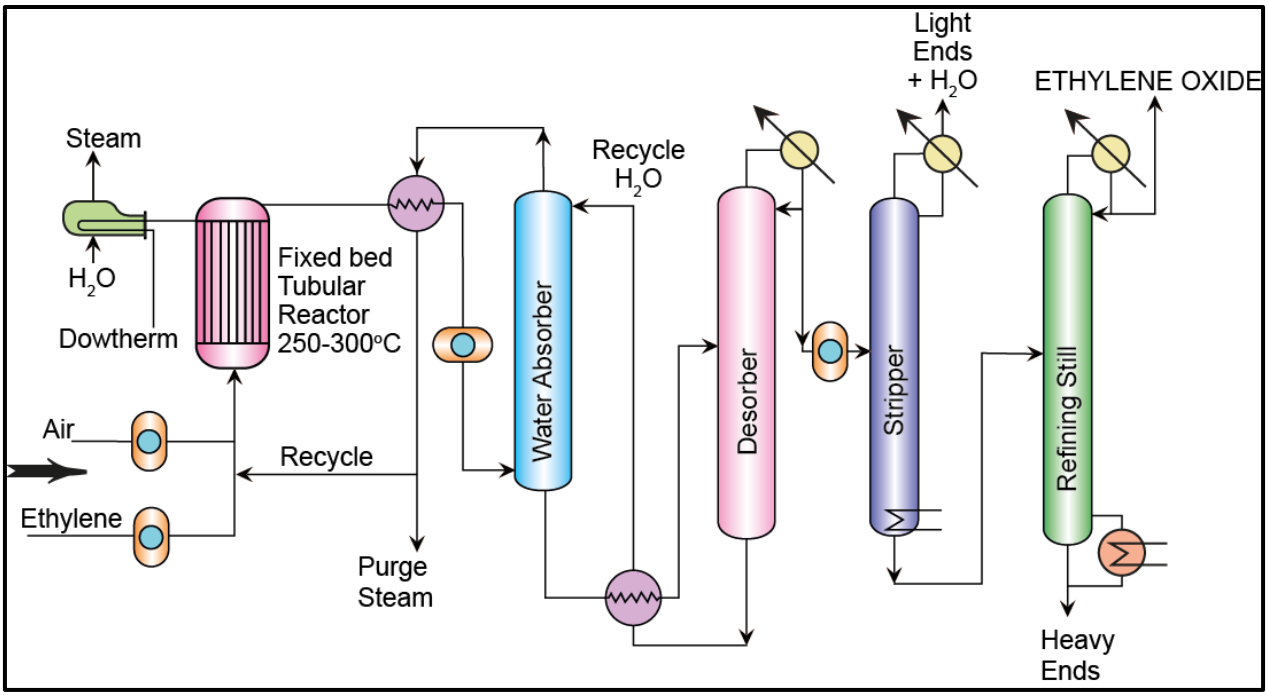

Figure 1-6: Air-based direct oxidation process for ethylene oxide

After the effluent of the reactor has been cooled, the ethylene oxide and CO_2 must be removed by scrubbing first with water and then with aqueous potassium carbonate solution. In the ethylene oxide scrubber, all ethylene oxide and small amounts of the other constituents of the recycle gas (CO_2, N_2, CH_4, CH_2CH_2, and aldehydes) are dissolved in water. The resulting aqueous ethylene oxide solution then passes to the ethylene oxide desorber. The ethylene oxide recovered as head product in the desorber is subsequently stripped of its low-boiling components and finally distilled, thereby separating water and ethylene oxide [26, 32].

Until 2002, ethylene oxide was produced in more than 30 countries in Asia, Australia, Europe, Middle East, North America and South America with a production capacity of 16.3 million tons per year. In 2009 the world consumption of EO reached already 19 million metric tons per year, making it the most utilized epoxide species [11]. The recent production and capacity of ethylene oxide in Europe is shown in Figure 1-7 [35].

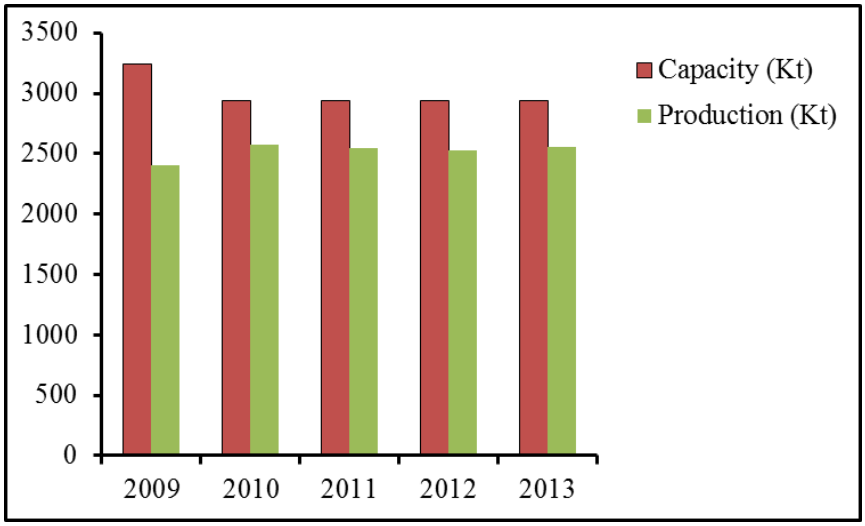

Figure 1-7: Production of EO in Europe [35]

In order to increase the yield in ethylene oxide, alternative catalysts doped with palladium and platinum were developed. During the last decades, the catalyst composition has been progressively improved. Now, the best catalysts show up to 81% selectivity in EO (ethylene conversion not reported) as shown in Table 1-2.

Table 1-2: Performance of the catalysts for direct oxidation of ethylene to ethylene oxide

Catalyst name	Temperature, °C	EO Selectivity, %	Reference
Pt-Ag/ α-Al_2O_3	250-300	70	[36]
Cs-Ag/ α-Al_2O_3	230-280	78	[37, 38]
Ag-Na-Cs-F/ α-Al_2O_3	217-224	79	[39]
Cs-Ag/α-Al_2O_3	224	81	[40]

Other additives were studied by Rashkin *et al.* such as alkali metal. The authors claimed high selectivity to ethylene oxide up to 78% at 9% conversion of ethylene. These results are surprising, as previously lithium, sodium, potassium and cesium were claimed to act as poison in the oxidation of ethylene. Rashkin *et al.* suggested that the quantity of alkali metal must be adapted wisely and showed that low amounts indeed improved both activity and selectivity relative to alkali-free silver catalysts. In 1982, Nojiri reported that not only the cation (sodium or

cesium) but also the anion is important for high selectivity. They claimed that halogen-ion (chlorine, bromine or fluorine) as an anionic component in addition to the Cs or Na cations are ideal dopants for the silver catalyst. Thus, an alkali metal-doped Ag-Na-Cs-F/α-Al_2O_3 catalyst showed 79% selectivity in ethylene oxide at 217 °C (ethylene conversion not reported). The highest performance for alkali metal-doped silver catalysts at 220-300 °C using 15% C_2H_4 with GHSV-5500h^{-1} and 21 bar pressure was reported by Kintoken claiming 81% selectivity for ethylene oxide (ethylene conversion not reported).

There were a number of studies about the effect of supports on epoxidation of ethylene. Rojluechai *et al.* [41] studied catalysts based on Au, Ag over Al_2O_3, TiO_2, and CeO_2. The best performance for ethylene epoxidation was found over Ag catalysts supported on Al_2O_3 with the optimum Ag loading of 13.18 wt.%, while Ag catalysts supported on TiO_2 or CeO_2 only promoted total oxidation. Beck *et al.* studied mesoporous silica in order to reduce the mass diffusion limitations and to provide the acidic properties of the microporous zeolitic aluminosilicates, which directly affected the catalytic activity [42]. Fotopoulos *et al.* found that the Ag catalysts supported on MCM-41 and HMS mesoporous silica were active in the ethylene epoxidation reaction, exhibiting ethylene oxide selectivity similar to those of the Ag catalysts supported on non-porous silica and conventional low surface area α-alumina at a relatively low temperature (~230 °C) [43]. Puangpetch *et al.* [44] successfully synthesized mesoporous-assembled $SrTiO_3$ nanocrystals via a sol-gel process. This mesoporous structured $SrTiO_3$ was used as the support for Ag, as it was hypothesized to facilitate the formation of uniform nano-sized Ag particles at high Ag loadings, which is supposed to facilitate the epoxidation reaction. Recently, Chongterdtoonskul *et al.* have studied the effect of different oxide supports on the ethylene epoxidation over Ag-based catalysts. They reported an Ag/$SrTiO_3$ catalyst which exhibits a very high EO selectivity of up to 99% and a EO yield of 4.5% [45].

1.2 Ethylene oxide production from ethanol

As we have seen, the ethylene oxide production is strongly dependent on a petrochemical-issued, non-renewable source, namely ethylene. However as the worldwide supply of petroleum will inevitably diminish, it will become increasingly expensive and accordingly less attractive as a carbon source. Furthermore, the use of fossil resources is associated with net increase in

greenhouse gas levels worldwide [46-49]. Hence, biomass has received considerable attention as a sustainable feedstock that can replace fossil fuels for the production of fine chemicals. Thus, during the last decades, concerns regarding global warming and fossil fuel depletion resulted in a wide interest in the use of environmentally friendly renewables as starting materials for the chemical industry. This is of course also the case for EO production and the best biosourced starting material in that particular case is of course bio-ethanol. The following paragraphs will draw a picture of the current state of art of the indirect or direct conversion of ethanol to ethylene oxide.

1.2.1 Indirect route

Recently, the production of ethylene oxide from bio-ethanol using an indirect process via ethylene was reported. Bio-ethanol is an environmentally friendly, versatile and sustainable renewable chemical derived from biomass. Currently, all industrial scale ethanol production belongs to the first generation using either sugar or starch as raw materials. However, the technology to produce second-generation ethanol is under development and will permit to use different types of lignocellulosic material as substrate.

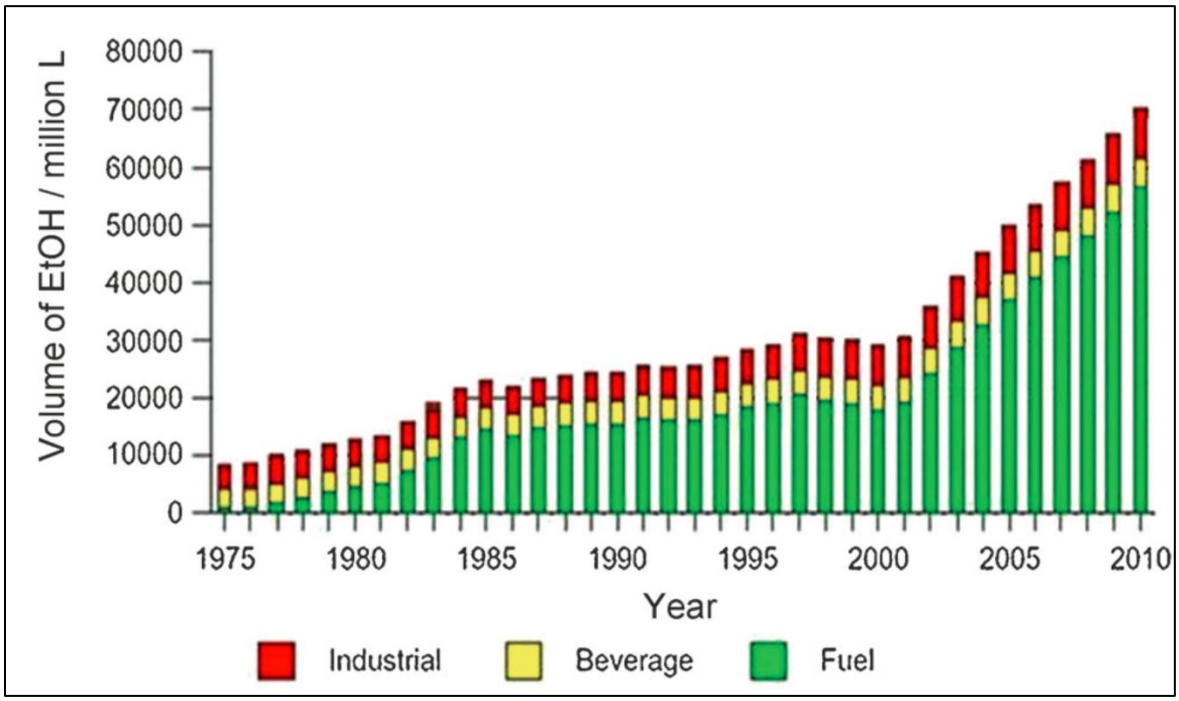

Figure 1-8: Worldwide production of ethanol [54]

Currently a negligible amount of second-generation bioethanol is produced around the world [50, 51] but it seems likely that cellulose-rich agricultural waste will gain importance as an even more sustainable and non-eatable feedstock in the future [52]. The production cost of ethanol has significantly decreased during the last decade notably due to continuous technological improvement [53] making it an attractive raw material. The worldwide production of bio-ethanol has significantly increased over the past years, as shown in Figure 1-8. The low price and large production capacities made bio-ethanol finding wide application as blending in gasoline whereby it enables to decrease the dependence on fossil fuels. But ethanol can also undergo different kinds of reactions like oxidation or dehydration.

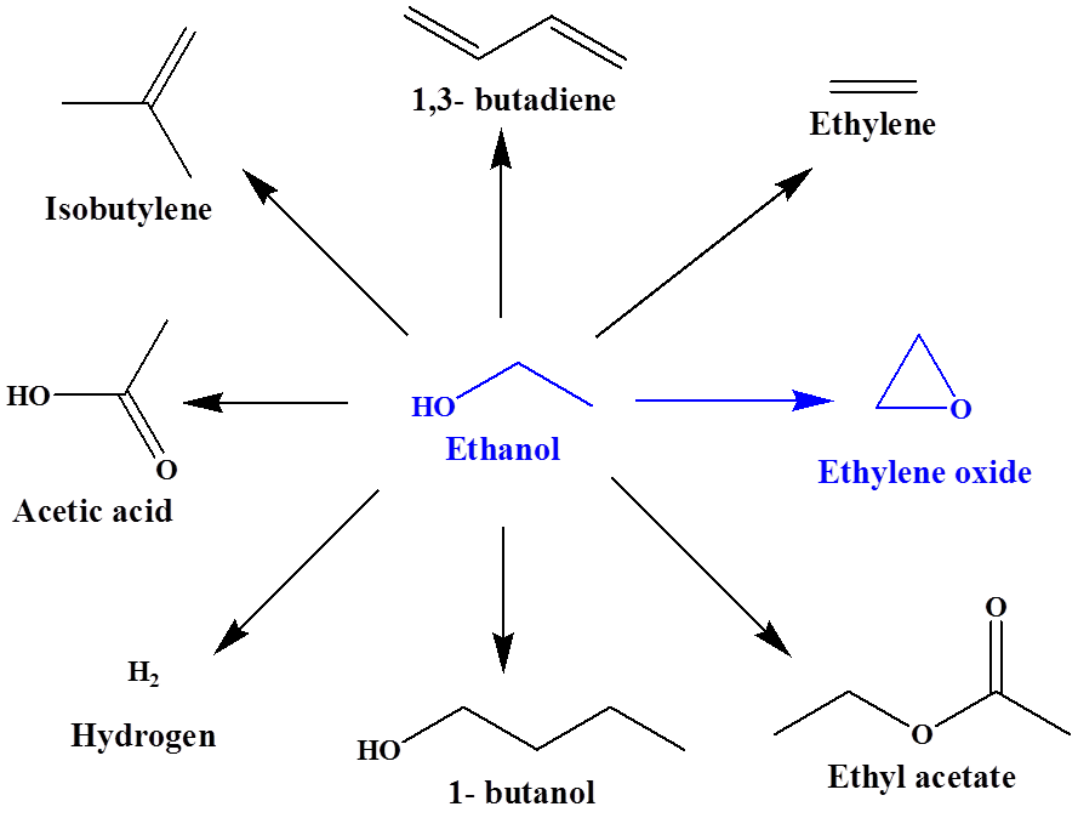

Figure 1-9: Valorization of bio-ethanol

It can – for example – be converted to acetaldehyde (oxidation), ethylene (dehydration), ethyl acetate (oxidation and consecutive esterification) as well as syngas (gasification) as shown in Figure 1-9 [55]. Nevertheless, among the various molecules derived from ethanol, ethylene oxide is one of the most valuable ones. It can be synthesized by successive dehydration of ethanol

and oxidation of the as-obtained ethylene. Therefore, the possibility of using a renewable feedstock - such as ethanol - has attracted much attention and interest.

The indirect route for the synthesis of ethylene oxide from ethanol was reported in a two-steps process by Chemtex Corp. [56]. The reaction is performed on the tandem mode without any intermediate (ethylene) separation between the two reactors. In the first step, ethanol is converted into ethylene via a dehydration reaction using an acid catalyst. In the second step, the as-prepared bio-ethylene is oxidized using conventional redox catalysts as shown in Figure 1-10.

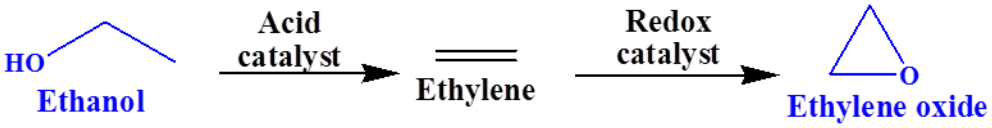

Figure 1-10: Indirect route for ethanol to ethylene oxide

Rockicki *et al.* disclosed a process for manufacturing ethylene oxide from ethanol via epoxidation of ethylene using silver-based epoxidation catalysts. The reaction was carried out at 225 to 280°C (pressure 1 to 30 atm) and GHSV between 1500 to 10000 h^{-1}. The yield in ethylene oxide was not detailed [57, 58].

1.2.2 Direct route

For the first time, the direct conversion of ethanol to ethylene oxide was reported by Lippits *et al.* as shown in Figure 1-11. In this study, different catalysts were screened in the dehydration, dehydrogenation and oxidation of ethanol. In addition, the influence of the reaction conditions was studied for different catalyst in order to optimize the selectivity in the targeted product.

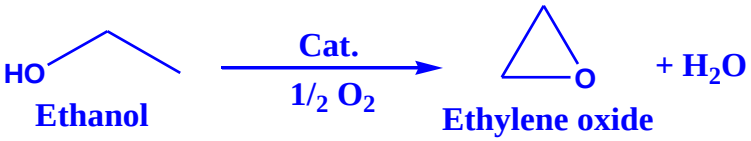

Figure 1-11: Direct route for ethanol to ethylene oxide

1.2.2.1 Catalysts

Up to now, the direct conversion of ethanol to ethylene oxide was only described using alumina-supported silver, copper and gold catalysts [59, 60]. These catalysts were prepared by a

deposition precipitation method. Prior to use the calcined catalysts were further reduced under hydrogen flow.

A. Influence of the metal

Lippits *et al.* reported that the supported gold, silver and copper catalysts were active for the direct conversion of ethanol to ethylene oxide. They studied the catalytic performance of alumina-supported gold, silver and copper catalysts and the effect of Li_2O and CeO_x at different temperatures. Each catalyst was screened for the oxidation, dehydration and dehydrogenation. Lippits *et al.* reported that all catalysts (gold, silver and copper) were active for the direct conversion of ethanol into ethylene oxide but that gold catalyst showed the highest yield towards ethylene oxide (up to 76%). On the other hand, silver and copper-based catalysts showed yield to ethylene oxide of 53% and 63%, respectively.

B. Influence of the addition of the oxides

- #### Effect of Li_2O

In all cases the addition of Li_2O had a significant positive impact on the selectivity to ethylene oxide. This effect is independent of the metal (gold, silver or copper), which is explained by the modification of the acidity of the alumina support. In fact, γ-alumina promotes the dehydration (ethylene) and condensation reaction (diethyl ether) due to its strong acid sites. It was also found that the Li_2O acts as a structural promoter for the Au/Al_2O_3 catalyst. So the lithium showed a double effect: (i) structural promoter by influencing the shape and size of the active gold particles and (ii) moderator of the activity of the alumina support by influencing the acidic sites. Addition of Li_2O was found beneficial in terms of selectivity to ethylene oxide.

- #### Effect of CeO_x

The addition of ceria has no significant effect on the selectivity to ethylene oxide. Ceria increases the acidity of the catalyst and thereby promotes the formation of diethyl ether and CO. Furthermore it does not prevent the coke formation on the active sites of the catalyst. In addition, ceria yields large amounts of acetaldehyde in absence and presence of oxygen (dehydrogenation or oxidation, respectively).

In Table 1-3 are summarized the most promising results obtained by Lippits and coworkers.

Table 1-3: Direct conversion of ethanol to ethylene oxide

Catalyst	Temperature (ºC)	Conversion of ethanol (%)	Selectivity in EO (%)	Yield in EO (%)
$Au/Li_2O/Al_2O_3$	200	80	95	76
	300	90	71	64
	400	100	10	10
$Ag/ Li_2O/Al_2O_3$	200	58	96	56
	300	90	54	49
	400	100	30	30
$Cu/ Li_2O/Al_2O_3$	200	70	90	63
	300	92	15	14
	400	100	4	4

Reaction operating conditions: *Catalyst wt.- 0.2 g, ratio O_2:Ethanol- 1:1,GHSV- 2500 h^{-1}, Carrier gas- Argon , Pressure- atmospheric*

1.2.2.2 Reported catalytic activity measurement and influence of the reaction conditions

In Lippits' work the catalytic tests were performed in a micro-reactor system at atmospheric pressure and oxygen was used as oxidizing agent. For the catalysts containing CeO_x and Li_2O, the amount of catalyst was adjusted in such a way that the amount of gold was similar for all the catalysts with and without additives. Prior to tests, the catalysts were reduced under hydrogen (4 vol.% in Ar) at 400 °C for 2 h. Two different ratios of oxygen/ethanol were used for the oxidation of ethanol: 1:1 and 6:1 (oxygen excess). Typically, a total gas flow of 40 mL^{-1} (GHSV = 2500 h^{-1}) was employed [59, 60].

A. Effect of oxygen

The amount of oxygen was found to play an important role notably to maintain high activity. Even if there is no information about catalysts stability in Lippits *et al.*'s publications one can assume that the main role of oxygen is to prevent coke formation. Nevertheless, at too high oxygen content, no ethylene oxide is formed as the latter is further oxidized to CO_2. Hence a good balance of the oxygen concentration might be important for high ethylene oxide selectivity and the maintaining of a constant activity.

B. Effect of reaction temperature

The selectivity towards ethylene oxide decreases at high temperature, which is ascribed to its further oxidation. In all cases (see Table 1-3), full conversion is reached at 400 ºC but the selectivity to ethylene oxide is then low. On the other hand, at low temperature (200 ºC), highest selectivity to ethylene oxide was observed, but the ethanol conversion was significantly lower (58-80%). Thus, moderate temperature (200 ºC) is the best compromise for high yields in ethylene oxide.

1.3 Aim and objectives of the thesis

As we have seen, until this date the commercial production of ethylene oxide is uniquely based on the direct oxidation of ethylene using air or pure oxygen as oxidizing agent. Many metal-supported catalysts were developed, but only silver-based catalysts are showing good activity for the selective ethylene oxidation. Obviously ethylene is a non-renewable resource mainly issued from oil and it is well known that fossil fuel resources are limited whereas the demand of fine chemicals is increasing. So, to find new routes from renewable resources for the production of fine chemicals is of significant importance. Taking all these criteria into account, ethanol, which is one of the most widely used biomass-derived sustainable chemical, is a very promising starting material. The literature survey showed very few reports on the synthesis of ethylene oxide from ethanol as only two kinds of processes are reported: a one-step direct process reported by Lippits *et al.* and a two-steps indirect process via ethylene proposed by Chemtex corporation. Of course the one-step process is the most attractive commercially. In this context, Lippits *et al.* used gold, copper and silver-based catalysts. Nevertheless, the authors limited their study to alumina-supported catalysts applying the deposition precipitation method. Furthermore, the catalytic activity and catalyst characterization were not reported in details. Hence, no correlation between the catalytic activity and the catalyst's properties was clearly established. Therefore, there is still a wide scope to study the catalyst properties using different characterization techniques. Furthermore, there is also still a large space to investigate the impact of the reaction conditions and to carry out their systematical optimization.

Hence, the challenge of this thesis is the development of a new catalytic system for the production of ethylene oxide from ethanol and to establish a correlation between the catalytic performance and the physical and chemical properties of the newly developed catalyst.

Our research work has been organized as follows. First we have synthesized the catalysts reported in the literature to try to reproduce the proof of concept. Then, on the basis of our preliminary results we have focused our work on the synthesis of copper-based catalysts using different synthesis methods and catalyst supports. These catalysts were deeply characterized using a large range of characterization techniques in order to determine their textural and redox properties. Further, a correlation between the catalysts properties and the catalytic performance was established which permitted to find the most determining factors for the optimization of the reaction. Finally, the effects of the different reaction parameters (temperature, GHSV, EtOH:O_2 ratio) were studied and optimized.

1.4 References

1. W. A. Goddard, E. A. Carter, Journal of Catalysis, **1988**, 112, 80-92.
2. N. Lopez, D. Torres, F. Illas, Journal of Catalysis, **2006**, 243(2), 404-409.
3. A. Wurtz, Annual Review of Physical Chemistry, **1859**, 110, 125-128.
4. T. E. Lefort, Societe Francaise de Catalyse Generalisee, **1931**, 41(254), 729-952.
5. T. E. Lefort, US1998878, **1933**, 402-438.
6. F. Maria, Verhaak M. Johannes, US0018557A1, **2014**.
7. Shell Chemicals Magazine, **2012**, 12.
8. J. Lacson, Zurich, SRI Consulting, CEH Marketing Research Report, **2003**.
9. K. F. George, J. P. Dever, W. C. Hoffman, H. Soo, Kirk-Othmer Encyclopedia of Chemical Technology, **2004**, 10, 632-673.
10. J. W. Ledford, V. Hal, J. S. Zhang, Xiankuan, Catalysis Today, **2007**, 123, 310-315.
11. J. Lacson, SRI International, Chemical Economics Handbook, **2003**.
12. PERP Report, NEXANT Chem Systems, **2006**, 5.
13. http://www.essentialchemicalindustry.org/chemicals/epoxyethane.html.
14. M. Baird C. Suna, H. A. Anderson, D. L. Brydon, Journal of Chromatography A, **1996**, 731, 161-169.
15. C. Podevin, G. Cretier, J-L. Rocca, Journal of Chromatography A, **2000**, 874, 305-310.
16. R. Srinivasan, I. A. Karimi, Proceeding of the 11th International Symposium on Process System Engineering, **2012**.

17. B. Delmon, A. Chauvel, W.F. Hölderich, Applied Catalysis A: General, **1994**, 115, 173.
18. S. Schwarz, D. R. Corbin, G.C. Sonnichsen, Catalysis Today, **1997**, 37, 71.
19. R. Wang, Feng, D. Liu, Z. Xie, Zaiku, Catalysis Communications, **2010**, 11(15), 1220-1223.
20. Y. S. Kardasheva, E.A. Karakhanov, A.L. Maksimov, V.V. Predeina, Journal of Molecular Catalysis A: Chemical, **1996**, 107, 235-240.
21. C. A. Coulson, Oxford University Press, New York, **1976**, 215-216.
22. A. Saika, L. H. Meyer, H. S. Gutowsky, Journal of american chemical society, **1953**, 75, 4567.
23. G. H. Twigg, H. J. Lichtenstein, Transactions of the Faraday Society, **1948**, 44, 357.
24. J. F. Norris, Journal of Industrial and Engineering Chemistry, **1919**, 11, 817.
25. H. J. Emeleus, F. G. A. Stone, Journal of the Chemical Society, **1950**, 2755, 521-563.
26. T. Kumazawa, I. Kiguchi, T. Nakai, Hydrocarbon Process, **1976**, 55, 69.
27. C. Backy, W. M. H. Sachtler, R. A. Van Santen, Catalysis Reviews: Science and Engineering **1981**, 23(182), 127-149.
28. R. M. Lambert R. F. Grant, Journal of Catalysis, **1985**, 93, 92-99.
29. C. P. M. de Groot, R. A. van Santen, Journal of Catalysis, **1986**, 98, 530-539.
30. B. Robert, L. Grant, M. Richard, Journal of Catalysis, **1985**, 92(2), 364-375.
31. K. Nakashiro, H. Kobayashi, T. Iwakuwa, Theoretical Chemistry Accounts, **1999**, 102, 237-243.
32. Shell Oil Co, EPA 266015 A1, **1988**.
33. Dutch Patent, **1964**, 6502927.
34. Brit. Pat., **1967**, 1075454.
35. http://www.petrochemistry.eu/about-petrochemistry/facts-and-figures/capacity-and-production-data.html. [cited 2014.
36. N. Ferlazzo, G. Antonelli, G. Aglietti, US3878126, **1975**.
37. N.J. Little Ferry, A. Jay Rashkin, U.S. 4774222, **1988**.
38. A. D. William, S. Conn, US4760042, **1988**.
39. S. Yukio, N. Naohiro, A. Akimi, EPA0059422A1, **1982**.
40. N.J Little Ferry, Kintoken Design Company, US5008413, **1991**.

41. S. Chavadej S. Rojluechai, J.W. Schwank, V. Meeyoo, Catalysis Communications, **2007**, 8, 57-64.
42. J.C. Vartuli, J.S. Beck, W.J. Roth, M.E. Leonowicz, C.T. Kresge, K.D. Schmitt, C.T.W. Chu, D.H. Olson, E.W. Sheppard, S.B. Mccullen, J.B. Higgins, J.L. Schlenker, Journal of american chemical society, **1992**, 114, 1-11.
43. K.S. Triantafyllidis, A.P. Fotopoulos, Catalysis Today, **2007**, 127, 148-156.
44. T. Sreethawong, T. Puangpetch, S. Yoshikawa, S. Chavadej, Journal of Molecular Catalysis A: Chemical, **2008**, 287, 70-79.
45. J. W. Schwank, A. Chongterdtoonskul, S. Chavadej, Journal of Molecular Catalysis A: Chemical, **2012**, 358, 58-66.
46. S. Iborra, W. George Huber, A. Corma, Chemical Reviews, **2006**, 106, 4044-4096.
47. J. H. Cushman, L.R. Lynd, R. J. Nichols, C. E.Wyman, Science, **1991**, 251, 1318-1323.
48. W. N. Delgass, N. R. Singh, F. H. Ribeiro, R. Agrawal, Environmental Science & Technology, **2010**, 44, 5298-5305.
49. Y. P. Zhang, Journal of Industrial Microbiology & Biotechnology, **2008**, 35, 367-375.
50. P. Erlandsson, P. R. Lennartsson, M. J.Taherzadeh, Bioresource Technology, **2014**, 165, 3-8.
51. T. L. Junqueira, M. O. Dias, O. Cavalett, M. P. Cunha, C. D. Jesus, C. E. Rossell, R. Maciel Filho, A. Bonomi, Bioresource Technology, **2012**, 103, 152-161.
52. B. E. Dale, S. Kim, Biomass Bioenergy, **2004**, 26, 361.
53. M. Ruth, R. Wooley, D. Glassner, J. Sheehan, Biotechnology Progress, **1999**, 15, 794.
54. OECD-FAO Agricultural Outlook 2011– 2020, **2011**.
55. B. M. Weckhuysen, C. Angelici, P. C. Bruijnincx, ChemSusChem, **2013**, 6, 1595-614.
56. http://www.chemtex.com/en/media/news?news=7 Chemtex corporation. 2009.
57. J. Durand, A. Rokicki, R. A. Morin, W. Suchanek, U.S. 0031568A, **2014**.
58. J. Durand, A. Rokicki, R. A. Morin, W. Suchanek, WO 2014/018474A1 **2014**.
59. M. J. Lippits, B. E. Nieuwenhuys, Catalysis Today, **2010**, 154, 127-132.
60. M. J. Lippits, B. E. Nieuwenhuys, Journal of Catalysis, **2010**, 274, 142-149.

Chapter 2

Catalysts Synthesis and Experimental Techniques

In this section are described the detailed procedures for the catalysts synthesis and catalytic tests – including the analytical techniques – and the characterization techniques employed for the study of the physicochemical properties.

2.1 Catalysts synthesis techniques

2.1.1. Materials

A list of the chemicals used in this work with the corresponding suppliers is given in the following Table 2-1.

Table 2-1: List of chemicals used and their suppliers

Material	Supplier
$Cu(NO_3)_2.3H_2O$ (99-104%)	Sigma-Aldrich
Titanium (IV) oxide (TiO_2-P25) (≥99.5%)	Sigma-Aldrich
Titanium (IV) oxide (TiO_2-Anatase)	Home made
Zirconium oxide (ZrO_2-Monoclinic) (99%)	Sigma-Aldrich
Zirconium oxide (ZrO_2-Monoclinic) (99.5%)	Clariant
Silicon dioxide (SiO_2) (CARIACT-Q10)	Fuji Silysia Chemical Ltd.
Activated carbon	CECA
Aluminum oxide (γ-Al_2O_3-98%)	Sasol
$Al(NO_3)_3 \cdot 9H_2O$ (99.99%)	Sigma-Aldrich
Titanium isopropoxide(99.99%)	Sigma-Aldrich
Ethanol (99.8%)	Sigma-Aldrich

2.1.2. Catalysts preparation

In the present work, the catalysts were prepared using three different techniques including impregnation, co-precipitation and sol-gel methods. In case of the impregnation technique different supports with different loadings of metal were employed. The supports used were TiO_2, Al_2O_3, activated carbon, SiO_2 and ZrO_2. The detailed procedures for all catalysts preparation methods are given below.

A. Impregnation method

Impregnation using diluted solutions of the precursors is often employed when low loadings of active metal are desired. When high metal loadings are required, then the

precipitation method is preferred. In the impregnation method, a metal ion is contacted with an oxide of high surface area with the idea to create small and highly dispersed metal particles with a large exposed surface area. Impregnation can be divided into two sub-methods, i.e. wet impregnation and incipient wetness impregnation. In the wet impregnation method the volume of the solution is substantially larger than the pore volume of the support while in the incipient wetness method the amount of the solution added is equal to the pore volume of the support.

In our case, most of the catalysts were prepared by the wet-impregnation method In a typical synthesis, the appropriate amount of the copper precursor [$Cu(NO_3)_2.3H_2O$] was dissolved in distilled water at room temperature under stirring. Afterwards, the support was added slowly to the aqueous solution at room temperature under constant stirring. The resulting solution was kept under vigorous stirring for 4 h at room temperature. Then, the solution was transferred to a round bottom flask and the water was removed on a rotary evaporator under reduced pressure at 60 °C. The obtained powder was dried at 105 °C for 16 h and calcined at 400 °C (heating rate of 2 °C min^{-1}) for 4 h under static air. The catalysts names and their theoretical compositions are summarized in Table 2-2.

Table 2-2: List of the catalysts prepared with their loadings

Sr. No.	Catalyst Name	Cu, wt.%	Support
1	0.2% Cu-TiO_2	0.2	TiO_2 (P-25)
2	1% Cu-TiO_2	1	TiO_2 (P-25)
3	2.5% Cu-TiO_2	2.5	TiO_2 (P-25)
4	5% Cu-TiO_2	5	TiO_2 (P-25)
5	5% Cu-Al_2O_3	5	Al_2O_3
6	50% Cu-Al_2O_3	50	Al_2O_3
7	5% Cu-SiO_2	5	SiO_2
8	5% Cu-ZrO_2-Ald	5	ZrO_2-Aldrich
9	5% Cu-Act. Carbon	5	Act. Carbon
10	5% Cu-ZrO_2-CL	5	ZrO_2-CLARIANT
11	5% Cu-TiO_2-Anatase	5	TiO_2-Anatase
12	5% Cu-TiO_2-Rutile	5	TiO_2-Rutile

The first four catalysts (entries 1 to 4) were synthesized with the same support but with different amounts of copper loadings. The remaining catalysts (entries 5 to 12) were synthesized using 5 wt. % of copper with different supports.

B. Co-precipitation method

Co-precipitation is one of the more convenient and facile methods used for the synthesis of nanomaterial catalysts. The corresponding metal salts in the form of nitrate, chloride, etc. are used as starting materials. These precursors, after calcination at suitable temperature, will give the corresponding metal oxide or mixed metal oxide. The major steps of the precipitation reaction are nucleation, growth and agglomeration [1-4].

In the present work, only copper-alumina-based catalysts were prepared by co-precipitation method [5]. Equimolar (0.5 M) mixtures of aqueous solutions of copper nitrate trihydrate [$Cu(NO_3)_2 \cdot 3H_2O$] and aluminium nitrate nonahydrate [$Al(NO_3)_3 \cdot 9H_2O$] in one addition funnel and aqueous solution (0.2 M) of potassium carbonate (K_2CO_3) in another addition funnel were added simultaneously to a beaker containing 15 mL of deionised water under constant stirring at room temperature. The obtained precipitate was matured for 5 h and then filtered and washed with deionised water to remove the traces of potassium. The precipitate was dried in an oven at 100 °C for 12 h, before the catalyst was calcined at 400 °C for 4 h under static air. The catalyst names and their theoretical compositions are shown in Table 2-3.

Table 2-3: List of catalysts prepared using co-precipitation method

Sr. No.	Catalyst Name	Cu, wt.%
13	5% Cu-Al_2O_3	5
14	50% Cu-Al_2O_3	50

C. Sol-gel method

Sol-gel is also one well-known method for catalyst synthesis [6, 7]. Sol-gel synthesis may be used to prepare materials with a great variety of shapes such as porous structures, thin fibers, dense powders and thin films.

In the present study, a Cu-TiO_2 catalyst was prepared using a sol-gel method to obtain pure anatase phase of TiO_2 (Table 2-4). An appropriate amount of copper nitrate trihydrate dissolved

in ethanol was added drop by drop to a solution of titanium isopropoxide in ethanol under vigorous stirring at room temperature. Then the sol was allowed to gel at room temperature. The obtained gel was dried at 100 °C for 12 h, before the sample was calcined at 400 °C for 4 h under static air.

Table 2-4: Catalyst prepared using sol-gel method

Sr. No.	Catalyst Name	Cu, wt.%
15	5% Cu-TiO2	5

2.2 Physicochemical characterization techniques

To determine the structural and textural properties, elemental composition and acid-base properties of the catalysts several techniques were used. They are described in details in this section including the parameters used.

2.2.1. X-Ray Diffraction (XRD)

Powder X-Ray diffraction (XRD) is a basic tool for the characterization of materials [8, 9]. X-ray diffraction is a versatile, non-destructive analytical technique for identification and quantification of the various crystalline compounds, known as 'phases', present in solid materials and powders.

The angular spread of the reflection from a crystal plane is affected not only by the perfection of the crystal but also by the size of the crystal. As the average size of the crystallites decreases, the angular spread of the reflection from a powder will increase. After suitable calibration, the half-height width of a reflection in a powder diffractogram can be used as quantitative measure of the mean crystallite size of the sample. The formula used for calculating the crystalline size is the Scherrer formula as given in the following equation (1):

$$K = \frac{0.9\lambda}{B\cos\theta} \qquad (1)$$

Where λ is the wavelength of the X-Ray, B is full width at half maximum of the pattern and θ is the Bragg angle. B is corrected for contribution from instrument line broadening by recording the pattern of a standard sample having very large particle size in the micrometer range.

In the current work, powder X-ray diffraction measurements were performed on a Bruker D8 advance diffractometer, using the CuKα radiation (λ = 1.5506 Å) as an X-Ray source. The 2θ range was of 10-80° with integration steps of 0.02° (2θ) per second.

High temperature XRD was also carried out on D8 Advance equipment (Bruker AXS) equipped with a HTK1200N high temperature chamber and connected to a VANTEC fast linear detector. The sample was deposited on a Pt sheet and the experiment was performed by increasing the temperature from ambient temperature to 600 °C using a heating rate of 10 °C/min acquiring a pattern every 50 °C. For high temperature XRD, the data acquisition parameters were the following: an angular range of 10°-80° with a step of 0.015° and acquisition time of 0.22 s per step. The phase identification was based on the comparison of the set of reflections of the sample with that of pure reference phases distributed by Joint Committee on Powder Diffraction Standards and International Center for Diffraction Data (JCPDS-ICDD).

2.2.2. X-ray Photoelectron Spectroscopy (XPS)

XPS is a surface sensitive technique since it has a relatively low penetration depth (0.5-10 nm) of the elastically scattered electron. XPS is based on the principle of the photoelectric effect, the emission of an electron when X-rays incident on a solid surface, discovered by Hertz in 1887. This technique has been widely used to characterize materials to get information about the elemental status [10, 11]. Through the electron spectra, the energy of the emitted photoelectrons can be measured. The solid material can characterize from the binding energies (BEs) of the element. Following equation (2) gives the relationship between the parameters involved in the XPS measurement:

$$E_B = h\nu - E_K - W \qquad (2)$$

Where $h\nu$ is the photon energy, E_K is the kinetic energy of the electron and W is the spectrometer work function. The binding energy can be calculated from the above equation and hence the information about elemental composition can be obtained. In addition to this, chemical information can be derived from the shift in binding energies, which depend on the chemical bounding (i.e. oxidation state) of the elements.

In this work, XPS for surface analysis of the catalysts was performed at the PRAS (Pole Regional d'Analyse de Surface, Villeneuve d'Ascq) on the KRATOS, AXIS Ultra^{DLD} apparatus equipped with a hemispherical analyzer and a delay line detector. The photoelectron source generated by Al-Kα operating at 150 W (15 kV, 10 mA) having initial kinetic energy up to 1486.69 eV. High resolution scans were acquired with 40 eV pass energy and 300 ms dwell time. All the resulting binding energy values were corrected using the C 1s peak (C-C) at 285 eV as a reference.

2.2.3. Textural properties measurement

The nitrogen physisorption technique is one of the important techniques for the characterization of porous solids [12]. On the basis of porosity, solids are classified into macroporous (pore diameters above 50 nm), mesoporous (pore diameters in the range 2-50 nm), and microporous (pore diameters less than 2 nm). To get the information about the surface area of a solid, one must determine the number of molecules that cover the surface area with single layer of adsorbate (monolayer capacity). The surface area can then be calculated from the cross section area of the adsorbate molecule. In this work, the monolayer capacity of the solids tested was calculated using the typical Brunauer-Emmett-Teller (BET) equation (3).

$$\frac{P}{v(P_0 - P)} = \frac{1}{Cv_m} + \frac{(C-1)P}{Cv_m P_0} \qquad (3)$$

Where P is adsorption equilibrium pressure, P_0 is saturation vapor pressure of the adsorbate at the experimental temperature, v is the volume of N_2 adsorbed at pressure P, v_m is the volume of adsorbate required for monolayer coverage and C is the constant that is related to the heat of adsorption and liquefaction.

The textural properties of the catalysts used in this work were measured by nitrogen adsorption-desorption at liquid nitrogen temperature (-196°C) using a Micrometrics ASAP 2010 instrument. Before analysis, the samples were evacuated at 130 °C for 4 h under vacuum and then adsorption-desorption was conducted by passing nitrogen. As said before BET equation was used to determine the specific surface areas of the catalysts. Desorption isotherms and BJH model

were used to calculate pore volume (Vp) and pore diameter at the relative pressure (P/P^0) of 0.98 [13].

2.2.4. Thermal Gravimetric Analysis (TGA)

TGA is a type of thermal analysis in which the physical properties of the studied material are measured as a function of temperature [16]. Information about any weight changes associated with thermally induced transformations can be obtained from TGA. The loss of weight as a function of temperature is the characteristic features of a material since there are physical and chemical changes over a wide temperature range.

Here, TGA analyses were performed using a thermobalance (SETARAM) to study the thermal weight loss behavior of the non-calcined and used catalysts. The catalysts were heated from room temperature to 800 °C with a heating rate of 5 °C min^{-1} under air flow (50 mL min^{-1} STP).

2.2.5. High Resolution Transmission Electron Microscopy (HRTEM)

In nanoscience and nanotechnology, observation is one of the key steps for studying an arrangement of atoms or structures and getting information about their size and shape [17]. In the present work selected catalysts were analyzed using a FEI Tecnai G2 20 S-Twin transmission electron microscope. The powder samples were dispersed in a solvent having low boiling point (isopropanol or ethanol) and dropped on the carbon and polymeric film coated copper grids for analysis. The coated samples were allowed to dry overnight to evaporate the solvent before analysis.

2.2.6. Temperature- programmed reduction (TPR)

Temperature-Programmed Reduction experiments were performed to understand the redox properties of the catalysts [18]. In this thesis, the reducibility of the catalysts was evaluated by TPR using hydrogen as a reducing agent at atmospheric pressure. A typical experiment was performed with 100 mg of catalyst loaded into a quartz reactor and pre-treated in a helium flow (30 mL min^{-1}) at 200 °C for 2 h. Afterwards, the catalyst was heated from 100 °C to 700 °C (heating rate of 5 °C.min^{-1}) under the reductive gas (5 mol.% H_2 in He; 30 mL.min^{-1} flow-rate). The effluent gas was analysed by a thermal conductivity detector (TCD).

2.2.7. X-Ray Fluorescence (XRF)

X-Ray Fluorescence is one of the most efficient analytical techniques to perform elemental analysis in all kinds of samples [19]. XRF combines highest accuracy and precision with simple and fast preparation method for the analysis of elements. In this work a M4 Tornado from Bruker was employed. This tool was used for element characterization using small-spot Micro X-ray Fluorescence (Micro-XRF) analysis. For each sample 30 points were measured in order to cover the whole sample surface, with spot sizes of 200 µm for each point. Then the standard deviations of the measures were calculated.

2.2.8. Energy Dispersive X-ray Analysis (EDAX)

EDAX is widely used to analyze the chemical components in a material during scanning electron microscope imaging [20]. This method detects the X-rays emitted as the result of the electron beam interaction with the sample, whereby the elemental dispersion can be obtained. In the present study, the atomic composition of the catalyst was further evaluated by EDAX analysis performed by on a Hitachi S3600N electron microscope equipped with a Thermo Ultra dry EDX detector using an acceleration voltage of 30 kV. During analysis of each catalyst 5 points were taken into account to determine the bulk amount of metal in the catalyst. Then the standard deviations of the measures were calculated.

2.3 Reactor setup and analytical techniques

In this section is described the setup of the vapor phase down-flow reactor employed to evaluate the performances of the catalysts. Furthermore, the analytical techniques used for the analysis of the reactor outlet stream are described in details.

2.3.1. Reactor setup employed for the catalytic activity

The performances of the prepared catalysts in the direct conversion of ethanol to ethylene oxide reaction were determined in a vapor phase down-flow fixed-bed reactor at atmospheric pressure. The detail structure of the reactor setup is shown in Figure 2-1. Mainly, the reactor setup is divided into three parts as follows:

- Feed-making zone
- Reaction zone

- Analysis zone

Feed-making zone: For testing the catalytic performance, ethanol, oxygen and helium are used as reactant flows. Helium is employed as an inert diluent and oxygen as oxidant agent. These gases were supplied from individual gas cylinders and the flow rates regulated separately by mass flow controllers (MFC-BROOKS). The addition of ethanol in to the feed was performed using a saturator at a calculated temperature depending on the desired composition of ethanol in the feed. The temperature and partial pressure of ethanol was calculated according to the following Antoine equation (4) [21].

$$\log_{10} p = A - \frac{B}{C+T} \qquad (4)$$

Where,

p = Ethanol vapor pressure (bar)

T = Temperature (K)

A (5.24677), B (1598.663) and C (-46.424) = Component specific constants [21]

Reaction zone: The reaction zone contains a heating box with two compartments (HB1 and HB2) (Figure 2-1). In the first are placed three valves (V-3, V-4 and V-5) and in the second is placed the reactor for the catalytic reaction. V-4 is a four-ways valve used as a bypass of the reactor, in order to stabilize the gas feed before starting the reaction. V-3 and V-5 are six-ways valves for injection of a sample from a calibrated loop to the on-line gas chromatograph. V-3 serves to analyze the reactant feed, whereas V-5 is for the effluent (after the reactor). The reactor is placed in the second part of the heating box (HB2). The reactor is made up of a stainless steel tube, with an inner diameter of 7 mm and a length of 140 mm. A thermocouple is inserted exactly at the position of catalyst bed for monitoring the internal reaction temperature. The detail of reactor is shown in Figure 2-2. The temperatures in HB1 (150 °C) and HB2 (200 – 275 °C) compartments were controlled using PID temperature controllers.

Analysis zone: The analysis of the reaction mixture (effluent) was carried out by injecting a sample of 1 mL (calibrated sampling loop) to the online GC. The GC analysis was performed on an ALPHA MOS PR 2100 device using a set of two columns arranged in series and a Thermal

Conductivity Detector (TCD). The detail schematic presentation of the analytical part is shown in the analysis zone on Figure 2-1. The first column was a RT-U BOND-RESTEK (Length - 30 m and Inner diameter - 0.53 mm) indicated PQ on the scheme specially installed for the separation of light products like ethanol, acetaldehyde, ethylene oxide, ethyl acetate, diethyl ether and CO_2. The permanent gases like CO, O_2 and N_2 were separated on the second column a RT-Msieve 5A-RESTEK (Length - 30 m and Diameter - 0.53 mm) indicated MS on the scheme.

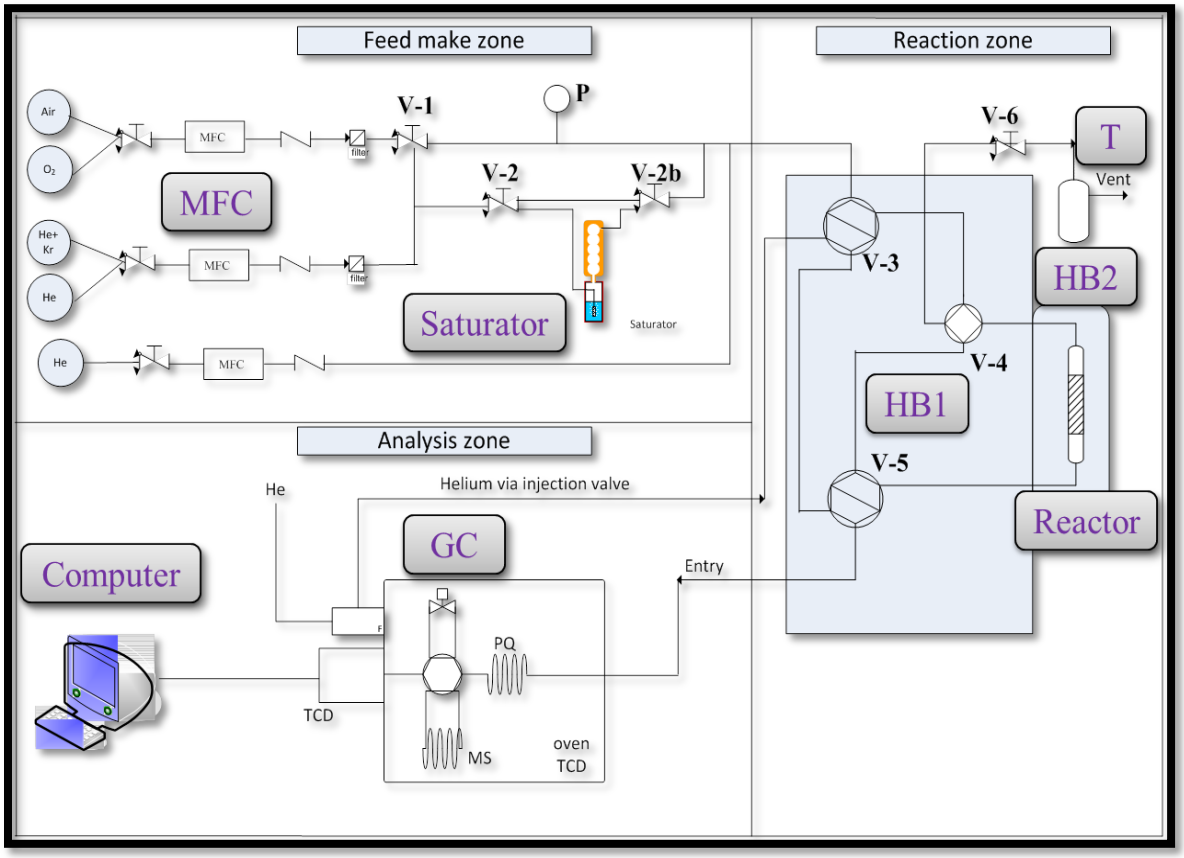

Figure 2-1: Schematic diagram of the vapor phase down-flow reactor setup

2.3.2. Catalytic activity measurements (typical conditions)

The performance of the prepared catalysts was determined using 0.1 g of powder catalyst at atmospheric pressure (101325 Pa). For the reactor loading, first compacted quartz wool was introduced at the bottom of the reactor to avoid fine particles entrainment by the gas flow. Then SiC (0.5 mm) was added to fill the reactor up to 6 cm from the bottom. Then the catalyst was introduced and the rest of the reactor was filled with SiC to reduce the void space. The detailed filling of the reactor is shown in Figure 2-2. In some cases, the catalysts were reduced using 5%

H_2/He at 250 °C for 2 h prior start to reaction. The reactants were fed using a mass flow controller and a saturator respectively. The ethanol concentration was 15 mol.% and the oxygen to ethanol ratio (O_2/ethanol) was adjusted to 2. Helium was used as an inert gas. For the latter conditions the Gas Hourly Space Velocity (GHSV) was 14040 h^{-1}. With the use of the by-pass valve V-4, the reactant flow was let stabilized without being in contact with the catalyst. The composition of the inlet, as well as the outlet flow, was analyzed by on-line gas chromatography as described above.

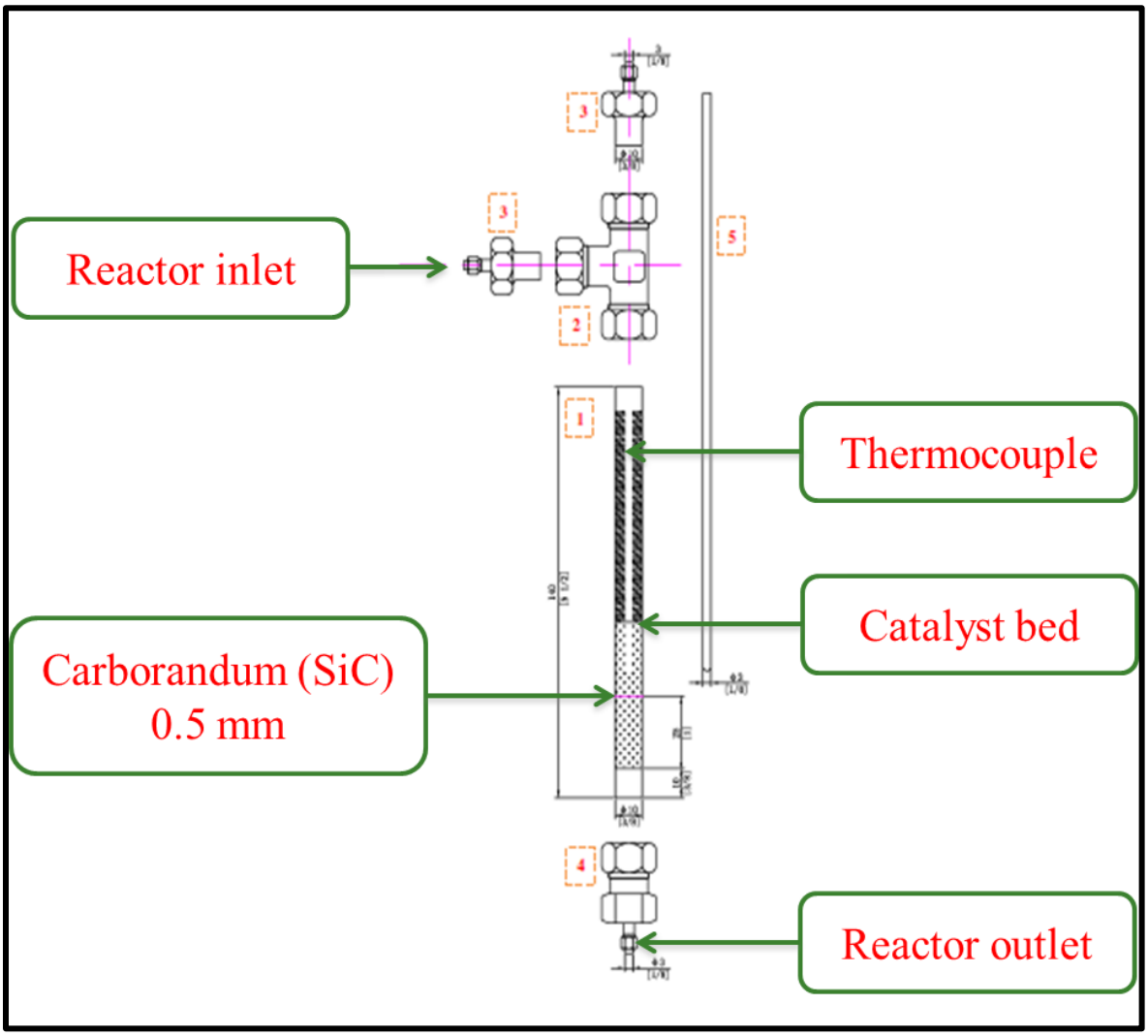

Figure 2-2: Schematic diagram of the reactor

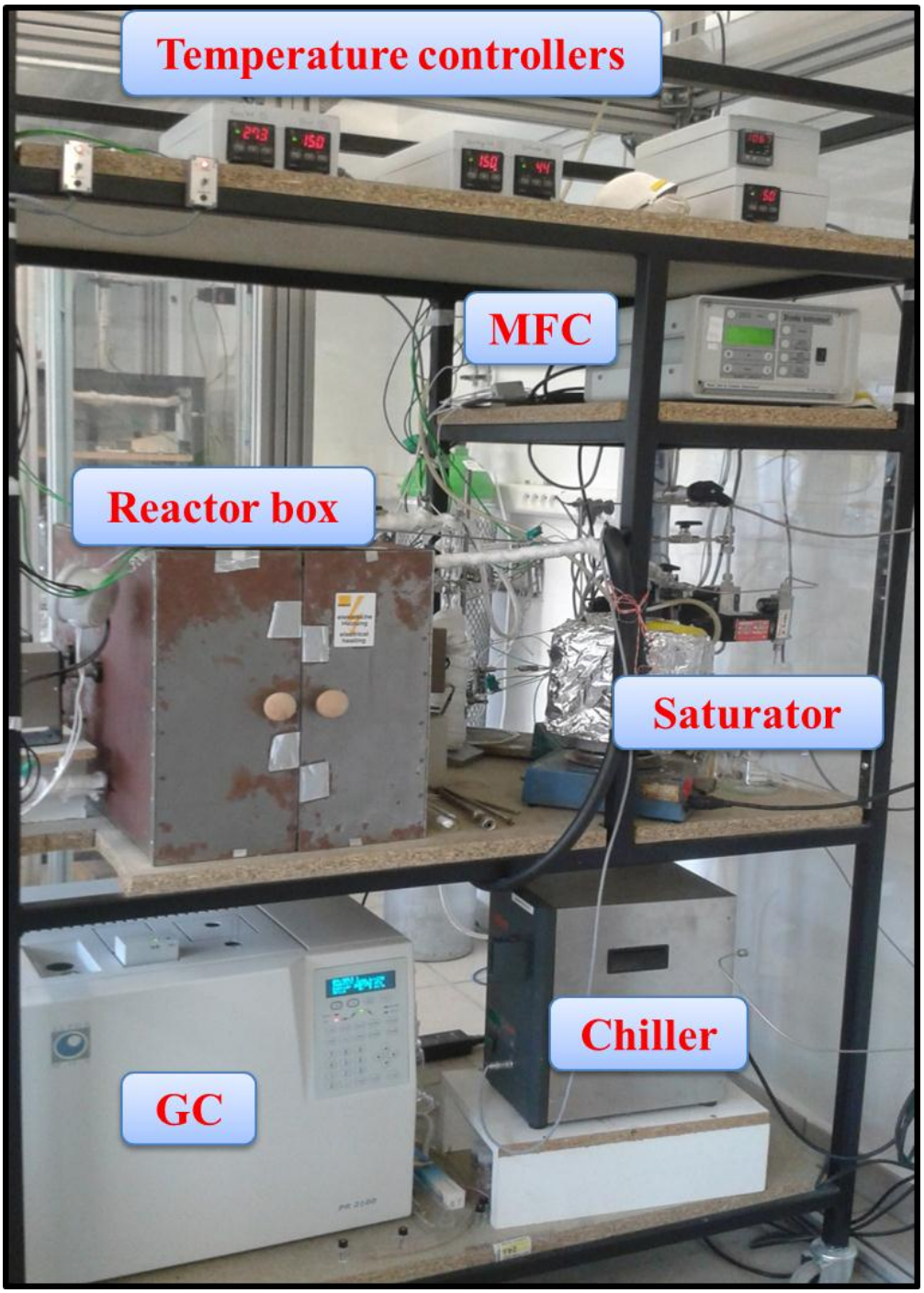

Figure 2-3: Reactor setup used for catalytic performance measurements

2.3.3. Analysis techniques

For the complete analysis of all the components of the effluent of the reactor two analytical methods were used. In the first one (Method 1), the entire sample passes only through the RT-U BOND column to analyze ethanol, ethylene oxide, acetaldehyde and ethyl acetate. The

second method (method 2) is more complicated. First (0 – 4 min), the sample passed through the RT-U-BOND column followed by the Molecular sieves (MS) column.

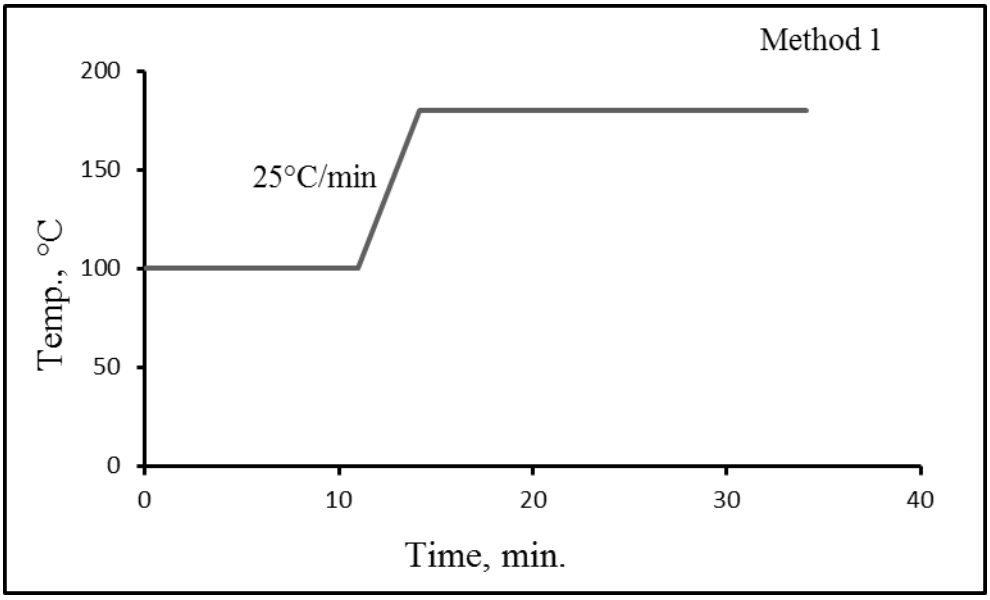

Figure 2-4: Gas chromatography Method 1 program of temperature

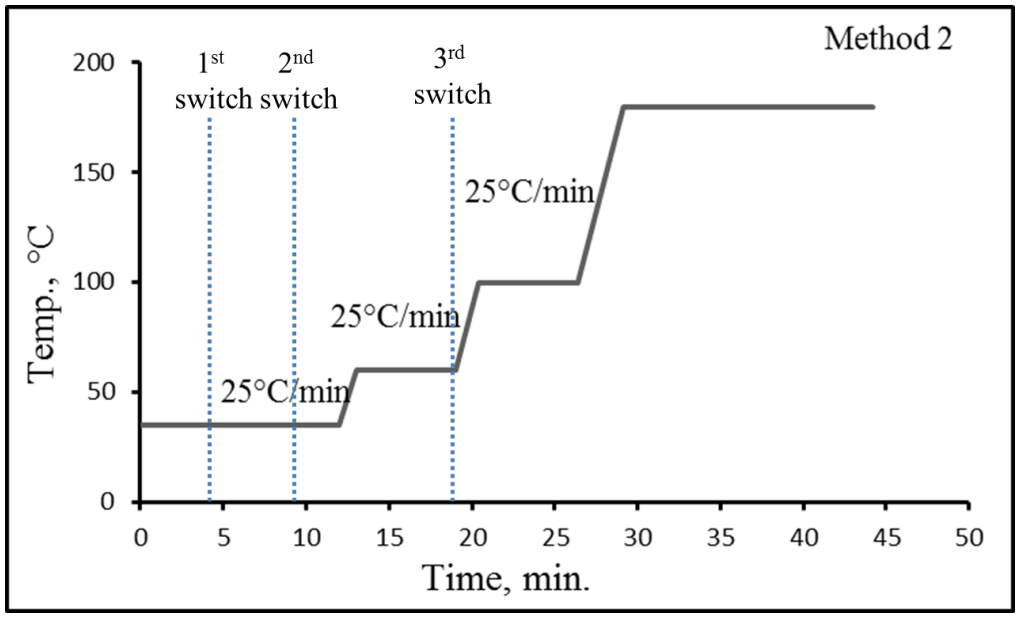

Figure 2-5: Gas chromatography Method 2 temperature profile

At this time the light gases (N_2, O_2 and CO) went into the MS column and got "stocked". After first inversion (4.00 min) only PQ column was connected to the TCD detector via a pressure drop. At this time CO_2 was detected. After the second inversion (9.00 min), the MS was

also connected to the detector and during this time all light gases were detected. Finally, after the third inversion (18.00 min) only the PQ column was connected to the detector and the ethanol and other heavier products were detected. The schematic temperature profiles of the methods used are shown in Figure 2-4 and Figure 2-5.

Typical chromatograms obtained using Methods 1 and 2 are shown in Figure 2-6 and Figure 2-7 respectively.

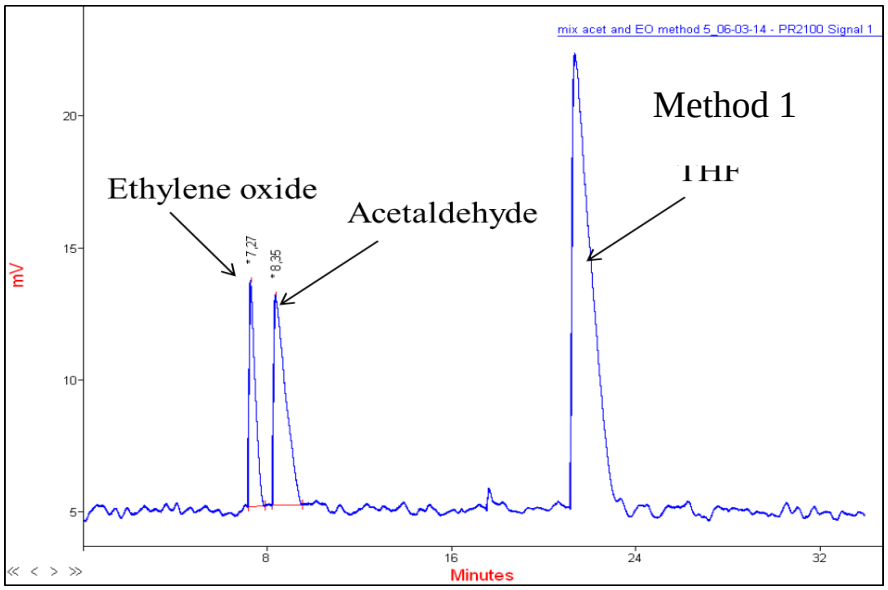

Figure 2-6: Typical GC chromatogram obtained using Method 1

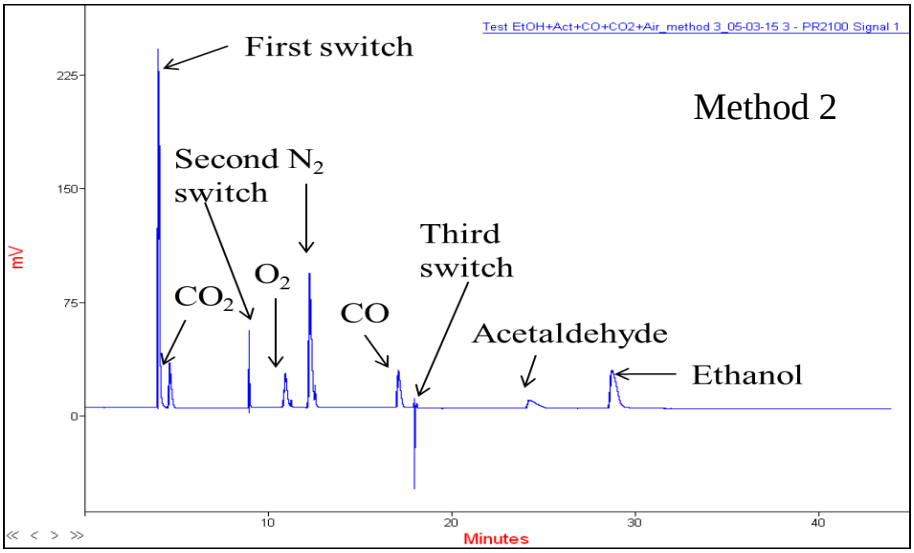

Figure 2-7: Typical GC chromatogram obtained using Method 2

2.3.4. Quantification

The GC was calibrated with standard products for quantification. Performing calibration, three different concentrations for each reactant or product were prepared and analyzed. The ethylene oxide in THF solution used for the calibration. Calibrations for light gases like CO, CO_2 were performed using calibrated mixtures. Finally, the linear equation obtained from the calibration curves was used to quantify all the products and to calculate ethanol conversion, product selectivity and carbon balance.

❖ The ethanol conversion (X) and ethylene oxide selectivity (S) were calculated using the following equations. (*n*: *moles; in : initial*)

$$X = \frac{n(\text{Ethanol})in - n(\text{Ethanol})final}{n(\text{Ethanol})in} \times 100 \quad (5)$$

$$S_{EO} = \frac{n(\text{EO})}{n(\text{Ethanol})in - n(\text{Ethanol})final} \times 100 \quad (6)$$

❖ The EO yield was calculated as follows:

$$Y = X.S /100 \quad (7)$$

❖ Carbon balance was calculated was according to the following equation

$$CB = \frac{\Sigma_i(n_i \times N_{ci}) + 2 \times n_{Ef}}{2 \times n_{\text{Ei}}} \times 100 \quad (8)$$

CB = Carbon balance in %,

n_i = Number of moles of outlet product 'i'

Nci = Number of carbon atoms in the outlet product 'i'

n_{Ei} = Initial number of moles of ethanol

n_{Ef} = Final number of moles of moles of unreacted ethanol

2.4 References

1. T. A. Ring, Fundamentals of Ceramic Powder Processing and Synthesis, 1996.
2. A. E. Nielsen, Kinetics of Precipitation, 1964, Pergamon.
3. H. Furedi-Milhofer, Pure and Applied Chemistry, 1981, 53, 2041.
4. T. A. Ring, J. A. Dirksen, Chemical Engineering Science, 1991, 46, 2389.
5. R. B. Mane, C. V. Rode, Green Chemistry, 2012, 14, 2780.
6. G. W. Scherer, C.J. Brinker, Sol-Gel Science, 1990, ISBN 0-12-134970-5.
7. J. K. West, L.L. Hench, Chemical Reviews, 1990, 90, 33.
8. S. R. Stock, B. D. Cullity, Elements of X-Ray Diffraction, 1978, Addison-Wesley Reading, MA.
9. L. E. Alexander, H.P. Klug, X-Ray Diffraction Procedures, 1954, Wiley New York.
10. J. Wolstenholme, J.F. Watts, An Introduction to Surface Analysis by XPS and AES, 2003, John Wolstenholme.
11. A.S. Mujumdar, G.A. Somorjai, Introduction to Surface Chemistry and Catalysis, 1994, Wiley New York.
12. P. H. Emmett, S. Brunauer, E. Teller, Journal of American Chemical Society, 1938, 60, 309.
13. B. H. Hameed, K. Y. Foo, Chemical Engineering Journal 2010, 156, 2-10.
14. G. Onyestyak, J. Valyon, L. V. C. Rees, Langmuir, 2000, 16, 1331.
15. P. Yuan, D. Liu, H. M. Liu, J. G. Cai, Z. H. Qin, D. Y. Tan, Q. Zhou, H. P. He, J. X. Zhu, Applied Clay Science 2011, 52, 358.
16. L. L. Merrit, H. H. Willard, J. A. Dean, F. A. Settle, Instrumental Methods of Analysis, CBS Publishers & Distributers, 1986.
17. C. B. Carter D. B. Williams, The Transmission Electron Microscopy: A Text Book for Materials Science,, 2009, Springer 2nd edition.
18. G. V. Sagar K. V. R. Chary, C. S. Srikanth, V. V. Rao, Journal of physical Chemistry, B, 2007, 111, 543-550.

19. H. Schreiber, R. Glocker, Annalen der Physik, 1928, 83, 1089.
20. G. D. Danilatos, Journal of Microscopy, 1986, 142, 317-325.
21. W. Wagner, Cryogenics, 1973, 13, 470.

Chapter 3

Preliminary Tests - Performance and Characterization

3.1 Preliminary results

3.1.1 Proof of concept over Au-, Ag- and Cu-based catalysts

First of all, the synthesis and tests of previously reported in the literature [1, 2] for the direct conversion of ethanol to ethylene oxide were carried out. In further study, these catalysts were characterized using different characterization techniques for the determination of their physicochemical properties. The results of this preliminary work are presented in this section.

A. Blank tests

Blank tests were performed in order to determine whether there was a thermal activation of ethanol at the reaction conditions and the effect of the bare support. The tests were carried out using the typical configuration of the reactor described in section 2.3.2, with SiC (VWR, particle diameter 0.5 mm) as filling material and bare γ-Al_2O_3-Sasol (60-150 µm) support was used instead of catalyst. This experiment was carried out in the same experimental conditions as the once reported in the literature [1]. The reaction temperature was 250 °C and the reactant feed composition was 15 mol.% ethanol with an O_2/ethanol ratio of 0.5.

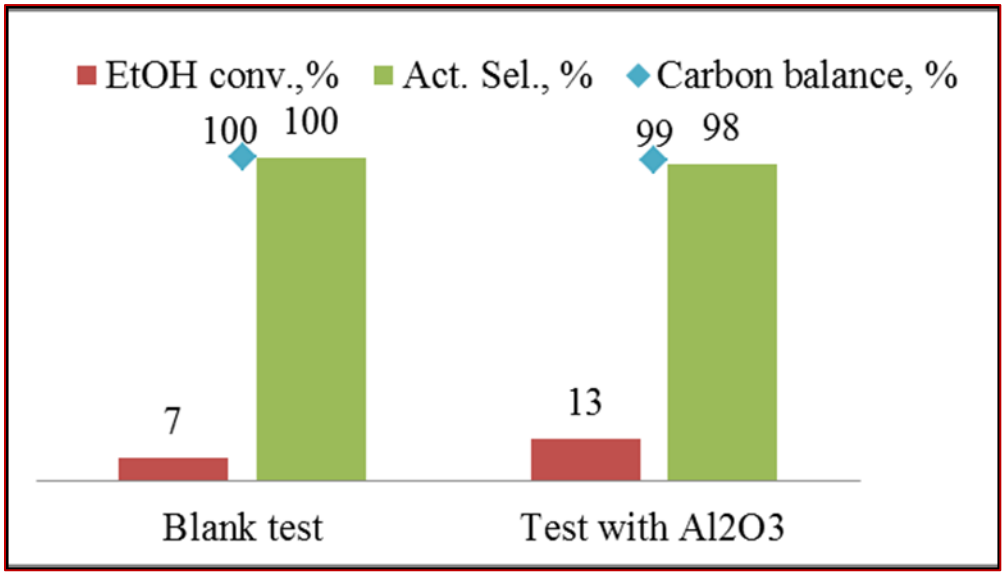

Figure 3-1: Blank tests results

Reaction conditions: *Ethanol: 15 mol.%, Carrier gas: Helium, Al_2O_3. wt.: 0.3 g, EtOH:O_2=2:1 (molar); Total gas flow at RT: 20 mL/min, Pressure: 1 atm.*

The ethanol conversion (EtOH conv. %) and selectivity to acetaldehyde (Act. Sel.,%) as a product are shown in Figure 3-1. A marginal ethanol conversion of 7 % and 100% selectivity to

acetaldehyde were observed using only SiC in the reactor. Hence, one can conclude that no significant thermal activation takes place under the used conditions. For the test using the bare support, under the same reaction conditions, the conversion of ethanol was increased compared to the blank test (13% vs. 7%). However, it is still relatively low. A very high selectivity to acetaldehyde was also observed in that case (98%). No EO was detected in both experiments.

From these blank tests it was therefore concluded that the reactor, the SiC used for dilution and the bare support (γ-Al_2O_3) are not significantly active in the formation of ethylene oxide in the operating conditions used in this work.

B. Catalytic results

In order to confirm the feasiability of the direct conversion of ethanol into ethylene oxide over gold, silver and copper-based catalysts as reported by Lippit's *et al.* [1, 2] we have tried, in a first approach, to reproduce the synthesis of the catalysts and to test them on our experimental set-up. Then, further developments on the catalysts and study of the reaction parameters were carried out in order to improve the catalytic performance.

In the first part of our study gold, silver and copper-based catalysts were prepared with similar metal loading (namely 0.53 at.%) using a deposition precipitation method, γ-Al_2O_3 as support and Li_2O as promoter. These catalysts were used for the direct conversion of ethanol to ethylene oxide and the catalytic performances were determined under the same reaction conditions as the ones reported in the literature [1] (ratio of $EtOH:O_2$ = 2:1 and react. Temp.= 200 and 250 °C). Prior to catalytic performance measurement the catalysts were reduced at 400°C in 5% H_2/He for 2 hours. The results are presented in Figure 3-2 (A and B).

On one hand, one can see from these results that low temperature (200 °C) was not favorable for ethylene oxide formation over silver and copper catalysts. Moreover, over these catalysts the ethanol conversion was low at 200 °C (13 and 11% respectively). On the other hand, the gold catalyst showed a good ethanol conversion of 50% with 18% selectivity in ethylene oxide (EO sel. %). All catalysts showed activity towards ethylene oxide formation at 250 °C.

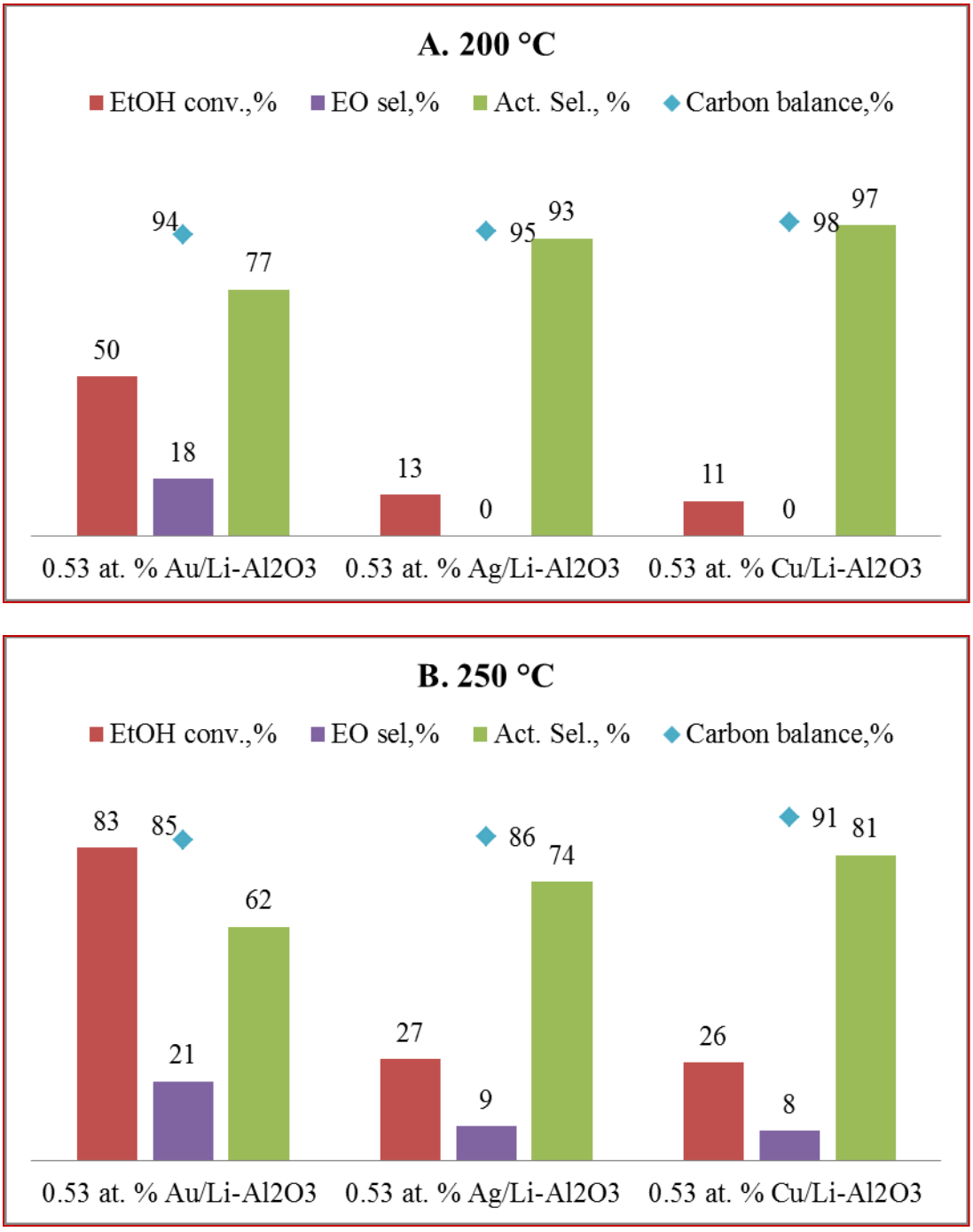

Figure 3-2: Catalytic performance A- 200°C and B- 250°C

Reaction conditions: *Ethanol: 15 mol.%, Carrier gas: Helium, Reaction temperature: 200 °C (A) and 250 °C (B), Cat. wt.: 0.3 g, EtOH:O_2=2:1 (molar) ; Total gas flow at RT: 20 mL/min, Pressure: 1 atm., Time on stream: 15 h*

The gold-based catalyst showed highest ethanol conversion (83%) with a rather good selectivity to ethylene oxide of 21%. Silver and copper-based catalysts showed lower

performance with ethanol conversion of 27 % and 26%, and selectivity to ethylene oxide of 9% and 8%, respectively. In all cases, acetaldehyde was the major byproduct obtained in the ethanol oxidation reaction. The carbon balance was always superior to 85%.

The results obtained on the gold, silver and copper-based catalysts were compared with Lippits *et al.*'s result (Table 3-1).

Table 3-1: Comparison of catalytic results

Catalyst names	**Au/Li-Al_2O_3**	**Ag/Li-Al_2O_3**	**Cu/Li-Al_2O_3**
Reported EO yield, %	76	56	63
Present study EO yield, %	9	0	0

Reaction conditions: *Ethanol: 15 mol.%, Carrier gas: Helium, Reaction temperature: 200 °C, Cat. wt.: 0.3 g, EtOH:O_2=2:1 (molar) ; Total gas flow at RT: 20 mL/min, Pressure: 1 atm., Time on stream: 15 h*

The literature reported that gold-based catalyst showed the highest yield to ethylene oxide 76%. It was the same with our work, but at a much lower level (9%). Moreover, the silver and copper-based catalysts in the present study were completely inactive for ethylene oxide synthesis at 200 °C whereas in the literature, it was reported that similar catalysts were active and showed 63 and 56% yield in EO respectively. We have not studied the higher temperature (300 °C) in the present study because of the decomposition of EO reported by Lippits et al. We can conclude that we were not able to reproduce the published results, probably because of differences in the catalyst physicochemical properties. In the following, the catalysts are characterized in details in order to try to understand the differences between of our catalysts and those reported in the literature.

C. Characterization

Detailed characterization studies of the synthesized catalysts were carried out using different characterization techniques in order to establish a correlation between their physico-chemical properties and their performance.

➢ X-ray diffraction results

The X-ray diffraction patterns of the gold-, silver- and copper-based catalysts are shown in Figure 3-3. All catalysts exhibited the characteristic diffraction peaks of γ-alumina. No characteristic peaks for specific phases containing gold, silver or copper were observed. However, according to Lippits's *et al.* [1, 2] the size of the gold, silver and copper particles is below the XRD detection limit (i.e. ≤ 3 nm). The absence of characteristic peaks for the metal species could also be linked to an uniform distribution on the support.

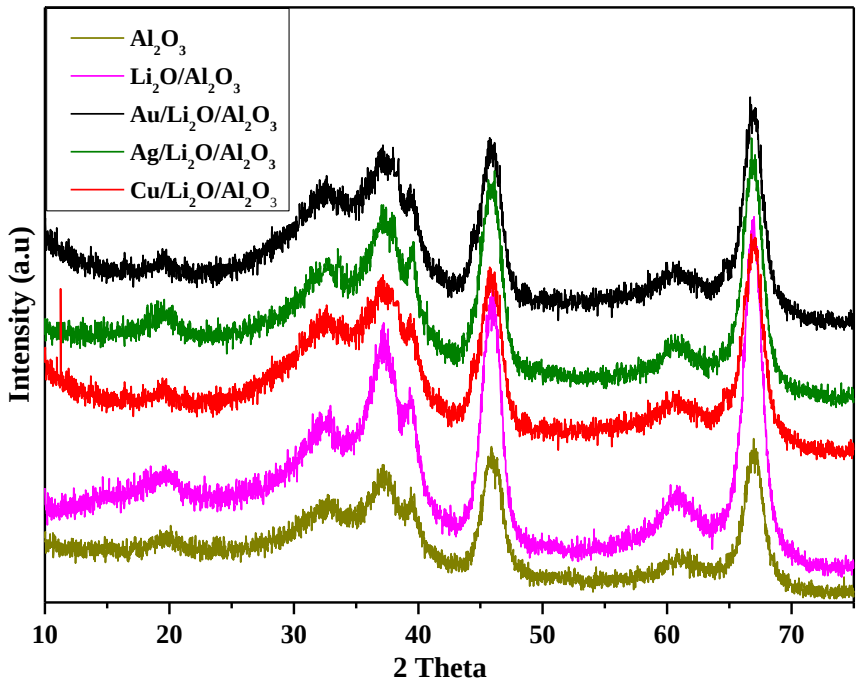

Figure 3-3: XRD patterns of Au, Ag and Cu-based catalysts and bare supports

➢ Textural properties

Synthesized gold-, silver- and copper-based catalysts were characterized by nitrogen physisorption for the determination of their textural properties. Their surface areas, pore volumes and pores mean diameters are reported in Table 3-2.

The surface area of the alumina support slightly decreased with the introduction of 0.53 at.% of metal (Au, Ag or Cu). This may be attributed to pore blockage after the impregnation by the metal oxide. It is noteworthy that the pore volume and specific surface did not decrease in the same extend for the different metals, which can be attributed to the different molar mass of gold, silver and copper. In fact, since the catalysts were loaded with constant atomic metal content, the

decrease for the metal with the highest molar mass (gold) is less pronounced than in the metal with the lowest molar mass (copper).

Table 3-2: Textural properties of the Au-, Ag- and Cu-based catalysts

Catalyst Name	S_{BET} (m^2g^{-1})	V_P (cm^3g^{-1})	Metal content (EDS) (at.%)	Metal content (XPS) (at.%)
γ-Al_2O_3	201	0.479	-	-
0.53 at.% Au/Li_2O/Al_2O_3	165	0.409	0.65	0.40
0.53 at.% Ag/ Li_2O/Al_2O_3	175	0.480	0.52	0.21
0.53 at.% Cu/Li_2O/Al_2O_3	180	0.474	1.13	0.71

- Elemental composition

The atomic compositions of the bulk and of the surface of the catalysts were determined by EDAX and XPS respectively. The results are gathered in Table 3-2. The quantity of gold determined in the bulk of the catalyst was slightly higher than the theoretical value (0.65% vs. 0.53%). In case of the silver catalyst the quantity of metal is identical to the expected one. In the case of copper, the quantity in the catalyst is the double than the expected theoretical value (1.13% vs. 0.53%). Concerning the surface composition determined by XPS, the surface atomic ratio of gold was found lower than the theoretical ratio (0.40% vs. 0.53%), this was also the case for the silver catalyst but to a higher extent (0.21% vs. 0.53%). For the copper, an increase of the concentration was observed compared to the bulk value (0.71% vs. 0.53%).

The XPS analysis also permits to determine the oxidation states of the metal species formed on the surface of the catalyst. The XPS spectra for Au 4f, Ag 3d and Cu 2p regions are presented in Figure 3-4

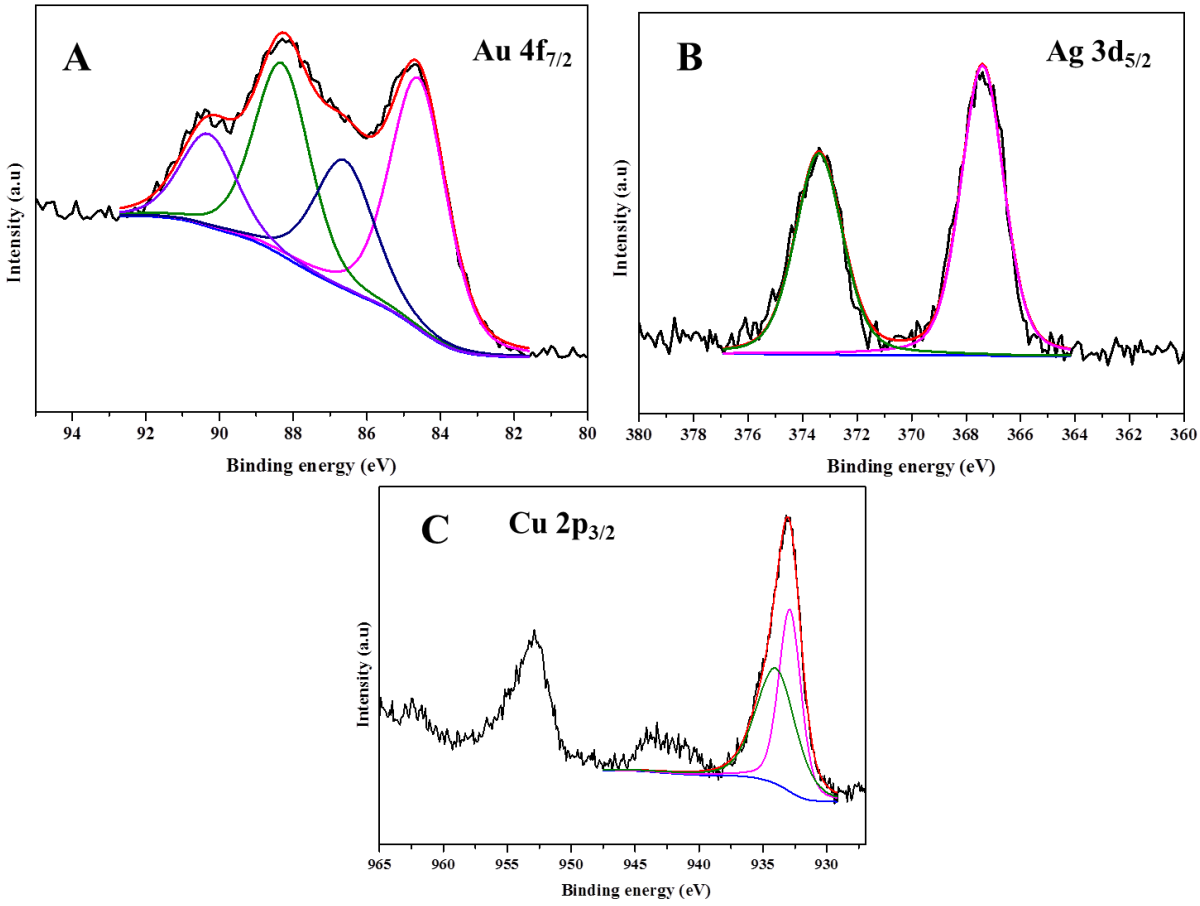

Figure 3-4: XPS analyses of A – gold-, B – silver- and C- copper-based catalysts

The deconvoluted peak in the Au $4f_{7/2}$ region of the spectrum for gold-based catalyst contains peaks at 84.6, 86.6, 88.3 and 90.3 eV. The peaks at 86.6 and 90.3 eV indicate the presence of Au^{3+}. The peaks at 84.6 and 88.3 have been assigned to metallic Au [3, 4]. One can hence conclude that drying in air at 110 °C resulted in the formation of two kinds of gold species (Au^{3+} 50% and Au° 50%).

XPS analysis was performed for silver catalyst in order to explore the Ag 3d region. The reported binding energies (BE) for silver are 368, 367.7 and 367.3 eV for Ag°, Ag_2O and AgO species, respectively [5]. Lambert *et al.* observed BE of 367 eV for metallic silver supported on α-alumina [6]. In our case, peaks at 367.4 eV and 374.2 eV were observed which indicates the presence of Ag^{+} species [7, 8]. The width of the latter did not allow distinguishing clearly

between oxide and metallic silver however. Nevertheless, the presence of silver oxide was clearly observed from TPR (*vide infra*).

The XPS spectrum of the $Cu/Li_2O/Al_2O_3$ catalyst is presented in Figure 3-4 C. The Cu^{2+} species are characterized by a Cu 2p binding energy of 934.0 eV with shake up or satellite peaks located at 938 to 946 eV. The binding energy at 932.9 was assigned to Cu^{+} species [9, 10]. From the deconvolution, the surface concentration of Cu^{2+} and Cu^{+} species was estimated to 48.3% and 51.6%, respectively.

- H_2-TPR analysis

The reduction behavior of the catalysts was studied by H_2 Temperature Programmed Reduction method. The H_2-TPR profiles of γ-alumina-supported Au, Ag, and Cu catalysts are shown in Figure 3-5. As expected, the reduction behavior of the catalyst samples was dependent on the metal used for the catalyst. The amount of hydrogen consumption for the Au, Ag and Cu catalyst was 0.23, 0.1 and 0.198 $mmol.g^{-1}$ respectively. The reduction temperature profile also varied from one metal to another. The TPR profile of gold catalyst manifests two intensive peaks. The main peak was observed at 190 °C with a shoulder at 303 °C. These peaks were ascribed to the reduction of Au^{3+} nanoparticles (190 °C) and of the big particle of metallic gold (303 °C) [11, 12].

In the case of the silver catalyst, two broad reduction peaks were observed at low temperature (142 °C and 183 °C). The first peak at 142 °C is ascribed to the reduction of highly dispersed silver oxide species (below XRD detection limit) to Ag° while the second reduction peak at 183 °C corresponds to the reduction of isolated Ag^{+} species [13-16]. From Table 3-3 one can see that, in case of silver catalyst the hydrogen consumption is less than the expected value, it may be due to the presence of Ag_2O species in the catalyst and these results are in the agreement with the XPS study.

The TPR profile of the copper catalyst shows two reduction peaks: a sharp peak at low temperature (239°C) and a broad shoulder peak at a higher temperature (295 °C). The peaks are explained by the successive reduction of copper species at low temperature followed by the reduction of bulk CuO at high temperature. Thus, the TPR peak in the low temperature region suggests the presence of highly dispersed CuO species on the surface with a weak metal-support interaction. On the other hand the TPR peak observed in the high temperature region is attributed to bulk CuO with strong metal support interaction [17-20].

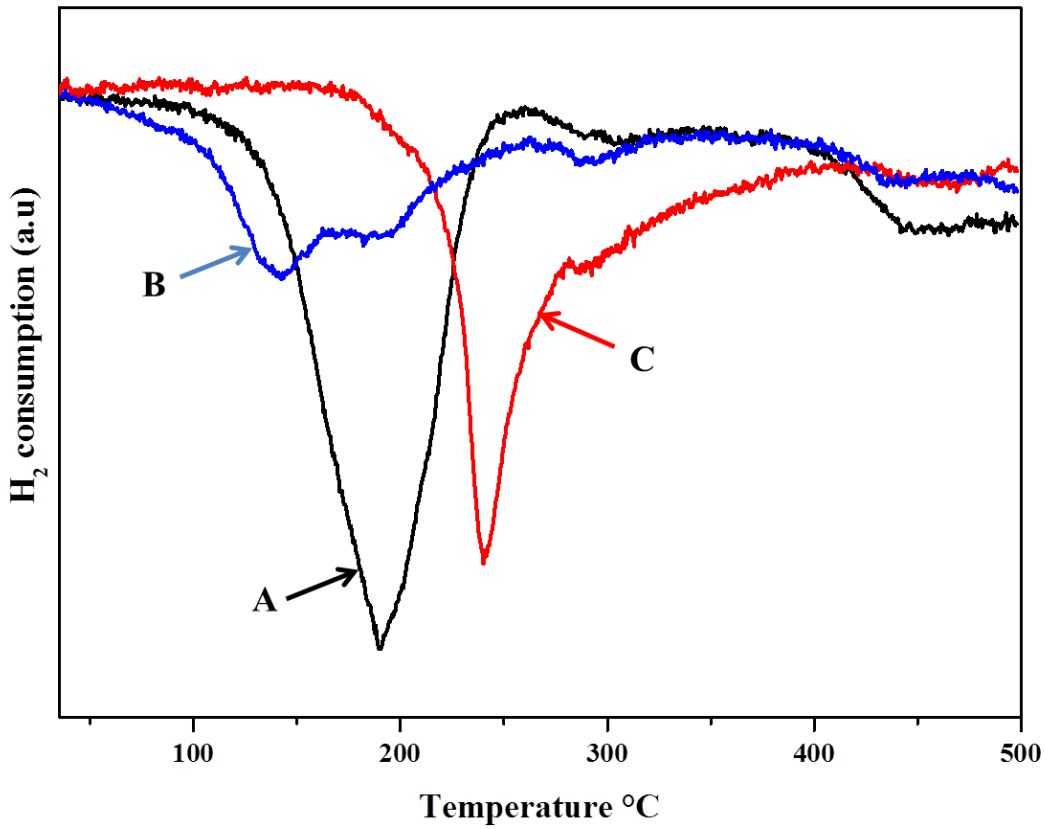

Figure 3-5: TPR profiles of A- gold-, B- silver- and C- copper-based catalysts

Table 3-3: Hydrogen consumption by TPR study

Catalyst Name	H_2 consumption ($mmol.g^{-1}$)	Temp. °C	Theoretical amount of H_2 required
0.53 at.% $Au/Li_2O/Al_2O_3$	0.236	186.8 °C	0.38
0.53 at.% $Ag/ Li_2O/Al_2O_3$	0.1	141.4 °C	0.232
0.53 at.% $Cu/Li_2O/Al_2O_3$	0.198	238.5 °C	0.234

D. Conclusion

As said above, the results reported by Lippits *et al.* were not reproduced successfully in our work, but several reasons can be proposed to explain this:

- The supports γ-Al_2O_3 used for the catalysts synthesis were not the same, but not a lot information is given in the literature concerning the properties.

- The experimental setup used for the tests were different and as EO is highly reactive, this might have a strong impact on the results,
- Instead of quartz, a stainless steel reactor was used in the present study.

However, as we have seen from the results in the previous section, gold-, silver- and copper-based catalysts are active for the selective oxidation of ethanol to ethylene oxide. Compared to gold and silver, copper is cheaper and it has been previously reported that the dispersion of copper nanoparticles is maintained during the reduction and reaction (temperature range 250-300 °C) [21]. During the last decades, copper-based catalysts have been extensively studied as eligible catalysts for a number of heterogeneous reactions like CO oxidation, water gas-shift reaction and hydrogenation reactions [22-25]. In the following of our work we decided to put the focus on γ-Al_2O_3-supported copper catalysts, studying the effect of the catalyst preparation method and of the copper loading on the support.

3.1.2 Effect of the catalyst preparation method on Cu/Al_2O_3 catalyst

In order to study the effect of the catalyst preparation method, Cu/Al_2O_3 catalysts were prepared by impregnation and co-precipitation varying the copper loading (5 and 50 wt.%). In the case of the impregnation method γ-alumina was used as a support while for the co-precipitation method we used aluminum nitrate as a source for the alumina. Of course the nature of the support is changed when using the co-precipitation method. Hence, the phases and textural properties were also characterized in details for the catalysts prepared by the different methods.

A. Catalytic results

The catalytic performance of the Cu/Al_2O_3 catalysts prepared using different preparation methods were measured at 250 °C and the results are gathered in Figure 3-6. From this figure, one can see that the 5%Cu/Al_2O_3 catalyst prepared by the impregnation method showed a good selectivity to ethylene oxide (15%) with an ethanol conversion of 39%. On the other hand, the impregnated catalyst with higher copper loading (50%Cu/Al_2O_3) was completely inactive for the ethylene oxide formation but promoted the formation of acetaldehyde (selectivity 78%) with ethanol conversion of 33%. Furthermore, when comparing the ethanol conversion of both catalysts, the catalyst containing 50 wt.% of copper showed surprisingly a significantly lower

conversion than the one with 5 wt.% Cu loading. It may be due to the fact that sintering or agglomeration of copper particles at higher copper loading occurs during the impregnation.

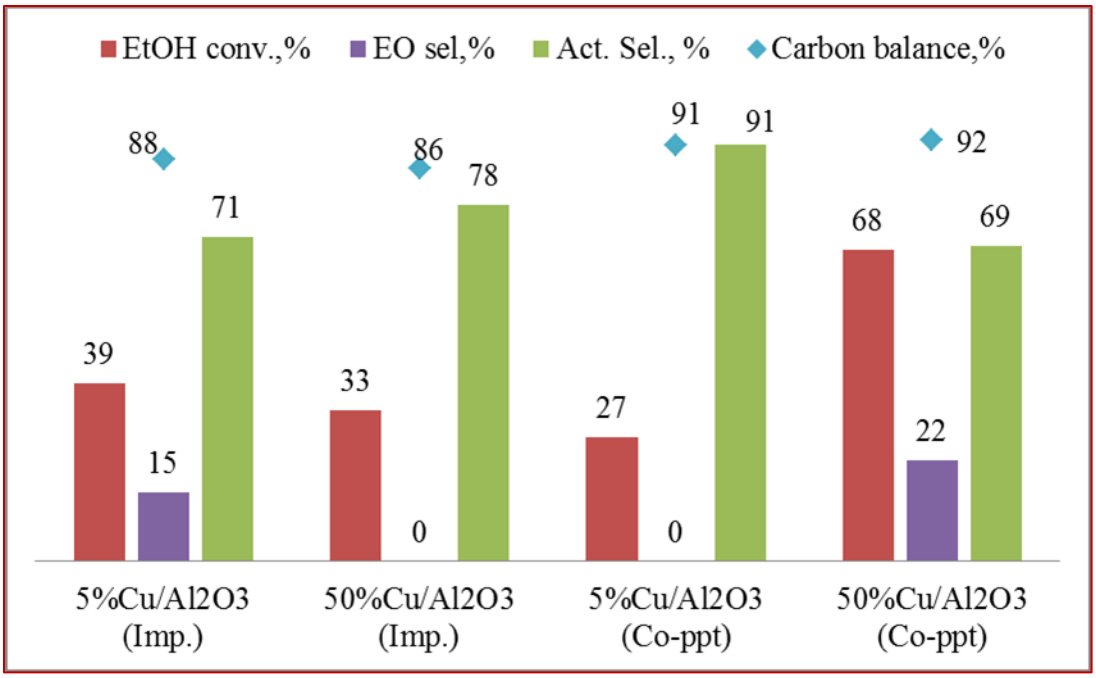

Figure 3-6: Catalytic performance of catalysts prepared by co-precipitation (Co-ppt) and impregnation (Imp.) method

Reaction conditions: *Ethanol: 15 mol.%, Carrier gas: Helium, Reaction temperature: 250 °C, Cat. wt.: 0.3 g, EtOH:O_2=2:1 (molar) ; Total gas flow at RT: 20 mL/min, Pressure: 1 atm., Time on stream: 15 h*

In the case of the co-precipitation method, the 5%Cu/Al_2O_3 catalyst yielded acetaldehyde as a major product with a selectivity of 91% and an ethanol conversion of 27% without showing any EO formation. On the other hand, the co-precipitation catalyst containing 50 wt.% of Cu exhibited the formation of ethylene oxide with 22% selectivity at an ethanol conversion of 68%.

When comparing the results for both preparation methods, one can see that in all cases, acetaldehyde was the major side product but its formation depended largely on the catalyst preparation method and copper loading. For the impregnation method, lower copper loading showed better results, whereas for the precipitation method higher copper loading showed increased ethylene oxide formation. The correlation between the catalytic performance and the catalysts physicochemical properties are discussed in the following section.

B. Characterization

The Cu/Al_2O_3 catalysts were characterized by nitrogen physisorption, XRF and XRD techniques.

➢ Textural properties

The textural characteristics of the catalysts were investigated by nitrogen physisorption measurements. The surface areas, pore volumes and mean pores radius of the Cu/Al_2O_3 catalysts are summarized in Table 3-4.

Table 3-4: Textural properties of the Cu/Al_2O_3 catalysts

Catalyst Name	S_{BET} (m^2g^{-1})	V_P (cm^3g^{-1})	Mean pore radius, nm	XRF, Cu content. (SDV*)
γ-Al_2O_3	201	0.47	3.2	-
5% Cu/Al_2O_3-Imp.	193	0.42	3.1	5.3 (0.44)
50% Cu/Al_2O_3-Imp.	137	0.32	3.6	41.8 (2.1)
5% Cu/Al_2O_3-Co-ppt.	271	0.82	4.8	7 (0.39)
50% Cu/Al_2O_3-Co-ppt.	73	0.34	8.5	57 (0.51)

* Standard Deviation Value

The surface area and cumulative pore volume of pure γ-alumina sample have been measured to 201 m^2g^{-1} and 0.47 cm^3g^{-1} respectively. When the alumina was impregnated with 5wt.% of copper a slight decrease in the surface area was noticed (193 m^2g^{-1}). On the other hand, surface area and pore volume significantly decreased with increasing copper loading which may be due to the filing of the pores with copper oxide particles as will be evidenced by the following XRD results. The Cu/Al_2O_3 catalysts prepared by co-precipitation method showed a very high surface area (271 m^2g^{-1}) with 5 wt.% loading of copper. The surface area and pore volume of the catalyst gradually decreased with higher loading (50 wt.%) of copper (73 m^2g^{-1}) following the similar trend observed for the impregnation method.

➢ Atomic composition

The bulk compositions of the catalysts were determined using XRF technique and the results are shown in Table 3-4. As previously mentioned in section 2.2.10, 30 points were measured per catalyst sample and then the standard deviations of the measures were calculated. For the 5% Cu impregnated catalysts, the amount of Cu measured was the one expected by the theoretical calculation. Nevertheless, at higher loading of 50%, an important deviation was observed and from the analysis of different points (standard deviation), one can also see that the copper species were non homogeneous and tended to agglomerate. In the case of the catalyst prepared by the co-precipitation method the experimentally determined amounts of Cu were always higher than the theoretical expected values. Nevertheless, the deviation values observed for both high and low loadings of copper was close to zero, suggesting thus an homogeneous mixture of the copper species.

➢ X-ray diffraction analysis

Figure 3-7 shows the powder X-ray diffraction patterns of the Cu/Al_2O_3 catalysts prepared by different preparation methods. In the case of the catalyst prepared by impregnation, only the characteristic peaks of γ-Al_2O_3 were observed at 37.4, 42.5, 45.7 and 67.2 (JCPDS File no. 10-0425) [26]. For the 5 wt.% Cu catalyst, no characteristic peaks for Cu was found, suggesting that the latter was well dispersed or that the particles are very small. In the case of the catalyst with 50 wt.% Cu loading intense characteristic peaks at 32.3°, 35.64°, 38.85°,48.5°, 58.0°, 61.3°, 65.9° and 68.0° were observed and ascribed to the presence of CuO phase in agreement with the reference (JCPDS File no. 65-2309) [27-29]. The formation of this bulk CuO at higher loading can be attributed to the agglomeration of copper species. Increase in the copper loading results in an increase of the XRD peak intensity suggesting the formation of crystalline CuO. On the other hand, no peak for other phases of copper like Cu_2O or $CuAl_2O_4$ were observed even at higher copper loading.

The catalysts prepared by the co-precipitation method showed amorphous phase of alumina in low as well as in high loadings of copper. The 5 wt.% Cu loading catalyst was found completely amorphous. No characteristic peaks for copper or copper oxides neither than for alumina were observed. Thus, one can conclude on the uniform dispersion of copper particles in amorphous Al_2O_3. In case of 50 wt.% on alumina, characteristic peaks for CuO species were observed. The intensity and full width at half maximum (FWHM) of the CuO peaks were found

to be weaker and broader compared to the catalyst prepared by the impregnation method. The intensity and crystalline size of the CuO peaks can be taken as an indirect measure of the copper dispersion [30, 31]. The trend observed in the degree of crystallinity and crystalline size indicated that the co-precipitation method gave better copper dispersion compared to the impregnation method. This can be explained on the basis of the anionic species formed during the precipitation method. In the precipitation process, carbonate species formed such as $Cu_2(OH)_2CO_3$, along with $Cu(OH)_2$ and CuO [32].

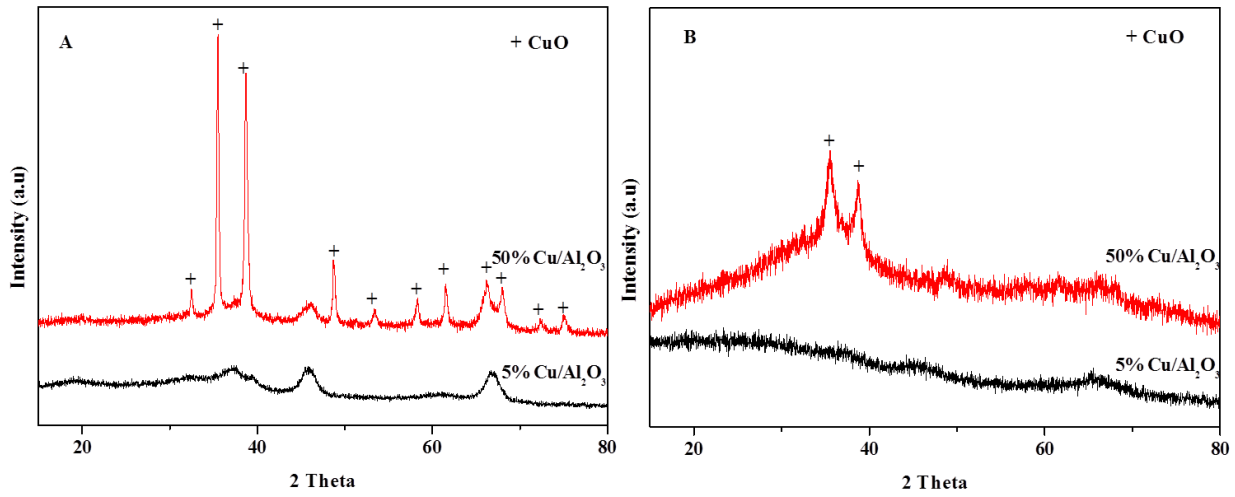

Figure 3-7: X-ray diffraction pattern of Cu/ Al_2O_3 catalysts prepared by A-Impregnation method and B- Co-precipitation method

On the other hand, in the impregnation method, the formation of higher amount of the crystalline CuO phase was ascribed to the direct calcination of the nitrate species. Also, inter-diffusion of copper and aluminum during the calcination may be responsible for the variation in crystallinity of copper. Here, one can see that the XRD results are in agreement with the results of XRF technique, in terms of homogeneity.

3.1.3 Effect of support

Nowadays, attention is paid to the development of catalysts with appropriate support. The main idea behind is that the active phase should be dispersed on a suitable support to make the active species stable in order to obtain optimal performance and to decrease the amount of the costly metal used, which accordingly decrease the total catalyst expense [33, 34]. Furthermore, the porous characteristics of the support materials offer the possibility of high dispersion of metal

nanoparticles which contributes to better catalytic activity [35, 36]. Obviously, the performance of catalytically active components depends upon both chemical and physical properties of the support used, such as, for instance, its chemical composition, crystal structure, porosity, particle size and surface area.

Usually Al_2O_3, TiO_2, SiO_2 and ZrO_2 are considered to be thermally stable supports with reasonably good chemical stability and low cost. Therefore extensive studies were reported on these supports [37-39]. γ-alumina is one of the most commonly used, cheap and stable material for catalyst support. Its high surface area properties are in good agreement with the requirements of gas phase catalytic reactions carried out at high space velocities. The catalytic properties of TiO_2 are also investigated as it is a promising reducible semiconductor metal oxide support with excellent stability. TiO_2 has been frequently demonstrated as an efficient catalyst support as well as a photocatalyst for many reactions to decompose a variety of organic compounds [40]. In various combustion reactions ZrO_2 is reported as an active support. The anionic vacancies, even in small amount, lead to better oxygen mobility in ZrO_2 lattice [41, 42]. For comparison a SiO_2 support was also investigated in our study even if the pore volume and surface area of silica supports have lower dominance on the metal dispersion [43]. Activated carbon is environmentally friendly, easily available and a cheap support as compared to other supports. However it is generally not stable in oxidative conditions.

In this part of the study, we have tried to identify the most appropriate support for copper species. Therefore, γ-Al_2O_3 from SASOL, TiO_2-P25 from Aldrich, ZrO_2-Monoclinic from Aldrich, SiO_2 from Fuji Silysia Chemical Ltd. and activated carbon from CECA were tested for the selective oxidation of ethanol to ethylene oxide. All the catalysts prepared contained 5wt.% of Cu.

A. Results of catalytic performance

The catalytic performance of all catalysts based on the different supports was determined at 250 °C. The detailed reaction conditions and distribution of products of ethanol oxidation are shown in Figure 3-8. From the results one can see that only the catalysts based on TiO_2 and Al_2O_3 promoted the formation of ethylene oxide. The catalyst based on TiO_2 showed higher selectivity for ethylene oxide than the catalyst based on Al_2O_3. Over the TiO_2–based catalyst mainly two products – namely acetaldehyde and ethylene oxide – were identified. The selectivities for

ethylene oxide and acetaldehyde (27% and 45% respectively) were observed at an ethanol conversion of 58%. On the other hand the catalyst based on Al_2O_3 showed less selectivity for ethylene oxide (15%) and more selectivity for acetaldehyde 56% with an ethanol conversion of 39%. For the latter the production of acetic acid (AA) was also observed (1%).

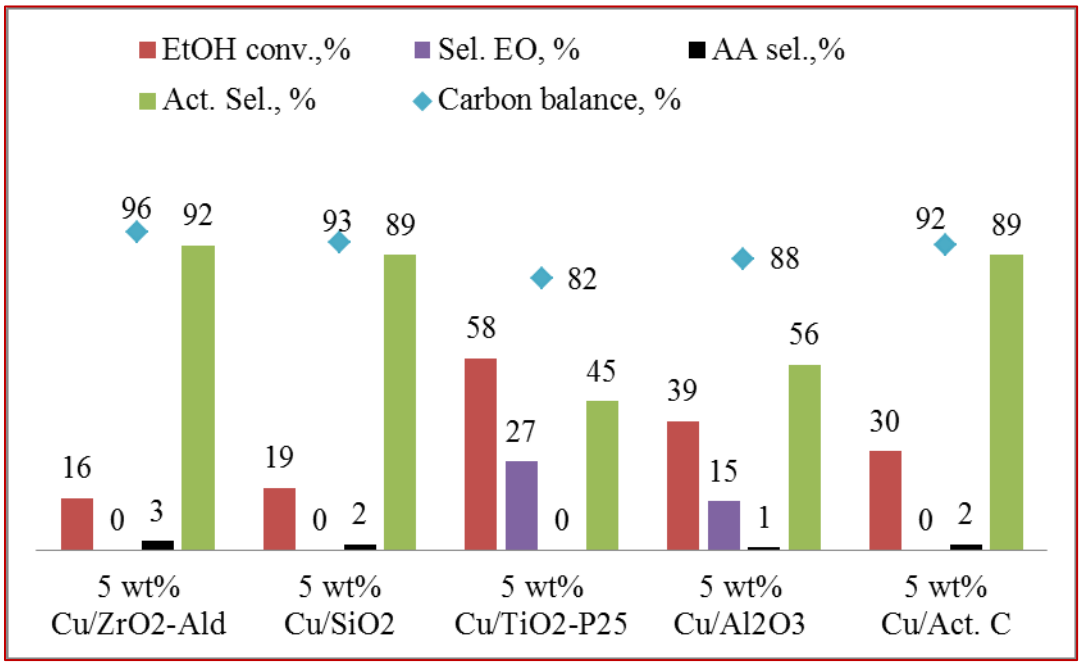

Figure 3-8: Catalytic performance of the catalysts based on different supports

Reaction conditions: *Ethanol: 15 mol.%, Carrier gas: Helium, Reaction temperature: 250 °C, Cat. wt.: 0.3 g (activated), EtOH:O_2=2:1 (molar) ; Total gas flow at RT: 20 mL/min, Pressure: 1 atm., Time on stream: 15 h*

The catalysts based on the other supports (ZrO_2, Act.C and SiO_2) promoted only the formation of acetaldehyde at very low ethanol conversion. The ZrO_2, Act.C and SiO_2–based catalysts showed acetaldehyde selectivity of 92%, 89% and 89% respectively with an ethanol conversions of 16%, 30% and 19% respectively.

B. Reproducibility of the catalytic performance

The TiO_2-supported copper catalyst showed the best performance among all the catalysts series based on various supports. Since, the reproducibility of the catalytic test was evaluated using 5 %wt. Cu/TiO_2(P25) as a catalyst. Figure 3-9 shows the results of the reproducibility test.

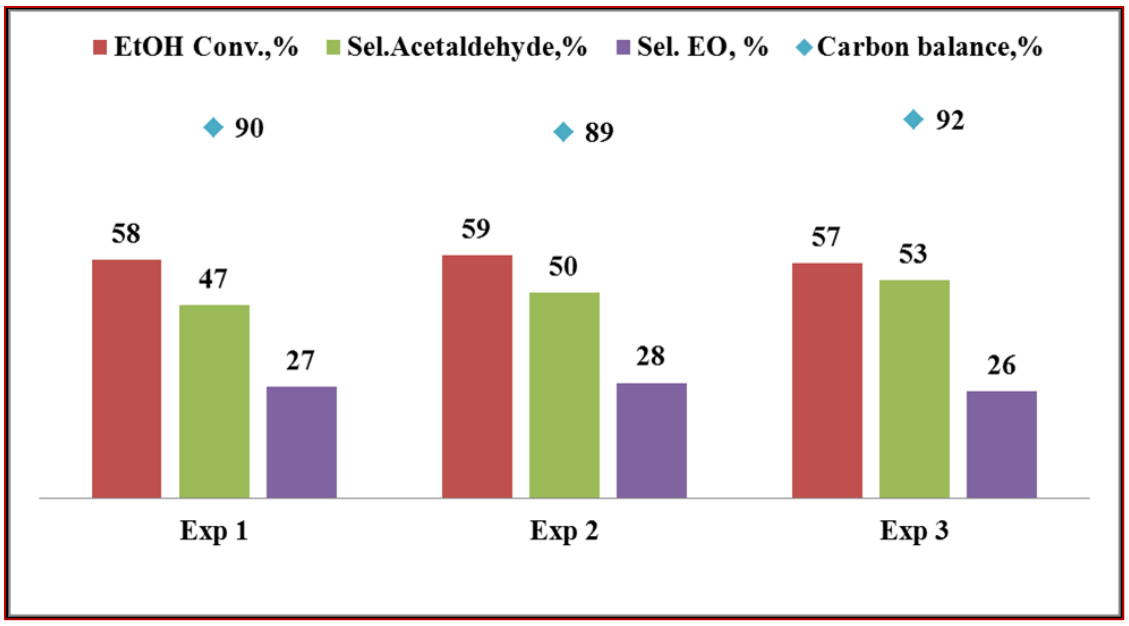

Figure 3-9: Reproducibility of catalytic test

Reaction conditions: *Ethanol: 15 mol.%, Carrier gas: Helium, Reaction temperature: 250 °C, Cat. wt.: 0.3 g of 5wt.% Cu/TiO_2-P25 (activated), EtOH:O_2=2:1 (molar) ; Total gas flow at RT: 20 mL/min, Pressure: 1 atm., Time on stream: 15 h*

From Figure 3-9, it is observed that ethanol conversion as well as ethylene oxide selectivity are reproducible for the three repeated experiments. The results are within the accuracy limit of the catalytic test and analysis technique. One can conclude that the catalytic test is reproducible and thus the results are reliable.

C. Reproducibility of catalyst synthesis

The 5wt.% Cu/TiO_2-P25 catalyst was resynthesized three times using the same preparation method and tested to check the reproducibility of the synthesis protocol. The results are reported in Figure 3-10. According to the results, it is proven that the catalyst synthesis is successfully reproduced. The minor changes in performance are within the margin of error of the experiment.

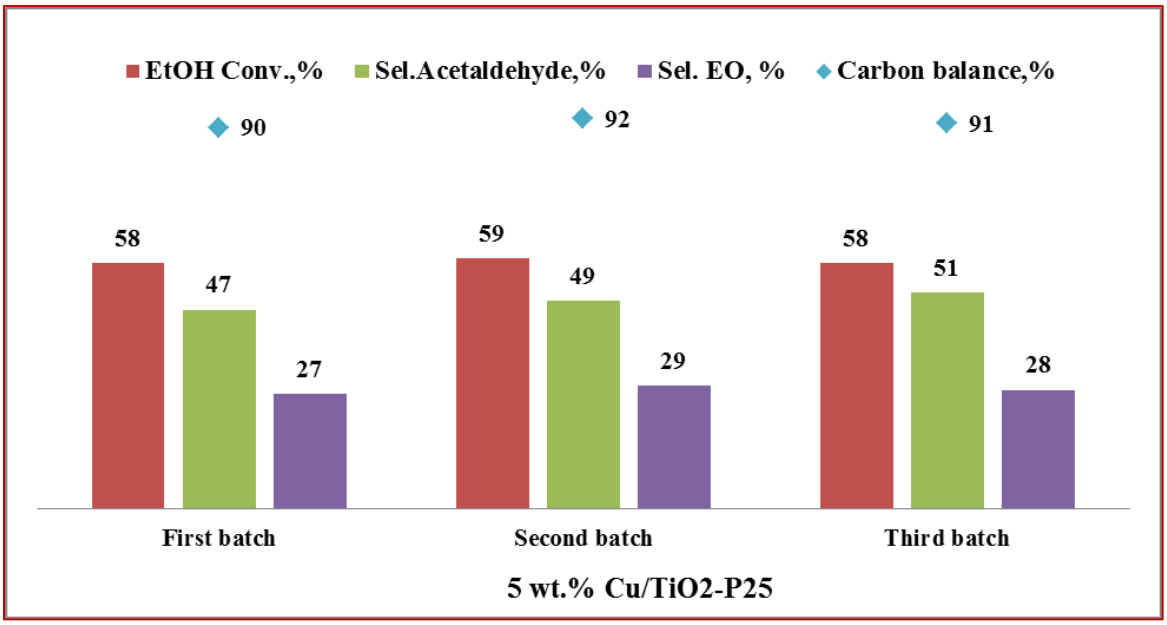

Figure 3-10: Reproducibility of catalyst synthesis

Reaction conditions: *Ethanol: 15 mol.%, Carrier gas: Helium, Reaction temperature: 250 °C, Cat. wt.: 0.3 g of 5wt.% Cu/TiO_2-P25 (activated), EtOH:O_2=2:1 (molar) ; Total gas flow at RT: 20 mL/min, Pressure: 1 atm., Time on stream: 15 h*

D. Preliminary characterization of the catalysts

Generally the performance of catalytically active components depends on both chemical and physical properties of the support used, such as chemical composition, crystal structure, porosity, particle size and surface area. The study of the crystalline and textural properties of the catalysts was performed by XRD and nitrogen physisorption measurement. The composition of the synthesized catalyst was also verified by XRF. The results are presented in the following sections.

➢ Atomic compositions of copper catalysts based on different supports

The bulk composition was determined using X-Ray Fluorescence (XRF) technique and the results are presented in Table 3-5. For all the catalysts the amount of copper was very close to the theoretical value except for activated carbon-based copper catalyst. It may be due to the calcination performed in static air for the all support to keep the homogeneous catalyst treatment. The carbon support as expected may have lost some carbon during that step in the form of CO_2

release. The standard deviation value suggested an homogeneous mixture of the metal over the supports. It is observed that the standard deviation value is higher for carbon-based catalyst.

Table 3-5: Textural properties of the catalysts based on different supports

Catalyst Name	S_{BET} (m^2/g)	V_P (cm^3/g)	Mean pore radius (nm)	XRF Cu content. (wt.%) (SDV*)
5 wt.% Cu/Al_2O_3	193	0.42	3.1	5.3 (0.44)
5 wt.% Cu/SiO_2	267	1.1	6.4	5 (0.98)
5 wt% Cu/TiO_2-P25	40	0.37	13.4	5 (0.19)
5 wt. % Cu/ZrO_2-Ald.	6	0.02	6.1	5 (0.29)
5 wt.% Cu/Act.C	300	0.19	2.7	6.7 (1.6)

*SDV- Standard Deviation Value

- Textural properties of the copper catalyst based on different supports

The BET surface areas, pore volumes and mean pore diameters for the supported copper oxide catalysts were measured and listed in Table 3-5. Carbon and silica-supported catalysts showed very high surface areas (300 and 267 m^2g^{-1}) together with large pore volumes (0.19 and 1.1 cm^3g^{-1}). In comparison, zirconia-supported catalyst showed a very low surface area (6 m^2g^{-1}) and pore volume (0.02 cm^3g^{-1}). One can assume that due to the low surface area and pore volume the dispersion of copper on zirconia was decreased.

The presence of hysteresis loop (Figure 3-11) shows the mesoporous nature of the catalysts. The surface area of the catalysts as a function of supports varies in the order: Activated carbon > SiO_2 > Al_2O_3 > TiO_2 > ZrO_2. The pressure range of capillary cohesion of the different supports is consistent with the pore size, as larger pore size is expected to show capillary cohesion at higher pressure. The pore diameter follows the decreasing trend: TiO_2 > SiO_2 > ZrO_2 > Al_2O_3 > Activated carbon. A closer look clearly shows that, although the activated carbon possesses a very high surface area there is no uniformity or order in the pores (Figure 3-11-E2). Apart from non-uniform pore the support ZrO_2 consists of very low surface area (Figure 3-11-D2). Among the supports Al_2O_3 and SiO_2 the former shows a higher surface area when compared to the latter and at the same time a very sharp pore size distribution (Figure 3-11-A2, B2). The

support TiO_2 has a moderate surface area but it shows well-defined mesopores with a diameter of ~14 nm (Figure 3-11C).

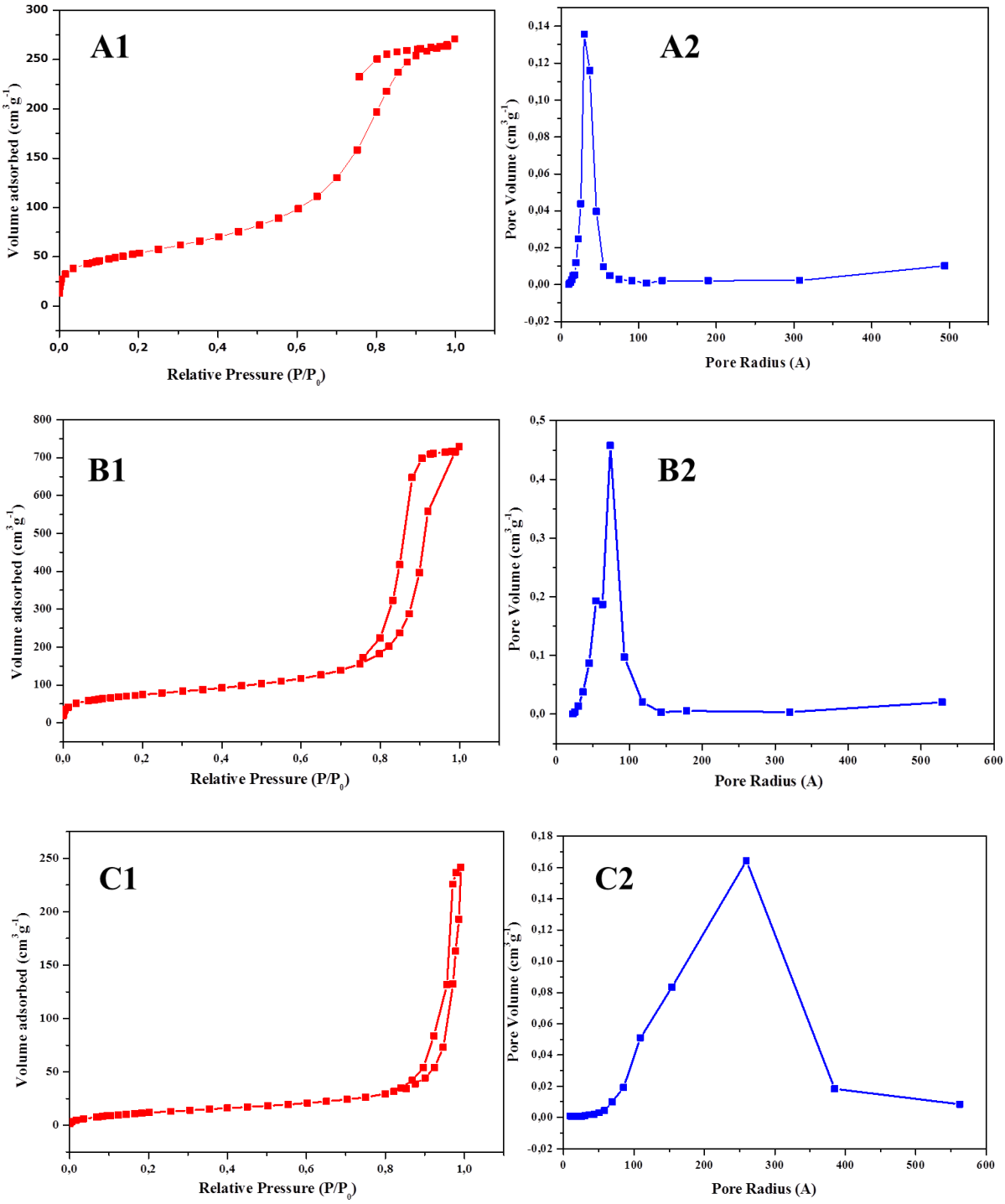

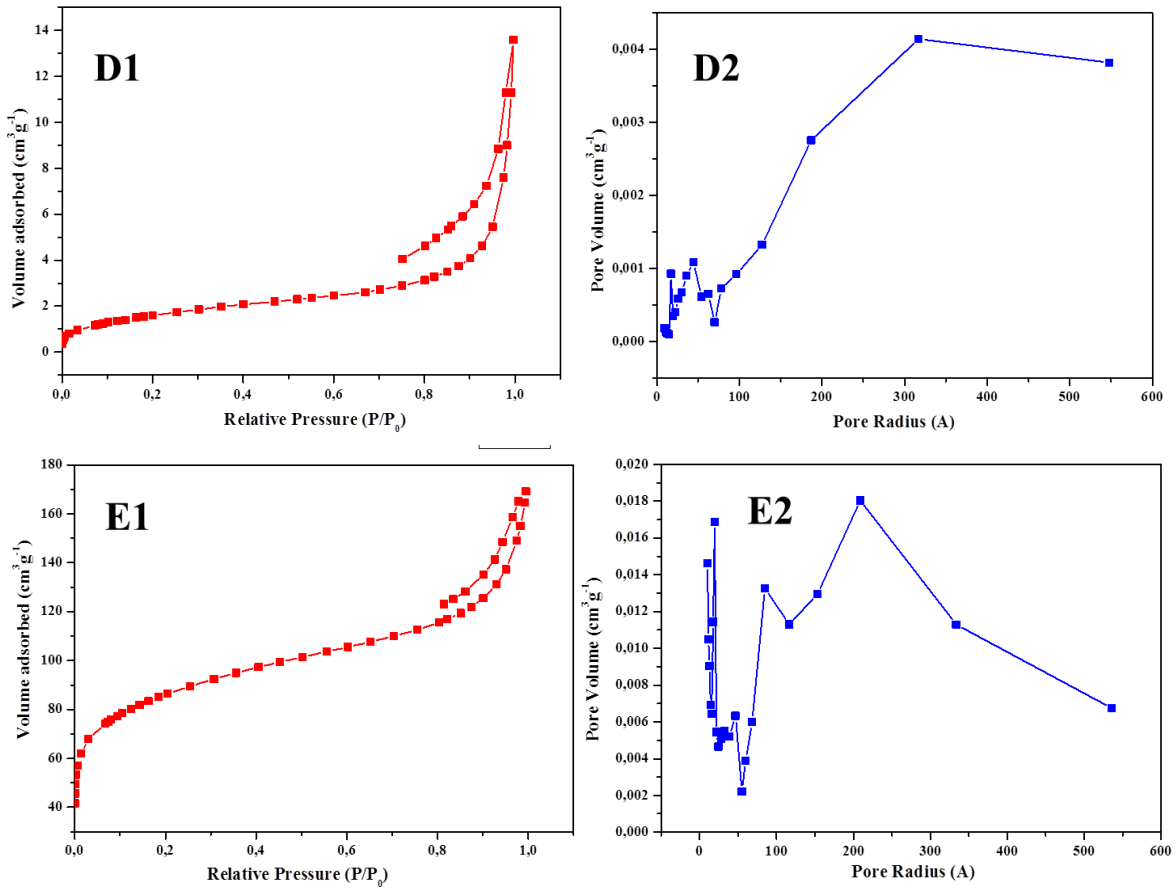

Figure 3-11: N_2 adsorption-desorption isotherms and pore size distributions A1&A2- 5% Cu/Al_2O_3, B1&B2- 5% Cu/SiO_2, C1&C2- 5% Cu/TiO_2-P25, D1&D2- 5%Cu/ZrO2-Ald and E1&E2- 5% Cu/Act.C

➢ XRD analysis

XRD patterns of the catalysts based on different supports are shown in Figure 3-12. For the copper catalysts based on silica, zirconia and active carbon, the prominent characteristic peaks appeared at 35.64° and 38.85° and were ascribed to oxidized copper (CuO/Cu^{2+}) phase (JCPDS File no. 65-2309) [27-29]. In the case of the alumina and titania-based catalysts, no characteristic peaks for copper species were observed. In case of TiO_2 typical diffraction pattern of P-25 were found, characterized by peaks attributed to anatase and rutile phases (JCPDS File no. 21-1272 and 21-1276 respectively). In case of alumina and titania-supported Cu, the absence of diffraction peaks corresponding to CuO_x phases implies a good dispersion or very small particle size of the impregnated copper species.

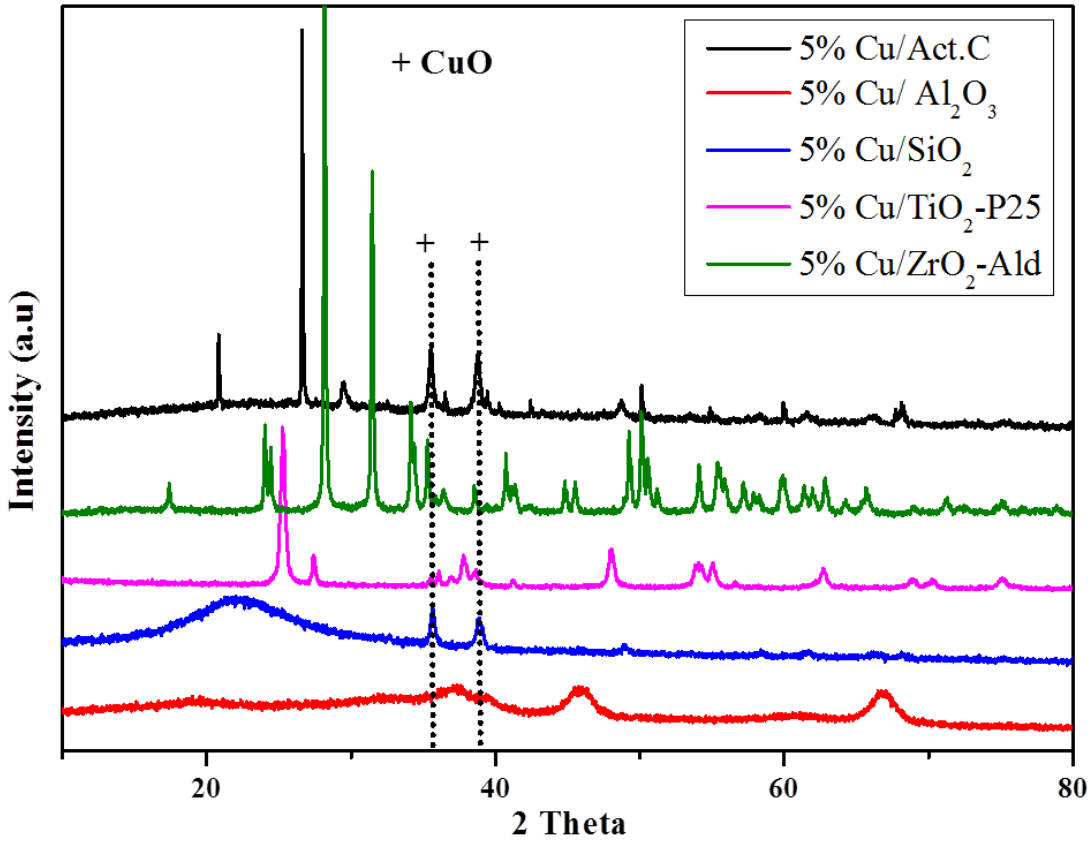

Figure 3-12: XRD patterns of the copper catalysts based on different supports

In the preliminary characterization part, the N_2 adsorption and desorption study of TiO_2-based catalysts showed the well-defined broad mesoporous structure. This was not the case for SiO_2, ZrO_2 and activated carbon-based catalysts. Moreover a uniform distribution of copper particles was observed in the TiO_2-based catalyst. In conclusion, 5%Cu/TiO_2 was the catalyst presenting the best results. Further reaction conditions optimization study was therefore performed using the TiO_2 as a catalyst support.

3.2 Results optimization over 5% Cu/TiO_2-P25

In the following of the study an optimization of the reaction conditions (including temperature, GHSV, EtOH:O_2) was carried out. Then the stability of the catalyst's performance over time on stream was investigated.

3.2.1 Effect of reaction parameters

A. Effect of temperature

The effect of the reaction temperature on the catalytic performance of 5 wt.% Cu/TiO_2–P25 catalyst was investigated between 190 °C and 275 °C keeping the EtOH:O_2 ratio at 1:2. The conversion, selectivity and carbon balance are plotted in Figure 3-13 As expected, the ethanol conversion strongly increased with the temperature, reaching 98% at 250 °C. In terms of product distribution, the formation of CO_2 was also promoted with temperature increase reaching 41% at 275 °C. On the other hand, the selectivity to acetaldehyde decreases progressively with this increment in temperature. In the case of ethylene oxide, the formation was first observed at 230 °C with low selectivity (20%). It increased to a maximum of 59% at 250 °C, and finally dropped again to 46% at 275 °C.

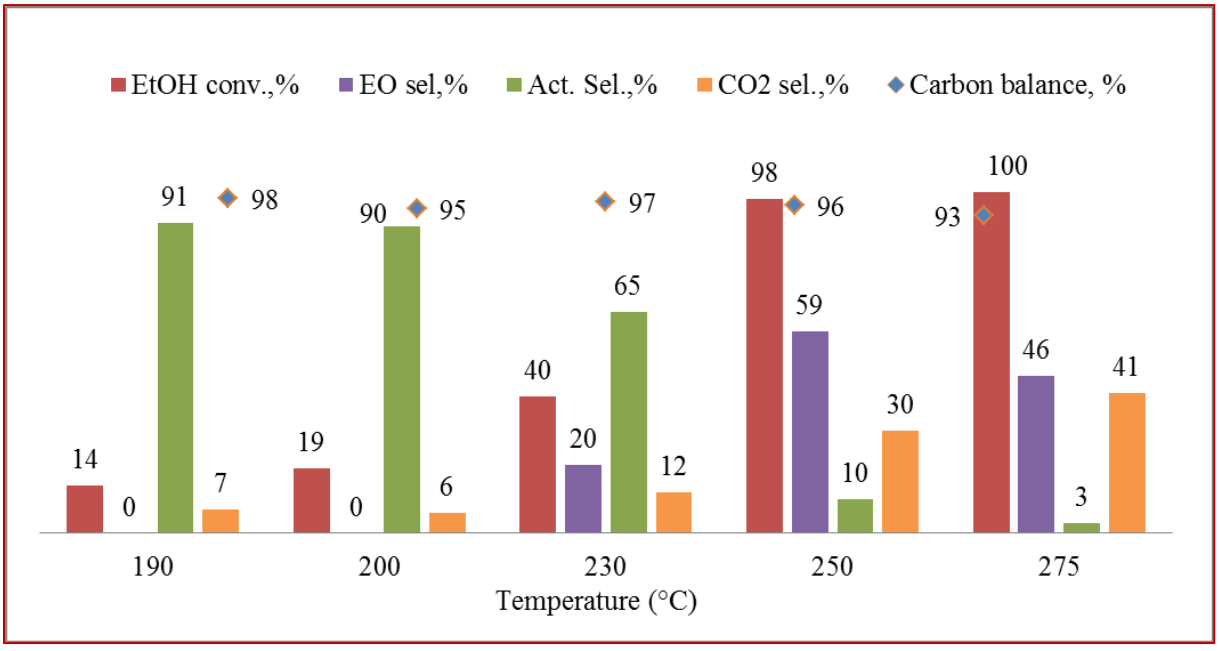

Figure 3-13: Evaluation of the catalytic performance as function of the temperature

Reaction conditions: *Ethanol: 15 mol.%, Carrier gas: Helium, Cat. wt.: 0.1 g of 5 wt.% Cu/TiO_2–P25, EtOH:O_2=1:2 (molar) ; Total gas flow at RT: 20 mL/min, Pressure: 1 atm., Time on stream: 15 h*

Since at 200 °C no ethylene oxide was detected one can conclude that 230 °C is the minimum temperature required for the formation of ethylene oxide. Since both, conversion and

selectivity in EO increase with temperature; one can conclude that 250 °C temperature is desirable for the selective oxidation of ethanol to ethylene oxide.

B. Effect of ethanol: oxygen ratio

The effect of the oxygen concentration was investigated due to the positive response of ethanol oxidation to ethylene oxide on the continuous presence of molecular oxygen. The catalytic performance of 5 wt.% Cu/TiO_2–P25 catalyst was studied at 250 °C varying the EtOH:O_2 ratio in the range of 0.5 to 2. The results are reported in Figure 3-14. Here one can see that the conversion of ethanol is enhanced by increasing the oxygen content in the feed. In terms of product distribution, the selectivity to ethylene oxide increased as well as the formation of carbon dioxide with the increase of oxygen content in the feed. On the other hand, the selectivity to acetaldehyde decreased. The best results were obtained at an EtOH:O_2 ratio of 1:2. Almost full conversion of ethanol was observed (98%) with 59% selectivity in ethylene oxide, 10 % selectivity in acetaldehyde and 30% selectivity in carbon dioxide. The carbon balance was 96%.

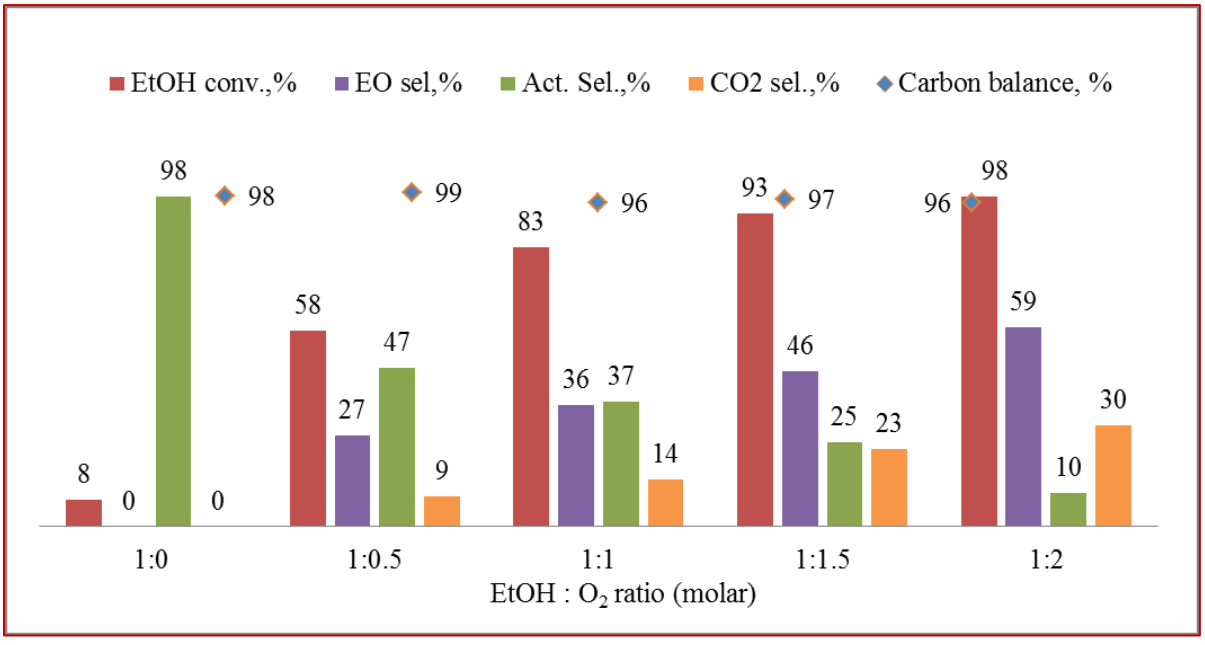

Figure 3-14: Influence of oxygen on catalytic activity

Reaction conditions: *Ethanol: 15 mol.%, Carrier gas: Helium, Reaction temperature: 250 °C, Cat. wt.: 0.1 g of 5 wt.% Cu/TiO_2–P25, Total gas flow at RT: 20 mL/min, Pressure: 1 atm., Time on stream: 15 h*

C. Effect of GHSV

To further optimize the performance several consecutive tests were performed varying the gas hourly space velocity (GHSV) in the range 7020 to 28080 h^{-1} using the 5% wt. Cu/TiO_2–P25 catalyst. The results are presented in Figure 3-15. An increase in the GHSV from 7020 to 14040 h^{-1} led to a higher selectivity in ethylene oxide (58%) with almost constant full conversion of ethanol (98-100%). On the other hand, at low GHSV 7020 h^{-1} selectivity for acetaldehyde was higher (37%) and traces of ethyl acetate (EA) were also observed (6%). A further increase in GHSV to 28080 h^{-1} did not show any impact on the ethylene oxide selectivity but decreased the ethanol conversion (71%). One can also see that the selectivity to CO_2 increased with increasing GHSV. In the present study, a slightly marked optimum in ethanol conversion (98%) and ethylene oxide selectivity (59%) was observed at GHSV of 14040 h^{-1}.

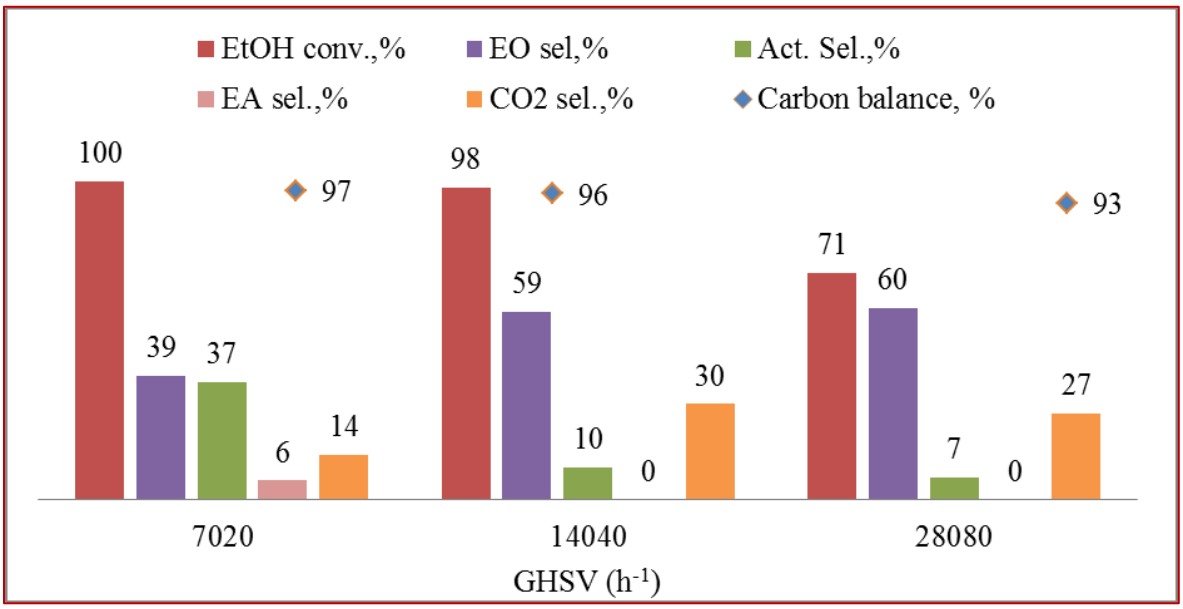

Figure 3-15: Effect of GHSV on catalytic performance

Reaction conditions: *Ethanol: 15 mol. %, Carrier gas: Helium, Reaction temperature: 250 °C, Cat. wt.: 0.1 g of 5 wt.% Cu/TiO_2–P25, EtOH : O_2=1:2 (molar), Pressure: 1 atm., Time on stream: 15 h*

3.2.2 Stability over time on stream

The time dependence of the ethanol conversion and ethylene oxide selectivity was investigated for 5wt.% Cu/TiO_2–P25 at 250 °C and at a GHSV of 14040 h^{-1}. The corresponding

results are shown in Figure 3-16. The ethanol conversion was stable and no significant change in ethylene oxide selectivity was observed for 50 h. The carbon balance stayed very close to 100%.

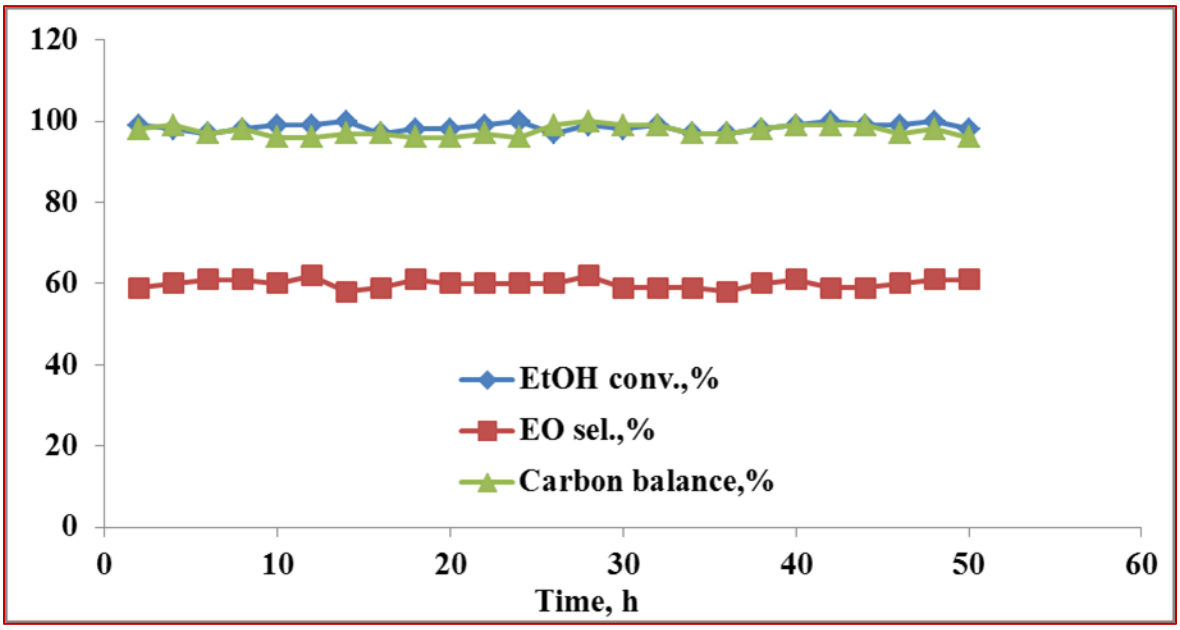

Figure 3-16: Time on stream study of 5%Cu/TiO_2–P25 catalyst

Reaction conditions: *Ethanol: 15 mol.%, Carrier gas: Helium, Reaction temperature: 250 °C, Cat. wt.: 0.1g of 5 wt.% Cu/TiO_2–P25, EtOH:O_2=1:2 (molar) ; Total gas flow at RT: 20 mL/min, Pressure: 1 atm., Time on stream: 50 h*

3.3 Conclusion

In the first part of our study, gold, silver and copper catalysts supported on LiO_2-doped γ-alumina were prepared using the deposition precipitation (DP) method and characterized using different techniques. From the XRD analysis the uniform distribution of metal nanoparticles on the support was confirmed. Furthermore, XPS and EDS analyses were carried out to determine the surface and bulk composition of the catalyst and the oxidation states of the metals. H_2-TPR study suggests that the silver metal reduction was facilitated over the alumina support. On the other hand, the copper catalyst requires high temperature for reduction. These catalysts were successfully applied for the selective oxidation of ethanol to ethylene oxide. The gold-based catalyst was more selective towards ethylene oxide compared to the silver and copper catalysts. For the latters, a minimum of 250 °C was required for the formation of ethylene oxide. Finally, the proof of concept for the oxidation of ethanol to ethylene oxide was delivered.

The obtained catalytic results were compared with the ones reported by Lippits *et al.* in the literature [1, 2]. It is clear that the results were not reproduced successfully but several conditions were different in the catalytic testing as described in Section 3.1.1 D. More data on the characterization of the catalysts reported in the literature would have been necessary to completely understand the difference in performance observed.

The catalytic activity of alumina-supported copper catalyst was optimized in the further study. Alumina-supported copper catalysts were prepared with different loadings and using different preparation methods (namely impregnation and co-precipitation method). These catalysts were characterized using XRD technique to study the phases and dispersion of the metal. The lower loading showed high dispersion of copper on alumina but with higher loading it showed the formation of copper oxide species. It can be concluded that higher copper loading leads to the formation of big particles of copper species. The highly dispersed copper catalysts are selective for the formation of ethylene oxide. BET analysis confirmed that the higher loading of copper decreased the surface area and pore volume of the support. Here, we can conclude that the impregnation method is good for the lower copper loading and the co-precipitation method better for higher copper loadings.

In the following of the study, 5 wt.% copper catalysts were prepared by impregnation method using different supports. The supports were selected on the basis of their different textural properties and stability. Silica, alumina, titania, activated carbon and zirconia supports were investigated. They were characterized using XRD technique and it was found that the copper dispersion over alumina and titania supports was better than over the other supports (zirconia, silica, act. carbon) because using titania and alumina-based catalysts the copper oxide species did not form. These catalysts were screened for the ethanol oxidation and it was found that titania was the best support for the ethylene oxide formation.

Further study with 5 wt.% Cu/TiO_2 catalyst were done for the reaction parameters optimization. First of all the catalyst synthesis and catalytic test reproducibility was confirmed by synthesizing the same catalyst several times and performing several times the tests with the same catalyst respectively. The reaction condition parameters were then optimized by changing reaction temperature, GHSV and ethanol:O_2 ratio. It was found that the temperature (250 °C),

GHSV (14040 h^{-1}) and ethanol: O_2 ratio (1:2) were the best experimental conditions for the selectively formation of ethylene oxide (58% yield).

In the next chapter some supplementary catalytic tests were performed including optimization of copper loading, effect of catalyst activation, effect of catalyst calcination temperature, effect of the nature of the TiO_2-phases in order to back optimized the performances. Furthermore, detailed characterization, including XRD, H_2-TPR, XPS, SEM and TEM of calcined and spent catalysts were performed in order to correlate the catalytic performance and the catalysts physicochemical properties.

3.4 References

1. M. J. Lippits, B. E. Nieuwenhuys, Catalysis Today, **2010**, 154, 127-132.
2. M. J. Lippits, B. E. Nieuwenhuys, Journal of Catalysis, **2010**, 274, 142-149.
3. N. Ichikuni, L. Fan, S. Shimazu, T. Uematsu, Applied Catalysis A: General, **2003**, 246, 87.
4. S. Scire, S. Minico, C. Crisafulli, S. Galvagno, Applied Catalysis B: Environmental, **2001**, 34, 277.
5. G. B. Hoflund, D.M. Minahan, Journal of Catalysis, **1996**, 158, 109.
6. J. M. Keel, S. Wodiunig, T. S. E. Wilson, F. W. Zemichael, R.M. Lambert, Catalysis Letters, **2003**, 87, 1.
7. G. Bernhardt, S. B. Rivers, M. W. Wright, D. J. Frankel, M.M. Steeves, R.J. Lad, Thin Solid Films, **2007**, 515, 8684.
8. X. Hou, X. Wang, W. Luan, D. Li, K. Yao, Applied Surface Science, **2012**, 258, 8241.
9. J. Zhu, C. Sun, Y. Lv, L. Qi, B. Liu, F. Gao, K. Sun, L. Dong, Y. Chen, Applied Catalysis B: Environmental, **2011**, 103, 206-220.
10. M. A. Brookshier, C. C. Chusuei, D. W. Goodman, Langmuir, **1999**, 15, 2806-2808.
11. D. Andreeva, Gold Bulletin, **2002**, 35, 82–88.
12. M. Fazio C. Milone, A. Pistone, S. Galvagno, Applied Catalysis B: Environmental, **2006**, 68, 28-37.
13. A. Chiorino F. Boccuzzi, M. Manzoli, D. Andreeva, T. Tabakova, L. Ilieva, V. Iadakiev, Catalysis Today, **2002**, 75, 169.

14. F. Epron, F. Gauthard, J. Barbier, Journal of Catalysis, **2013**, 220, 182.
15. S. Aouad, M. Skaf, S. Hany, R. Cousin, E. Abi-Aad, A. Aboukaïs, Journal of Catalysis, **2014**, 320, 137-146.
16. Z. Qu, D. Chen, S. Shen, X. Li, Y. Shi, Y. Wang, Q. Fu, J. Wu, Catalysis Today, **2011**, 175, 338-345.
17. M. W. Song, T. W. Kim, H. L. Koh, K. L. Kim, Applied Catalysis A: General, **2001**, 210, 35-44.
18. A. B. Lopez, F. E. L. Suarez, M. J. I. Gomez, Applied Catalysis B: Environmental, **2008**, 84, 651-658.
19. Y. J. Zhong, M. Feiluo, X. X. Yuan, X. M. Zheng, Applied Catalysis A: General, **1997**, 62, 121-131.
20. M. Turco, S. Esposito, G. Bagnasco, C. Cammarano, P. Pernice, Applied Catalysis A: General, **2011**, 403, 128-135.
21. A. Parmaliana, A. Basile, S. Tosti, A. Iulianelli, F. Gallucci, C. Espro, J. Spooren, Catalysis Today, **2008**, 137, 17-22.
22. K. I. Choi, M. A. Vannice, Journal of Catalysis, **1991**, 131, 22.
23. G. G. Jernigan, G. A. Somorjai, Journal of Catalysis, **1994**, 147, 567.
24. L. Song, L. Li, C. Chen, Y. Zhang, Y. Zhan, X. Lin, Q. Zheng, H. Wang, H. Ma, L. Ding, W. Zhu, International Journal of Hydrogen Energy, **2014**, 39, 19570-19582.
25. Y. Cui, C. Wen, X. Chen, B. Zong, W. Dai, Applied Catalysis B: Environmental, **2015**, 162, 483-493.
26. V. S. Prasad, B. Naik, N. N. Ghosh, Powder Technology, **2012**, 232, 1-6.
27. P. Niebryzydowska, A. Bialas, B. Dudek, Z. Piwowarska, L. Chmielarz, M. Michalik, M. Kozak, P. Kustrowski, Catalysis Today, **2011**, 176, 413-416.
28. M. P. Reddy, P. A. Kumar, L. K. Ju, B. H. Sook, H. H. Phil, Journal of Molecular Catalysis A: Chemical, **2008**, 291, 66-74.
29. A. M. Hengne, R. B. Mane, A. A. Ghalwadkar, S. Vijayanand, P. H. Mohite, H. S. Potdar, C. V. Rode, Catalysis Letters, **2010**, 135, 141-147.
30. N. Bakshi, R.O. Idem, Industrial & Engineering Chemistry Research, **1994**, 33, 2047.
31. C. K. Wu, M. Yin, Y. Lou, C. Burda, J. T. Koberstein, Y. Zhu, S. O'Brien, Journal of American Chemical Society, **2005**, 127, 9506-9511.

32. S. Mikhailenko, H. Praliaud, Z. Chajar, M. Primet, Applied Catalysis B: Environmental, **1998**, 16, 359-374.
33. H. Honda, N. Shibasaki-Kitakawa, H. Kuribayashi, T. Toda, T. Fukumura, T. Yonemoto, Bioresource Technology, **2007**, 98, 416-421.
34. N. Muhd Julkapli, S. Bagheri, S. Bee Abd Hamid, The Scientific World Journal, **2014**, 21.
35. N. Coustel, J. M. Planeix, B. Coq, Journal of American Chemical Society, **1994**, 116, 7935-7936.
36. J. E. Mondloch, P. D. Kent, R. G. Finke, Journal of American Shemical Society, **2014**, 136, 1930-1939.
37. P. B. Barbero N. F. Aguero, L. Gambaro, E.C. Luis, Applied Catalysis B: Environmental, **2009**, 91, 108-112.
38. P. J. Neill, E. M. Cordi, P. O. L. Falconer, Applied Catalysis B: Environmental, **1997**, 14, 23-36.
39. E. M. Holmgreen M. M. Yung, U. S. Ozkan, Journal of Catalysis, **2007**, 247, 356-367.
40. J. Belkouch, H. V. Van, D.A. Ould, B. Taouk, Journal of Hazardous Materials, **2009**, 169, 758-765.
41. N. Guilhaume, C. Bozo, J. M. Herrmann, Journal of Catalysis, **2001**, 203, 393-406.
42. L. N. Ikryannikova, G. L Markaryan, G. P. Muravieva, A. O. Turakulova, B. G. Kostyuk, E. V. Lunina, V. V. Lunin, E. A. Zhilinskaya, A. Aboukaıs, Colloids and Surfaces A, **1999**, 151, 435-447.
43. P. Shukla, A. Patel, T. Rufford, S. Wangc, J. Chena, V. Rudolph, Z. Zhu, Applied Catalysis A: General, **2011**, 409-410, 55-65.

Chapter 4

Back optimization of catalysts – performance and characterization

4.1 Back optimization of catalyst

In the previous chapter, some preliminary results were presented. They allowed the selection of copper as a promising active phase for ethanol conversion into EO, the choice of the best support (TiO_2-P25) to disperse and stabilize this metal and of the best synthesis method to get a catalyst giving a high and stable performance. Finally, a parameter optimization study was also carried out to select the right temperature, GHSV and EtOH:O_2 ratio. However, this preliminary work was not sufficient to understand why the catalyst is efficient.

In this chapter the optimization of the TiO_2-supported copper catalysts are pursued in more details and some supplementary catalytic results with copper catalysts using various supports are also presented. Then a more exhaustive characterization study of the catalysts is presented in a view to establish a clear correlation between the physicochemical properties of the catalysts and their catalytic performance.

4.1.1 Blank tests

A blank reaction test was performed in the optimized reaction conditions, without any catalyst nor SiC, in order to evaluate the thermal decomposition of ethanol with a higher ethanol/oxygen ratio (EtOH:O_2=1:2) at 250°C using the regular configuration of the reactor (described in Section 2.3.1). The conversion of ethanol was 6% with 99% selectivity in acetaldehyde (Figure 4-1). One can conclude that no significant thermal activation takes place under these conditions, even at increased ethanol/oxygen ratio.

A second blank test, using only TiO_2–P25 powder, was made in order to evaluate the activity of the catalyst support under the optimized reaction conditions (EtOH:O_2=1:2; 250°C). The conversion of ethanol was slightly increased compared to the blank test (9% vs. 6%) with 97% selectivity in acetaldehyde (Figure 4-1). In conclusion, in comparison with the first blank test, we can conclude that the catalyst support (TiO_2-P25) is inert under the reaction conditions used.

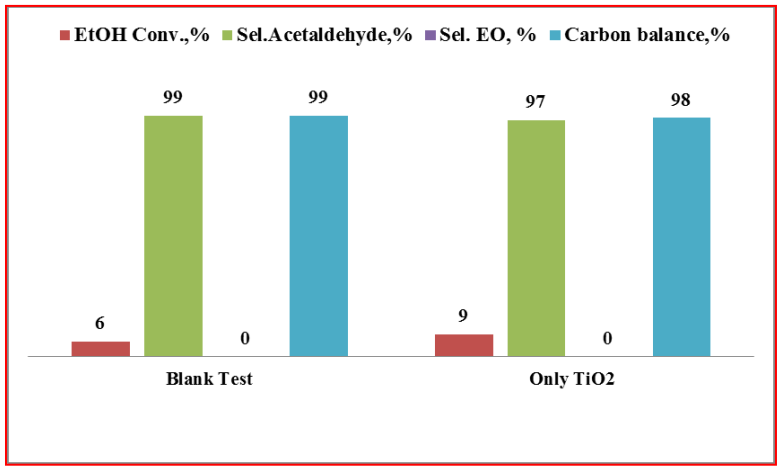

Figure 4-1: Blank test in optimized reaction conditions

***Reaction conditions**: Ethanol: 15 mol.%, Carrier gas: Helium, Reaction temperature: 250 °C, TiO_2-P25 wt.: 0.1 g, EtOH:O_2=1:2 (molar), Total gas flow at RT: 20 mL/min, Pressure: 1 atm.*

4.1.2 External diffusion limitations

A standard test was performed on the catalyst containing 5 wt.% Cu supported on TiO_2–P25 to evaluate the external mass transfer limitations. The standard methodology was to vary the total gas flow and the mass of the catalytic bed (proportional to the catalyst mass). While changing the flow of the reactant gas (F), the linear velocity changes proportionally. Hence, the volume of the catalytic bed (V) is adapted proportionally to ensure a constant contact time. In the absence of external mass transfer limitations the ethanol conversion should stay at a constant value. (Figure 4-2A)

From the results (Figure 4-2B) one can see that the decrease from 0.3 g to 0.1 g of catalyst mass does not affect the catalytic performance. On the other hand, a further decrease to a 0.05g mass clearly affected the catalytic performance, with a decrease in conversion (79% vs. 98-99%) as well as in selectivity (46% vs. 59-58%). Hence, in our conditions the use of 0.1g of catalyst at minimum is mandatory to assure the absence of external diffusion limitations.

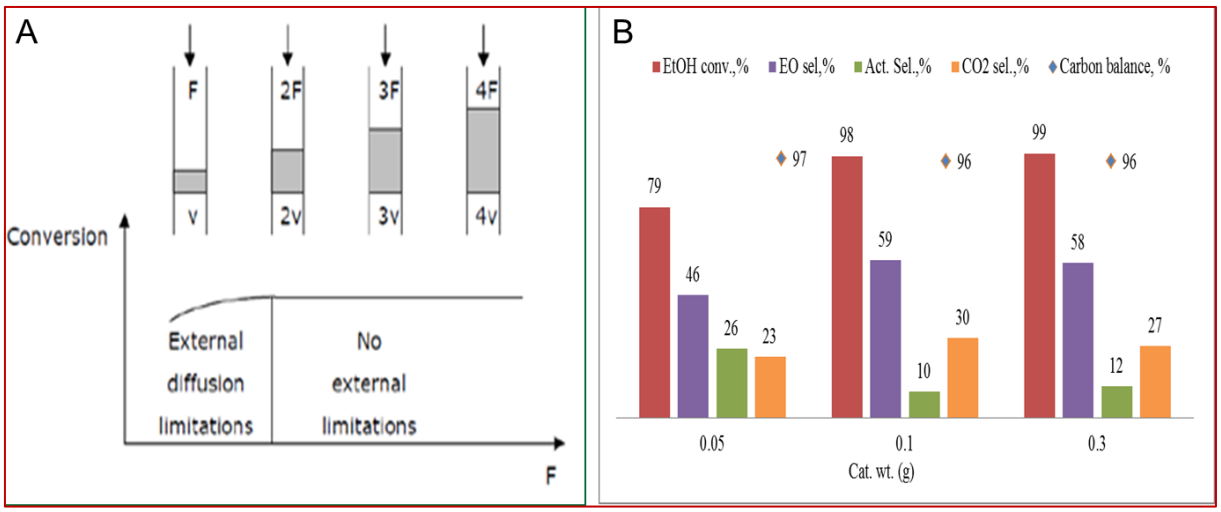

Figure 4-2: External diffusion study

***Reaction conditions**: Ethanol: 15 mol.%, Carrier gas: Helium, Reaction temperature: 250 °C, Cat. wt.: 0.05-0.3 g of 5 wt.% Cu/TiO_2-P25, EtOH:O_2=1:2 (molar) ; Total gas flow at RT: 10-60 mL/min, Pressure: 1 atm., Time on stream: 15 h, GHSV: 14040 h^{-1}*

4.1.3 Influence of copper loading

To investigate the optimum amount of Cu on the TiO_2 support, the oxidation of ethanol to ethylene oxide was studied using catalysts with different loading (0.2, 1, 2.5 and 5 wt.%). The results are displayed in Figure 4-3. One can see that the conversion of ethanol increases with the loading suggesting an increase in the number of active sites available for the reaction. However, it is further worth mentioning that the selectivities in EO and acetaldehyde were also significantly impacted by the copper loading: acetaldehyde selectivity decreases gradually from 92 to 10% for increased amounts of copper, whereby the selectivity in EO increased from 0% (0.2 wt.% loading) to 59% (5 wt.% loading). Among the Cu/TiO_2–P25 catalyst series, the 5 wt.% Cu/TiO_2 catalyst exhibited the best performance with 98% conversion of ethanol and 59% selectivity to ethylene oxide. A complementary test was carried out with bulk CuO whereby no ethylene oxide formation and only low conversion of ethanol was observed (21%).

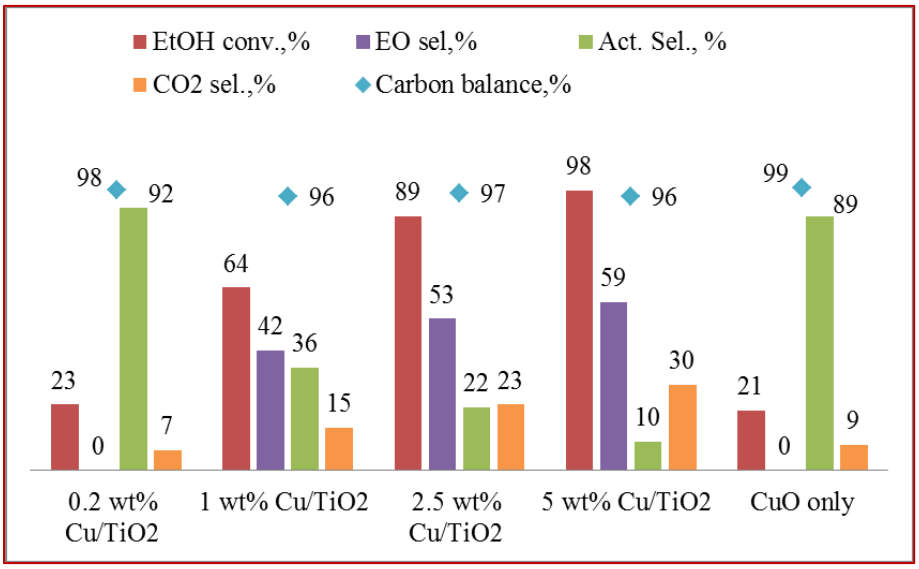

Figure 4-3: Effect of copper loading

***Reaction conditions**: Ethanol: 15 mol.%, Carrier gas: Helium, Reaction temperature: 250 °C, Cat. wt.: 0.1 g of 5 wt.% Cu/TiO_2-P25, EtOH:O_2=1:2 (molar) ; Total gas flow at RT: 20 mL/min, Pressure: 1 atm., Time on stream: 15 h*

4.1.4 Influence of the nature of the support

Copper catalysts with a constant amount of metal (5 wt. %), based on different supports (SiO_2, Al_2O_3, ZrO_2-Ald, ZrO_2-CL, activated carbon, TiO_2-anatase, TiO_2-rutile) were screened under the new optimized reaction conditions. Note that in Chapter 3 these catalysts were screened in other non optimized operating conditions. The catalytic performance is presented in Figure 4-4. As observed in the preliminary tests (*cf.* Section 3.1.3), the catalysts based on SiO_2, ZrO_2-Ald and activated carbon are not active in the formation of ethylene oxide but gave exclusively acetaldehyde as main product. Additionally, a zirconia-optimized support provided by CLARIANT was used as comparison to the standard commercial zirconia. It is clear that the nature of the ZrO_2 support strongly affects the performance. Actually, the catalyst based on the CLARIANT-provided ZrO_2 showed 89% ethanol conversion with 49% selectivity for ethylene oxide whereas the commercial ZrO_2 only gave 17% ethanol conversion without any selectivity for ethylene oxide. An increase in performance of the Al_2O_3-supported catalyst was also observed applying the optimized reaction conditions: conversion of ethanol (52% vs. 39% previously) and selectivity for ethylene oxide (21% vs. 15% previously).

From the performance point of view, TiO_2-supported catalysts always showed the best performance. On the other hand, the presence of anatase phase in TiO_2 seems to be crucial in the ethylene oxide formation as no EO is detected using the rutile phase alone. It has to be reminded here that the TiO_2–P25 catalysts contains mainly the anatase phase. The copper catalysts based on the other supports (SiO_2, ZrO_2-Ald and activated carbon) seem completely inactive for the ethylene oxide formation at optimized reaction conditions and showed selectivity towards acetaldehyde only.

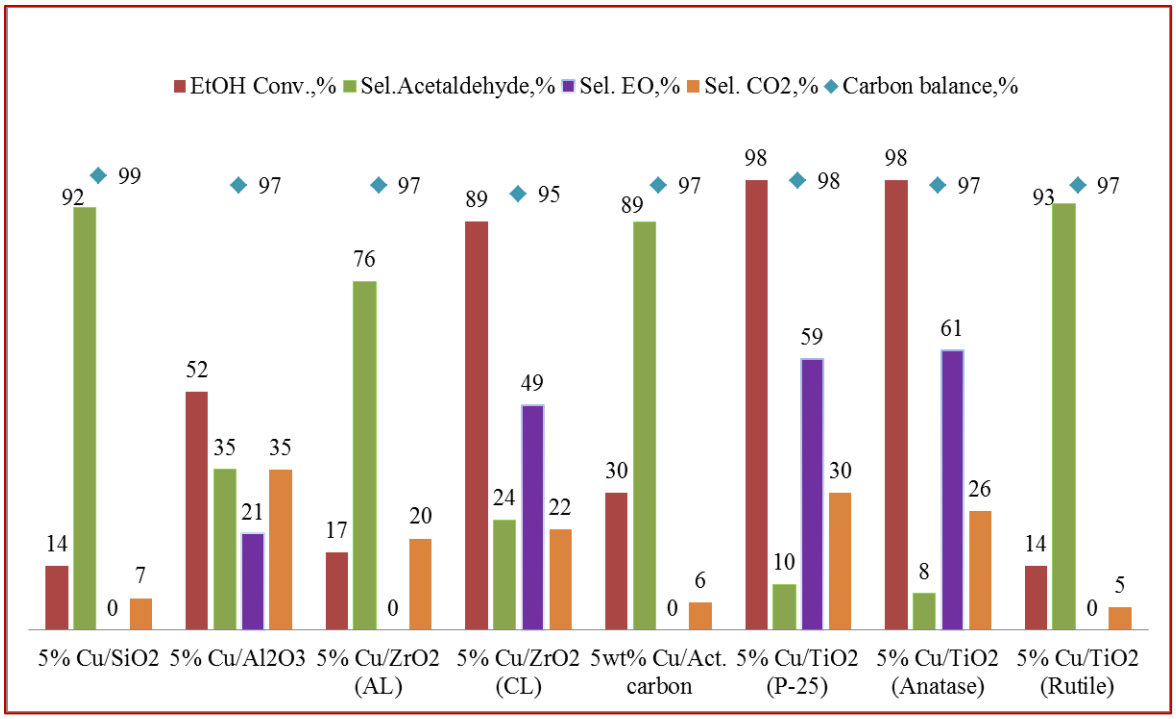

Figure 4-4: Catalytic performance of copper catalysts with various supports

***Reaction conditions**: Ethanol: 15 mol.%, Carrier gas: Helium, Reaction temperature: 250 °C, Cat. wt.: 0.1 g, EtOH:O_2=1:2 (molar), Total gas flow at RT: 20 mL/min, Pressure: 1 atm., Time on stream: 15 h*

4.1.5 Influence of the activation temperature

A study of the effect of a pre-reduction of the catalysts on the performance was also carried out. The catalysts were reduced at 300°C in the presence of 5% H_2/He flow prior to reaction. The catalytic performance of the as-reduced catalysts based on the various supports was determined at 250°C and the results were compared to those of the non-pre-reduced catalysts.

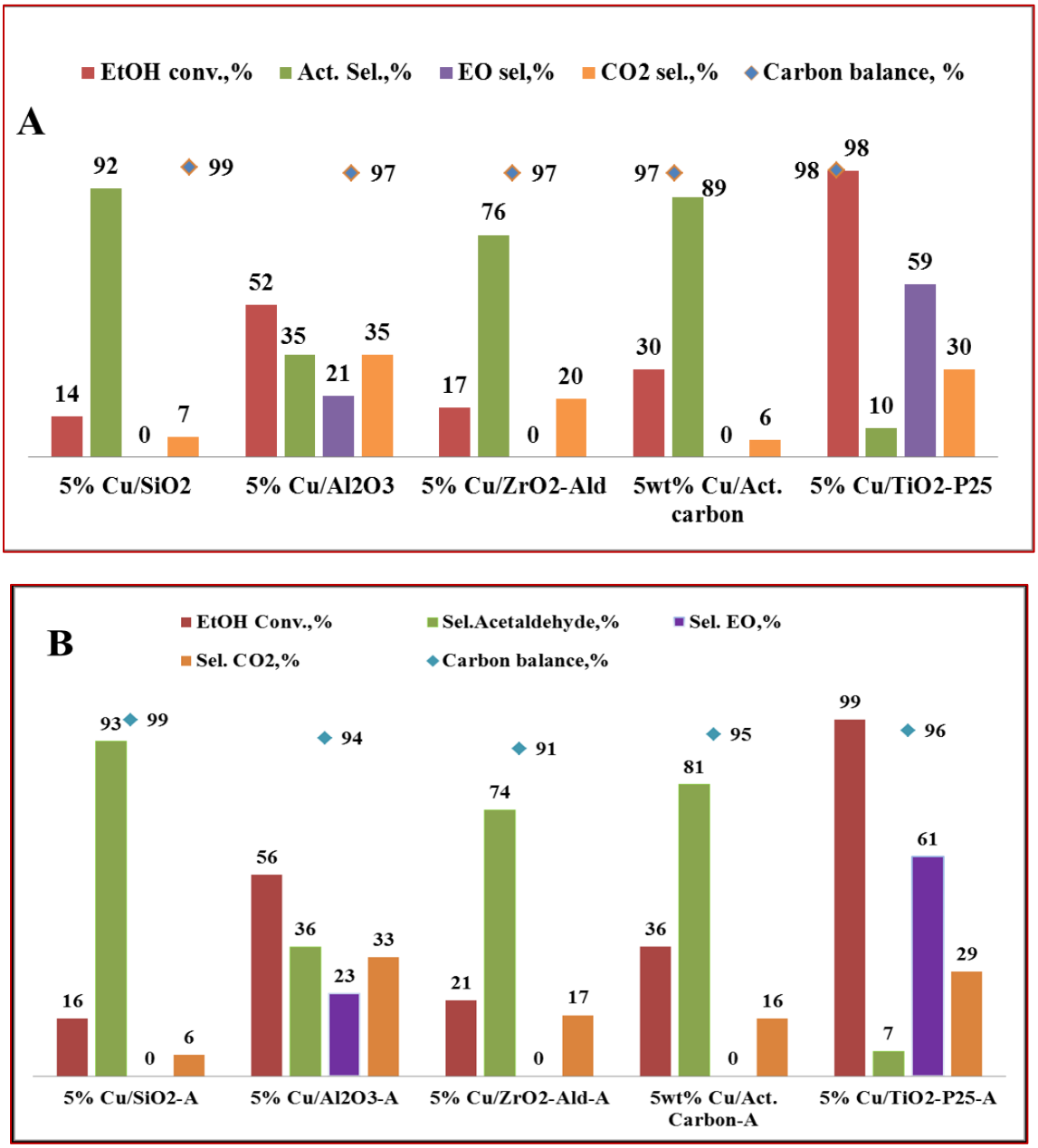

Figure 4-5: Catalytic activity of A- Non-activated and B- Activated copper catalysts

***Reaction conditions**: Ethanol: 15 mol.%, Carrier gas: Helium, Reaction temperature: 250 °C, Cat. wt.: 0.3 g, EtOH:O_2=1:2 (molar) ; Total gas flow at RT: 20 mL/min, Pressure: 1 atm., Time on stream: 15 h*

From Figure 4-5 B, one can see that the activated copper catalysts showed similar results as the non-activated ones (Figure 4-5 A), no matter the support used. To conclude, the hydrogen pre-activated catalysts showed no advantage over the non-pre-activated catalysts, meaning

probably that the activation takes place under the reaction flow conditions even if the oxygen is in stoichiometric excess.

4.1.6 Influence of the calcination temperature

The effect of the catalyst calcination temperature on the catalytic activity was investigated on 5 wt.% Cu/TiO_2–P25 by pre-treating the catalyst at different temperatures (400-800 °C). The main purpose of this study was to check the influence of copper particle size on catalytic activity. As shown in Figure 4-6, the activity of a catalyst for ethanol oxidation decreases with increasing the calcination temperature. The ethylene oxide selectivity as well as the conversion was decreased gradually as the catalyst calcination temperature increased from 400 °C to 800 °C (59% vs. 0% EO selectivity and 98% vs. 10% Ethanol conversion). It is clear from these data that the optimal calcination temperature is 400°C for the 5 wt.% Cu/TiO_2–P25 catalyst.

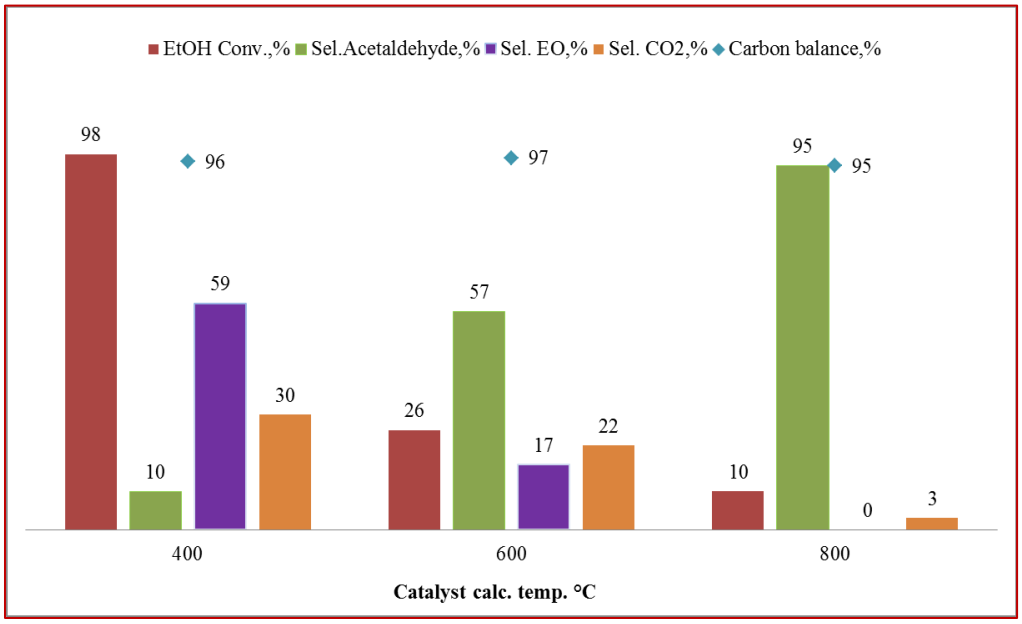

Figure 4-6: Effect of catalyst calcination temperature

***Reaction conditions**: Ethanol: 15 mol.%, Carrier gas: Helium, Reaction temperature: 250 °C, Cat. wt.: 0.1 g of 5%Cu/TiO_2-P25, EtOH:O_2=1:2 (molar) ; Total gas flow at RT: 20 mL/min, Pressure: 1 atm., Time on stream: 15 h*

4.2 Catalysts detailed characterization and discussion

Detailed characterization results for the calcined and spent catalysts are described and correlated to their catalytic performance in the following paragraphs. The catalysts were characterized by XRF, XRD, TPR, XPS, SEM and TEM techniques.

4.2.1 Copper catalysts supported on TiO_2-P25

A. Bulk composition of catalysts by XRF

The bulk compositions of the TiO_2-P25-supported copper catalyst with different loadings were determined by X-ray fluorescence. The results are shown in Table 4-1. The experimental values obtained were in all cases very close to the theoretical values. Furthermore, the standard deviations of the composition were close to zero, meaning that the composition of copper species was homogeneous on the support and that no agglomeration of Cu took place.

Table 4-1: Textural properties and Cu contents of TiO_2-supported copper catalysts

Catalyst	S_{BET} (m^2/g)	V_P (cm^3/g)	Pore radius (Å)	XRF Cu content (SDV)* (wt.%)
TiO_2-P25	52	0.44	137	-
0.2% Cu/TiO_2-P25	53	0.41	122	0.2 (0.01)
1% Cu/TiO_2-P25	50	0.38	128	1 (0.22)
2.5% Cu/TiO_2-P25	46	0.40	129	2.7 (0.15)
5% Cu/TiO_2-P25	41	0.37	134	5 (0.19)

***Standard Deviation Value**

B. Surface area and porosity

The textural properties of the TiO_2-P25-supported copper catalysts are also given in Table 4-1. The surface area and pore volume of the catalysts decreased gradually with the increase of copper loading, whereas the mean pore radius remained rather constant (Figure 4-7 B). This gradual decrease suggests that the pore network remains unchanged and fully accessible, confirming again the good dispersion of Cu on the support, as already found from XRF. Figure 4-7 (A and B) shows the N_2 adsorption-desorption isotherms and pore size distributions of pure TiO_2 and copper-impregnated TiO_2. The copper-impregnated TiO_2 displays a classical type IV

nitrogen isotherm compared with pure TiO_2, indicating the presence of well-defined mesoporous structure with pore diameter of ≈14 nm [1].

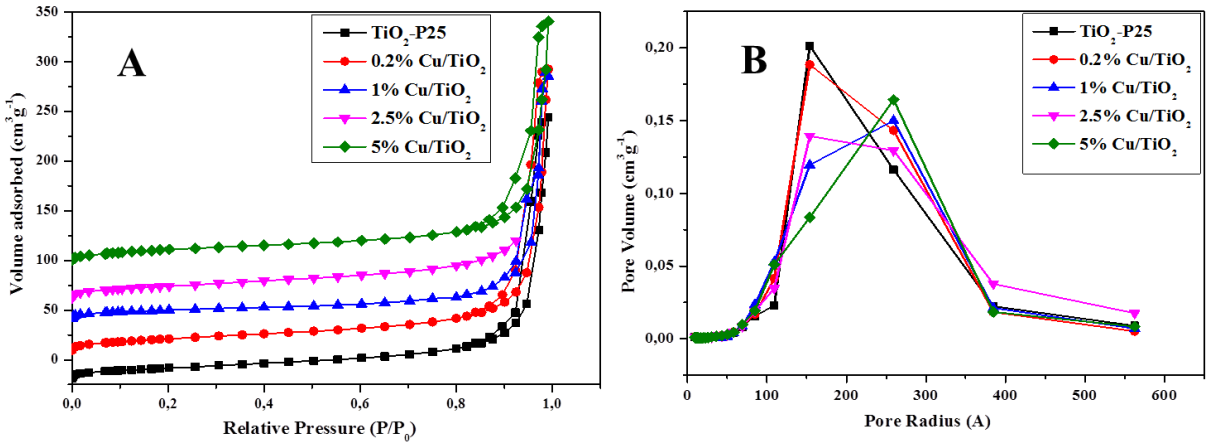

Figure 4-7: N_2 adsorption-desorption isotherm (A) and pore size distribution (B)

C. X-ray diffraction results

➢ Fresh catalysts

Figure 4-8 shows the XRD pattern of fresh TiO_2-P25-supported copper catalysts with different loadings. The only remarkable signals arise from the support in which anatase (JCPDS 21-1272) and rutile (JCPDS 21-1276) phases of TiO_2 were identified [2]. Even when the Cu loading increases from 0.2% to 5 wt.%, no characteristic diffraction peaks for copper species were observed, which can be explained by (i) uniform dispersion (ii) low Cu loading or (iii) weak crystallinity of copper particles. Since the titania patterns showed no change in intensities and width, one can conclude that the structure and crystalline size of TiO_2 where not significantly altered during the catalyst preparation. For comparison one catalyst was prepared with 10 wt.% copper loading. The latter exhibited characteristic diffraction peaks at 35.6° and 38.6° 2θ ascribed to the CuO species (particle size 17 nm). Thus one can assume that 5 wt.% copper loading is optimal for well dispersed Cu and controlled particle size of less than the 17 nm.

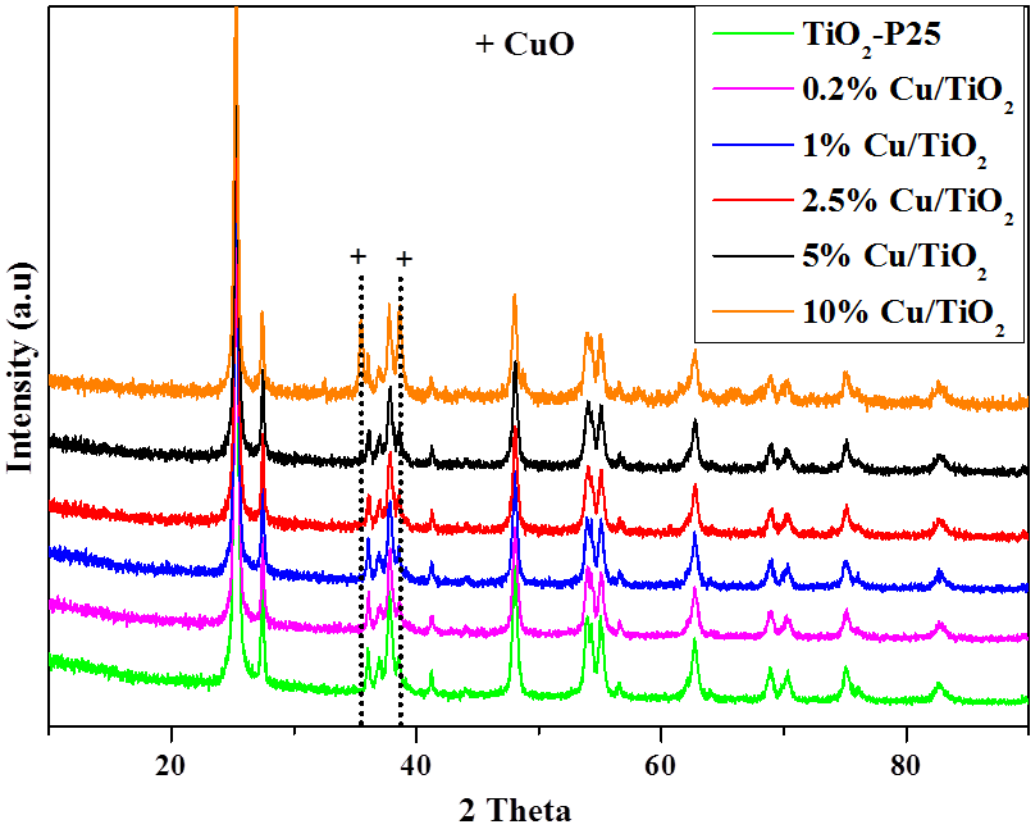

Figure 4-8: XRD pattern of TiO_2-supported copper catalysts

➢ *In situ* reduction followed by Temperature-Programmed XRD

The reduction of the 5 wt.% Cu/TiO_2 catalyst was studied by temperature-programmed XRD in presence of hydrogen as reducing gas (5% H_2/He). The experiment was performed from room temperature to 450 °C and the XRD patterns obtained are shown in Figure 4-9. A change in the diffraction pattern was observed with increasing temperature: Until 100 °C no change was observed but when the temperature increased from 100 to 400 °C a characteristic peak of Cu° species (2θ = 43.3°) became visible and more intense [3]. No characteristic peak of Cu_2O was observed [2], one can assume that a direct transformation of Cu^{2+} to Cu^0 took place during reduction without formation of Cu_2O crystallites. After cooling back to room temperature (under reducing atmosphere), the XRD pattern still exhibited the characteristic peak of Cu° with the same intensity. Thus, one can see from the temperature programmed XRD pattern of catalyst that

the minimum temperature required for the reduction of copper species on TiO_2 surface is in the range of 100-150°C.

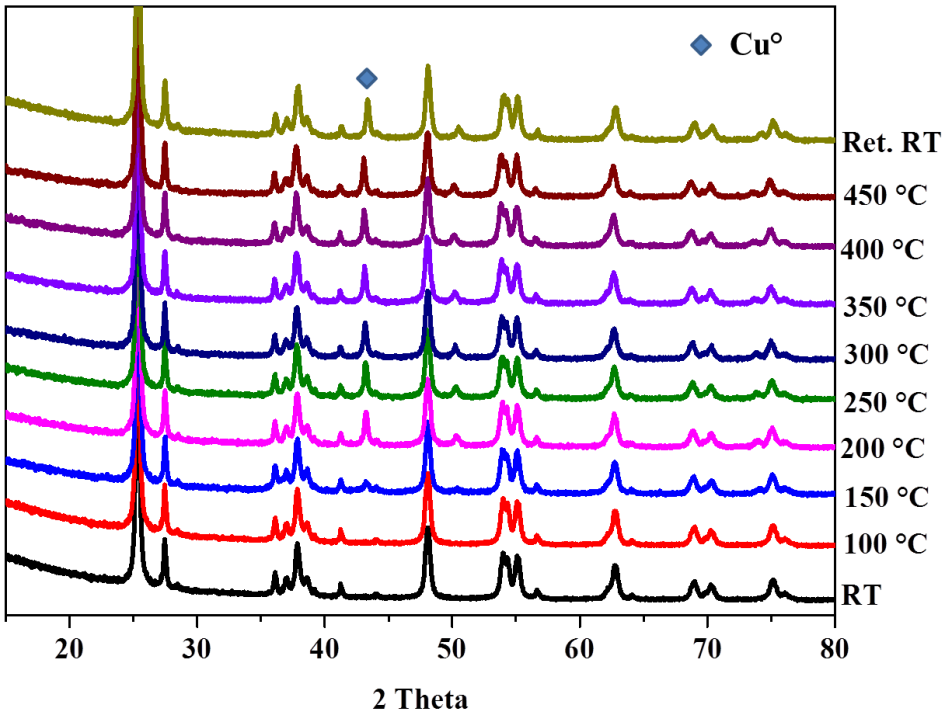

Figure 4-9: Temperature programmed XRD results over 5 wt.% Cu/TiO_2–P25 in presence of H_2

➢ X-Ray diffraction of spent catalysts

XRD analysis was performed on the 5 wt.% Cu/TiO_2–P25 catalyst recovered after the catalytic test to study any possible change in the copper phases under the stream. As aforementioned, the freshly calcined catalyst showed characteristic diffraction peaks of TiO_2 only without any pattern for copper species (*cf.* Section 3.1.3 Figure 3-12). Figure 4-10 shows the XRD patterns of the catalyst after reaction. One can distinguish the presence of metallic copper (Cu°) species at 43.2° and 50.3° 2θ (JCPDF 04-0836). No diffraction peak was observed for Cu_2O at 36.2° in the spent catalyst. However, it is difficult to distinguish Cu_2O peak due to overlapping with the diffraction peak of TiO_2 support. With respect to the previous study on the influence of the activation by pre-reduction (*cf.* Section 4.1.5 Figure 4-5), the activated (A) used catalyst was also analyzed by XRD after the test. As for the fresh activated catalyst, the presence of metallic Cu° was still observed. The particle size of metallic copper was calculated to be 24-25

nm for both – activated and non-activated – catalysts confirming the non-influence of the activation pre-treatment.

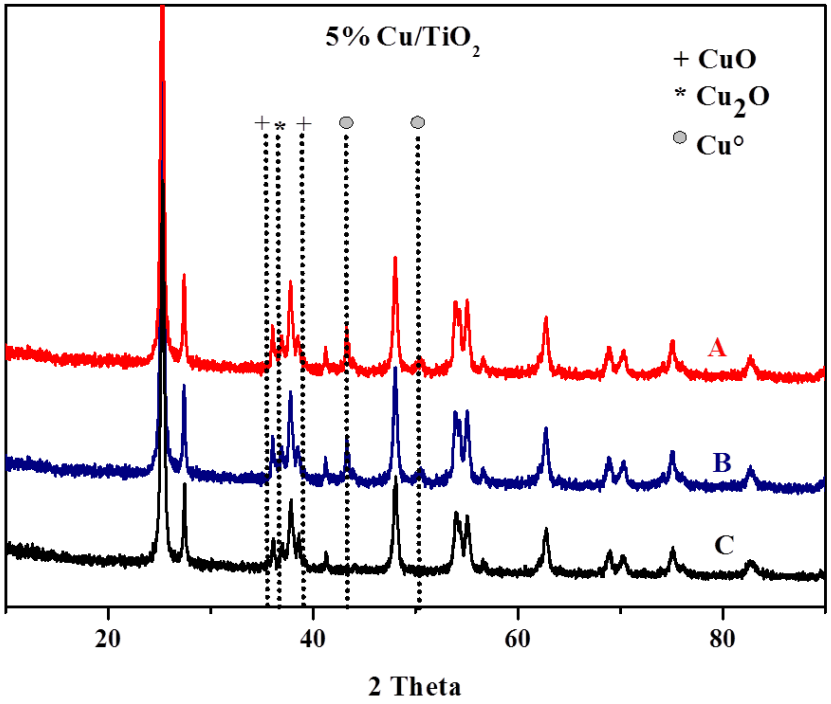

Figure 4-10: XRD patterns of spent catalysts (5 wt.% Cu/TiO_2-P25)

A - activated spent, B - non activated spent and C – calcined

D. H_2-TPR analysis

- TPR of calcined catalysts

The different copper species present on the TiO_2–P25 support were further investigated by temperature programmed reduction under hydrogen (H_2-TPR). The corresponding TPR profiles of the Cu/TiO_2 catalysts with different copper loadings are depicted in Figure 4-11A. Since the TiO_2 support is known [4] to be almost irreducible at temperatures lower than 400 °C, the reduction peaks should correspond exclusively to the reduction of the different types of copper oxide species.For the catalysts having a copper loading from 1 to 5 wt.%, three reduction peaks at 116 °C, 138 °C and 207 °C were observed.

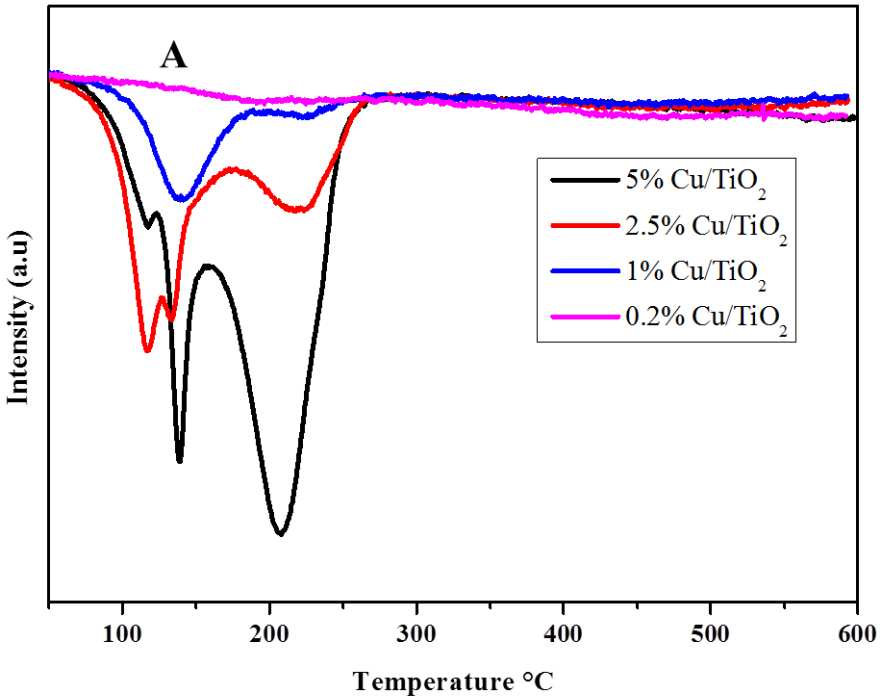

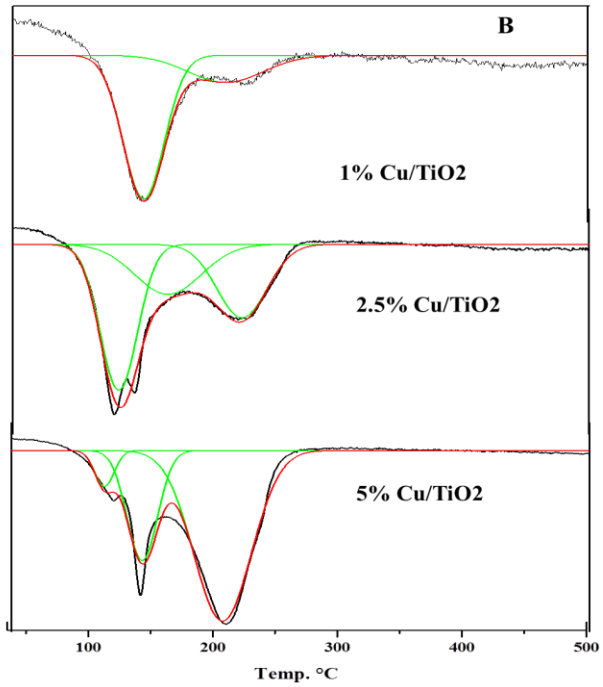

Figure 4-11: A- H_2-TPR and B- H_2 consumption distribution

The peaks at 116 °C and 138 °C correspond to the reduction of highly dispersed copper species on TiO_2 [5]. Besides, the reduction peak at 207 °C was assigned to the reduction of crystalline CuO [6]. It is worth mentioning that all the reduction peaks of the Cu/TiO_2 samples occur at lower temperatures than for pure CuO which can be explained either by an interaction between the copper species and the support [7], or by highly dispersed and small CuO particles [8-10]. In conclusion the H_2-TPR results are in good agreement with the *in situ* temperature-programmed XRD results presented previously (section 4.2.1-C)

The total hydrogen consumption, the hydrogen consumed for each peak and the corresponding quantity of copper oxide species were calculated. The results for each catalyst are shown in Figure 4-12. One can see that the total hydrogen consumption increased linearly with the copper loading and is close to the theoretical hydrogen consumption, meaning that most Cu is accessible to hydrogen, even at increased loading. Furthermore, the distribution of the different copper species (highly dispersed and bulk type) was determined by deconvolution (Figure 4-11B). The relative amount of highly dispersed copper species decreased with the amount of Cu, whereas bulk type CuO species gradually increased. Whereas the 5 wt.% Cu/TiO_2 catalyst showed 29% highly dispersed and 71% bulk type CuO, the 1 wt.% Cu/TiO_2 catalyst showed 74% highly dispersed and 36% bulk type CuO.

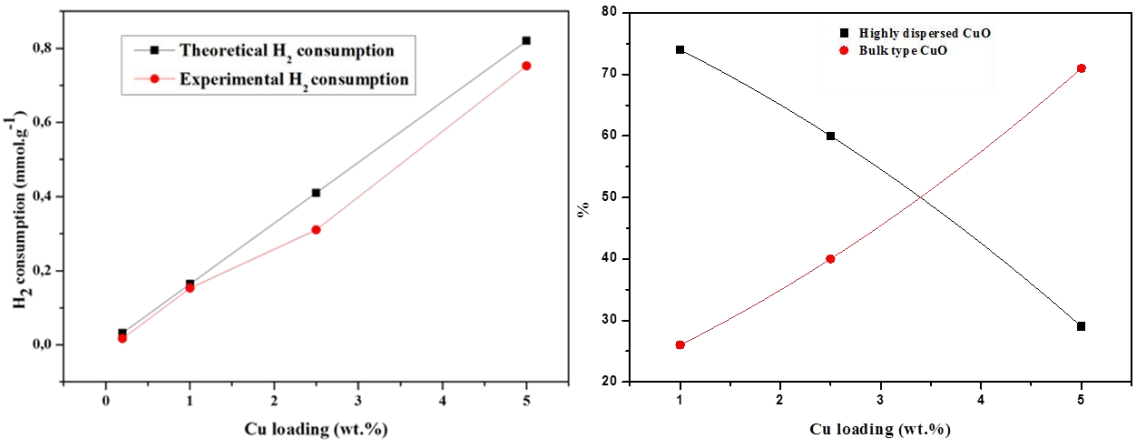

Figure 4-12: Total H_2 consumption and distribution of copper species

➢ TPR of spent catalyst

TPR was performed for the used 5 wt.% Cu/TiO_2–P25 catalyst and compared to the H_2 profile obtained before reaction (Figure 4-13). From the quantification one can see that the spent catalyst consumed less hydrogen compared to the corresponding freshly calcined one (0.211 $mmol.g^{-1}$ vs. 0.753 $mmol.g^{-1}$). This can be explained by the fact that the spent catalyst exhibited the presence of already reduced phase, meaning that most of the copper species are in Cu° form. The total amount of copper present in the fresh calcined catalyst was 0.0052 g and after reaction out of that 0.0014 g of copper is in the oxidized form. These results are in agreement with XRD analysis and XPS analysis (*cf.* Section 4.2.1) of the spent catalysts.

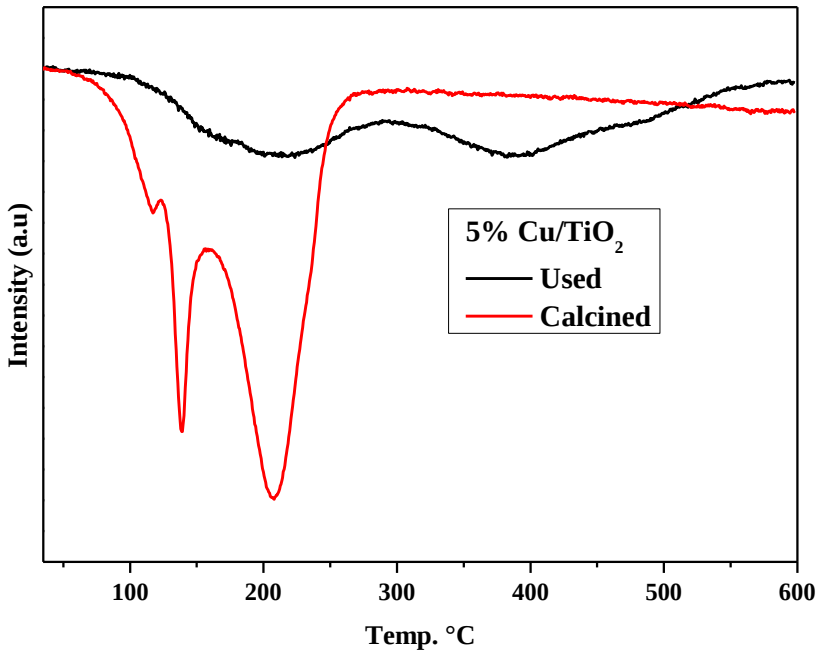

Figure 4-13: H_2-TPR study of calcined and used catalysts (5% Cu/TiO_2-P25)

E. X-ray Photoelectron Spectroscopy

XPS analysis was used to characterize the nature of the species constituting the surface layer of the calcined catalysts. X-ray photoelectron spectra of the catalyst with different amounts of copper loading on TiO_2 are shown in Figure 4-14 A, B, C and D. The XPS surface compositions are summarized in Figure 4-15. The binding energies of 932.5 eV and 952.3 eV corresponding to the Cu 2p region were associated to Cu° or Cu_2O (Cu^+) species [11]. On the other hand binding energies of 934.4 eV and 954.0 eV were assigned to CuO (Cu^{+2}) [2, 12]. The

small peak observed at about 944 eV was the Cu $2p_{3/2}$ satellite peak. In the catalyst with 0.2% Cu loading, one single peak at a binding energy of 932.1 eV was observed, meaning that the all copper species are in oxidation state Cu^{+} (highly dispersed). A shake-up satellite at about 942 eV was observed, ruling out the presence of Cu^{2+} species [13]. It should be noted that the satellite peak are not seen in the case of Cu^{+} species because of completely filled 3d shells. For higher loadings of copper (1 - 5%), the presence of at least two kinds of surface copper species (Cu^{+} and Cu^{2+}) is observed. According to the literature reports, the peak appearance of Cu^{+} was possible because of the reduction of Cu^{2+} to Cu^{+} resulting from the bombardment effect by X-ray irradiation under ultra-high vacuum, when Cu content was low and existed in highly dispersed state on TiO_2 surface [14]. It was found that highly dispersed copper oxide species gradually decreased with increasing the copper loading, giving rise to bulk copper oxide species (Figure 4-14). These results are in agreement with the temperature-programed reduction (TPR) (*cf.* section 4.2.1D Figure 4-11A). From the correlation with the catalytic results, we suggest that the selectivity to ethylene oxide is dependent on the nature of the copper species present in the catalyst and of course of its nature. For example, the catalysts presenting an exclusive presence of well-dispersed Cu^{+} species (0.2% copper loading) showed no selectivity at all for EO suggesting that the amount and the nature of the copper species in presence in this catalyst is not appropriate to reach a high catalytic performance (Figure 4-3).

Table 4-2: Surface composition and peak positions in the XPS analysis of Cu/TiO_2–P25 catalysts

Copper loading, wt.%	Cu^{+2} (eV)	Cu^{+} (eV)	Cu^{2+} (%)	Cu^{+} (%)	Cu/Ti
0.2	-	932.1	0	100	0.011
1	933.7	932.3	22	78	0.034
2.5	933.6	931.97	64	36	0.073
5	933.65	932.3	71	29	0.076

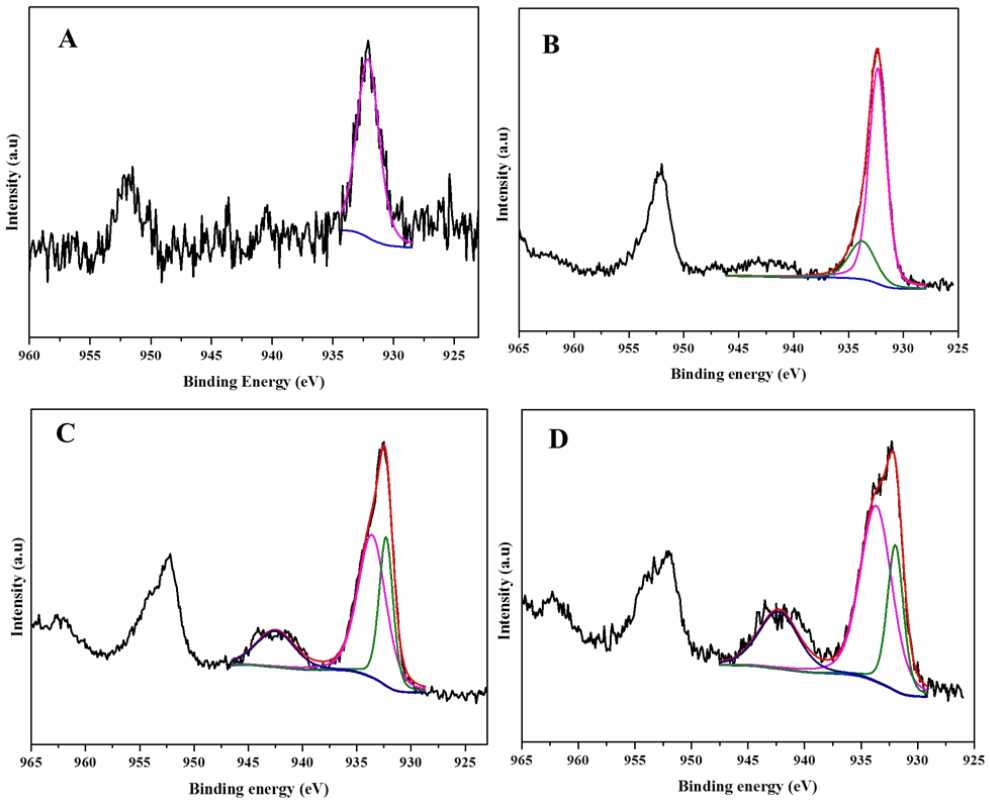

Figure 4-14: XPS spectra of TiO_2-P25-supported copper catalysts
A - 0.2 wt.%, B – 1 wt.%, C - 2.5 wt.% and D – 5 wt.%

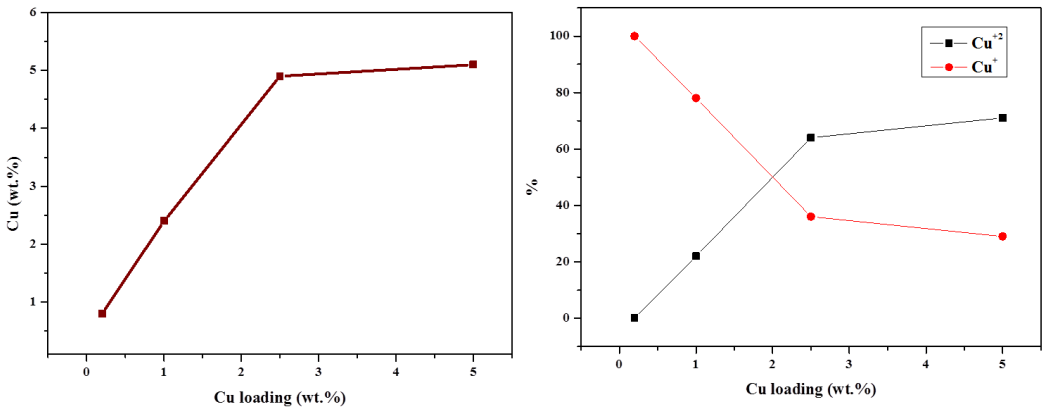

Figure 4-15: Surface composition (A) and oxidation states distribution of Cu (B) of Cu/TiO_2–P25 catalysts

➢ XPS of spent catalyst

The X-ray photoelectron spectra of the spent catalyst (5 wt.% Cu/TiO_2-P25) was recorded to check whether the Cu oxidation state changed during the reaction, as suggested by TPR and XRD (*cf.* Sections 4.2.1 C & D). The spectrum is shown in Figure 4-16. After deconvolution of the peaks, two kinds of copper species were observed in the spent catalyst: The binding energies 932.0 eV and 933.9 eV were attributed to the $Cu°/Cu^{+}$ and Cu^{2+} respectively. The amount of copper was found lower on the surface than for the calcined 5 wt.% Cu/TiO_2 (3.9% vs. 5.8%). The distribution of copper species was determined and the ratio of $Cu^{+}/Cu°:Cu^{+2}$ = 1:1, corresponding to a significant increase of the $Cu^{+}/Cu°$ compared to the calcined catalyst. These results are in good agreement with the XRD and TPR results of the spent 5 wt.% Cu/TiO_2 catalyst, showing the partial reduced phase: XRD confirmed the presence of a Cu° phase in the spent catalyst and TPR showed lower hydrogen consumption. Nevertheless, one should mention that XPS proved the presence of 50% Cu^{2+} copper species, which was not observed by XRD, maybe due to the too small size of the copper particles.

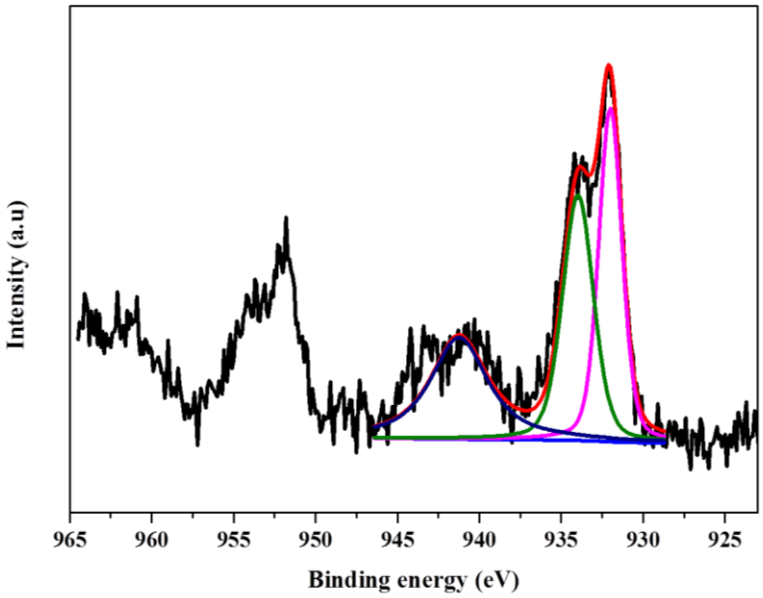

Figure 4-16: XPS of spent catalyst (5 wt.% Cu/TiO_2-P25)

F. Thermal Gravimetric Analysis (TGA)

The fresh and spent, 5 % Cu/TiO_2-P25 catalysts were analyzed using TGA in order to determine the optimal calcination temperature. The weight loss curves of the dried sample

exhibited two weight losses at 100 °C and 350 °C shown in Figure 4-17. The first one at 150 °C was due to the endothermic loss of surface adsorbed water molecules. The following weight loss in the range of 150 °C to 350 °C corresponds to the decomposition of the copper nitrate precursor. After 350°C, no further loss in the weight was observed up to 800 °C, indicating that the catalyst is thermally stable at high temperature. The heat flow data confirmed that the decomposition of copper nitrate was exothermic. In order to achieve full decomposition, the calcination temperature was fixed to 400 °C for all copper catalysts.

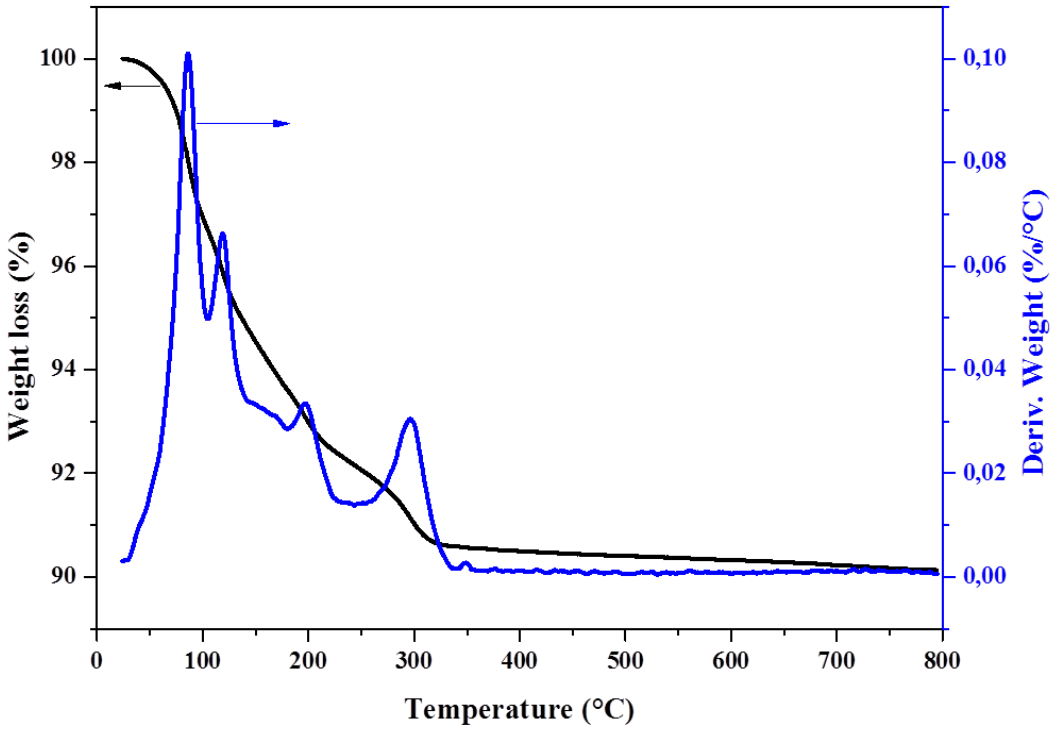

Figure 4-17: TGA profile of the fresh 5% Cu/TiO_2-P25 catalyst

After the stability test (*cf.* Section 3.2.3), the spent 5 wt.% Cu/TiO_2 catalyst was collected after 50 h under stream and characterized by TGA to determine if any coke deposition occurred on the surface (Figure 4-18). Two main different weight losses were observed, the first at around 150 °C ascribed to adsorbed surface water and two further at around 290 °C and 700 °C due to carbon deposit as shown by the formation of carbon dioxide which was confirmed by mass spectroscopy. Calles *et al.* reported that amorphous carbon is oxidized below 550 °C whereas, filamentous and graphitic carbons require high temperature for oxidation (>650 °C) [15]. In the present study, the intense peak at 290 °C may hence be due to the formation of amorphous carbon

and the less intense peak at 700 °C due to the formation of small amounts of graphitic carbon. Despite the formation of these carbonaceous species, the stability of the catalyst over time on stream was found constant up to 50 h under the stream. This may be explained by the presence of oxygen in the stream that limit the carbon deposit and hence regulate the deactivation process.

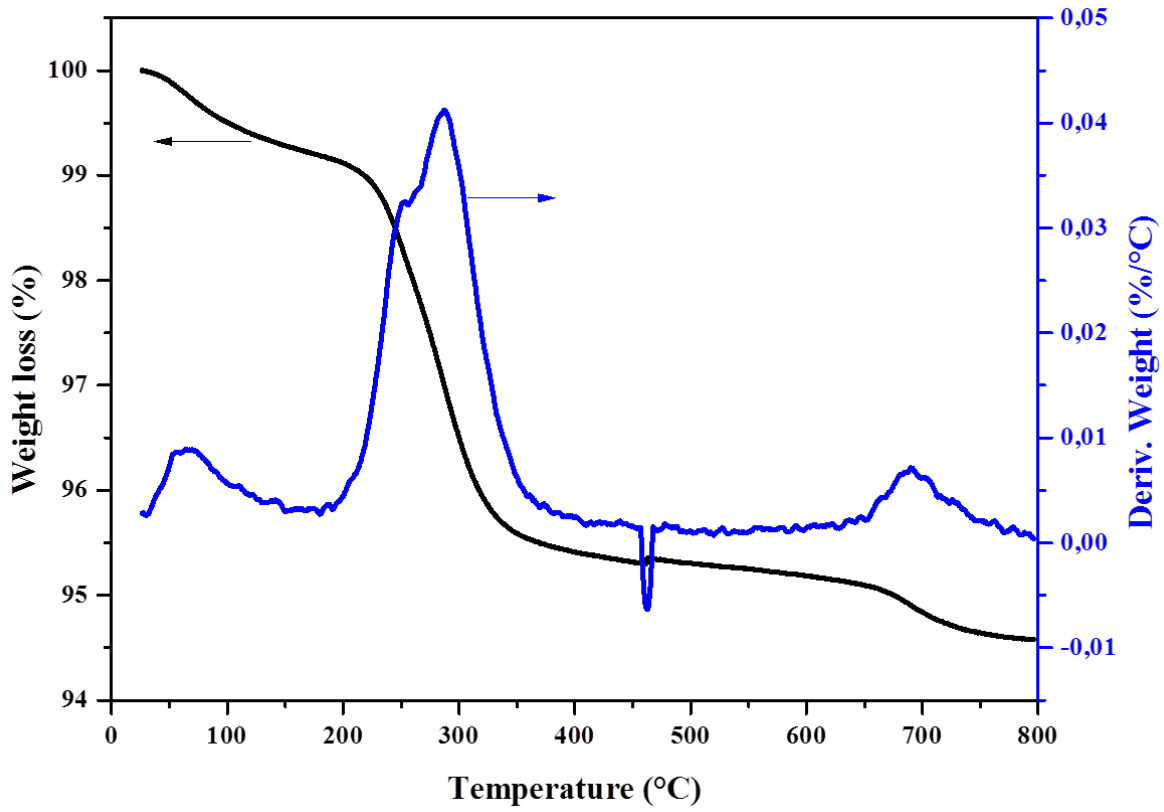

Figure 4-18: TGA profile of the spent 5% Cu/TiO_2-P25 catalyst

G. Transmission Electron Microscopy analysis (TEM)

Transmission Electron Microscopy (TEM) images offer the possibility to access to the metal particle size and the dispersion of the metal on the support. Figure 4-19 A, B, C and D shows the TEM images of the P25 titania-based catalysts with different Cu loadings. The TiO_2 support (P25) itself showed spherical particles with particle size around 25 nm. On the other hand, the copper particles were not only in the spherical shape but also polyhedral. For the catalysts with low loadings of copper, the particle size was smaller than for those with higher loading: The sample containing 0.2 wt.% Cu loading had copper particles with diameter around 7-14 nm whereas the copper catalysts with 2.5 and 5% loading showed the almost similar kind of

particle size of 7-22 nm, meaning that no significant agglomeration took place at increased Cu loading. In all cases a uniform distribution of copper particles was observed for all loadings. But of course, the copper particle density is less at low copper loading. These results are in good agreement with TPR and XRD analyses (*cf.* Section 4.2.1C).

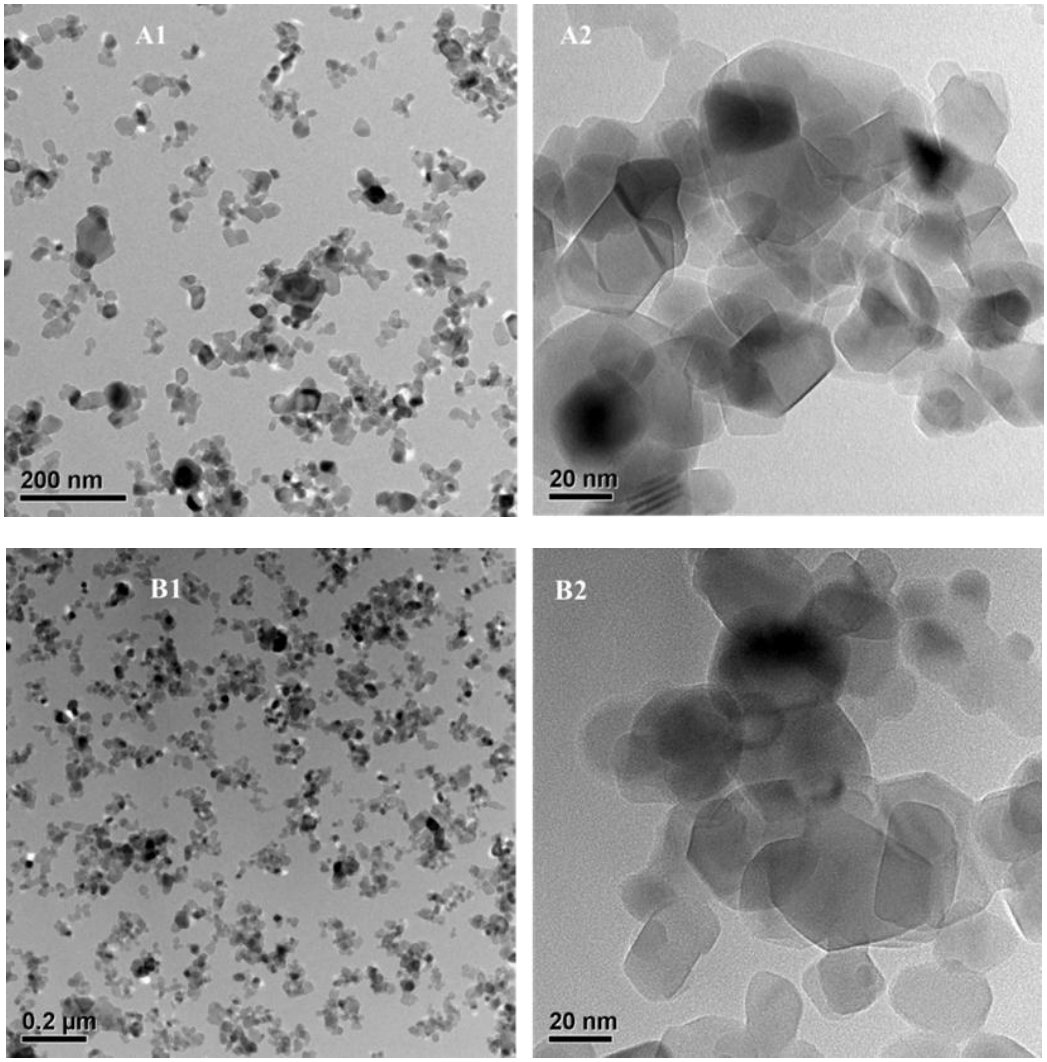

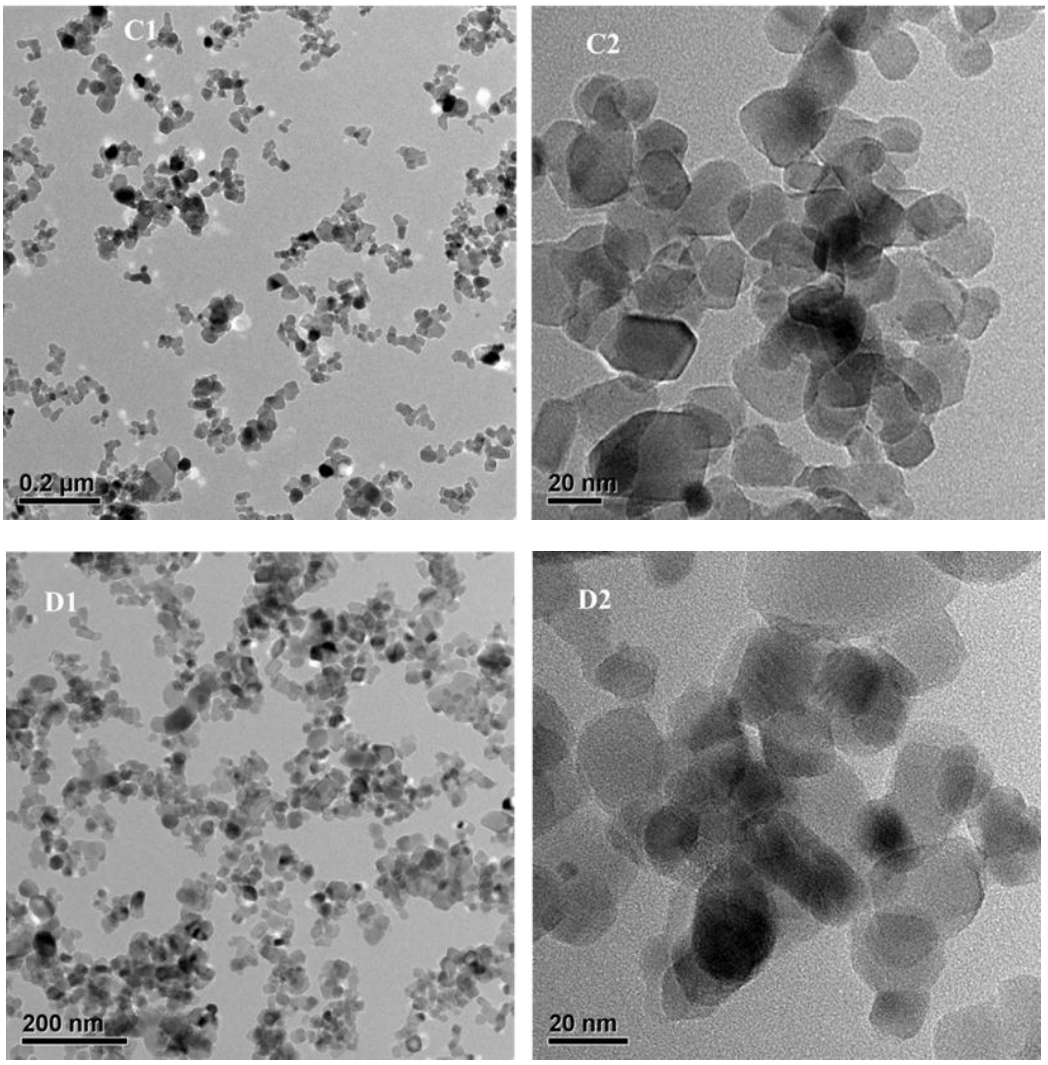

Figure 4-19: TEM images of Cu/TiO_2-P25 catalysts with different Cu loadings (A-0.2 wt.%; B-1 wt.%; C-2.5wt.% and D-5 wt.%)

H. Scanning Electron Microscopy (SEM) with EDX mapping

Scanning Electron Microscopy (SEM) with EDX mapping was performed to visualize the distribution of copper on the support. The SEM mapping images for all catalysts are shown in Figure 4-20. The red dots correspond to the copper particles in each catalyst. As expected, an increase in the copper particle density with the copper loading was observed. Furthermore the distribution of the Cu was found uniform in the all TiO_2-P25-supported copper catalysts.

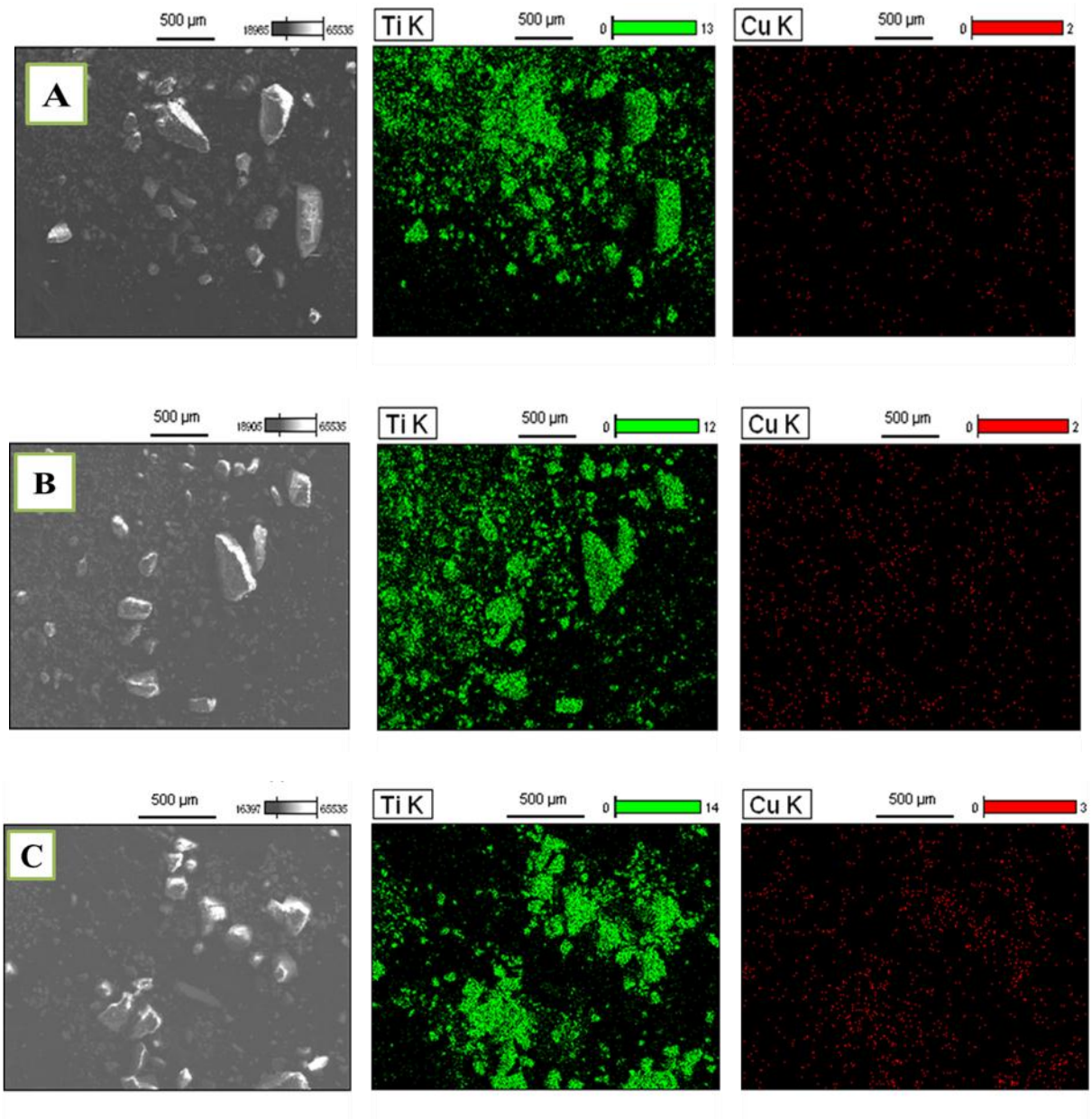

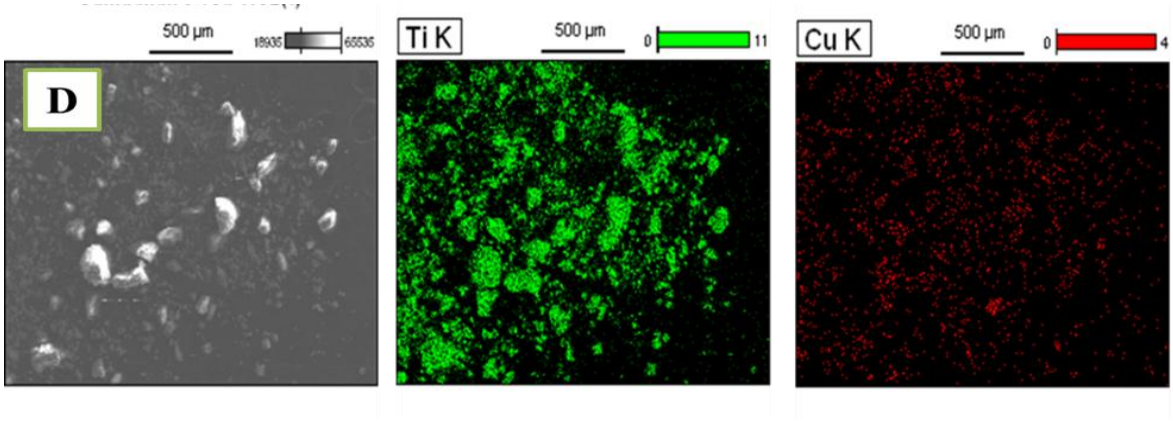

Figure 4-20: SEM images of of Cu/TiO_2-P25 catalysts with different Cu loadings (A-0.2 wt.%; B-1 wt.%; C-2.5wt.% and D-5 wt.%)

4.2.2 Copper catalysts based on various TiO_2 phases

A. Textural properties

The surface areas, porous volumes and mean pore radius of copper catalysts supported on different TiO_2 phases and calcined at different temperatures are shown in Table 4-3.

Table 4-3: Textural properties of Cu catalysts supported on different TiO_2 phases and calcined at different temperatures

Catalyst (Calc. temp.)	S_{BET} (m^2g^{-1})	V_P (cm^3g^{-1})	Pore radius (Å)
5% Cu/TiO_2-Anatase (400 °C)	72	0.36	80
5% Cu/TiO_2-P25 (400 °C)	41	0.37	134
5% Cu/TiO_2-Rutile (400 °C)	6	0.023	167
5% Cu/TiO_2-P25 Calc. 600°C	17	0.12	136
5% Cu/TiO_2-P25 Calc. 800°C	2	0.0014	38

The surface area decreased according to the following order anatase>P25>rutile. Pore volumes of the anatase and P25 phases were similar (0.36 vs. 0.37 $cm^{3}.g^{-1}$) whereas it is much lower for rutile (0.023 $cm^{3}.g^{-1}$). The rutile phase also presents a considerably lower surface area (6 $m^{2}.g^{-1}$) compared to P25 and anatase.

The surface area as well as the porosity of the catalysts decreased strongly when the calcination temperature is increased. The corresponding surface areas of the 600 and 800°C calcined catalyst are 17 and 2 $m^{2}.g^{-1}$ resp. After a calcination at 400, 600 and 800 °C, the pore volume decreased from 0.37 to 0.12 and 0.0041 $cm^{3}.g^{-1}$ respectively.

B. XRD patterns

The XRD patterns of the catalysts based on copper supported on different kinds of TiO_2 (anatase, P25 and rutile) are shown in Figure 4-21. The copper supported on anatase and P-25 did not exhibit any peaks for copper oxide. On the contrary, the sample based on rutile support showed visible peaks of CuO. One may assume that the copper particles were not well dispersed over the rutile phase, which may be ascribed to the low surface area of this support.

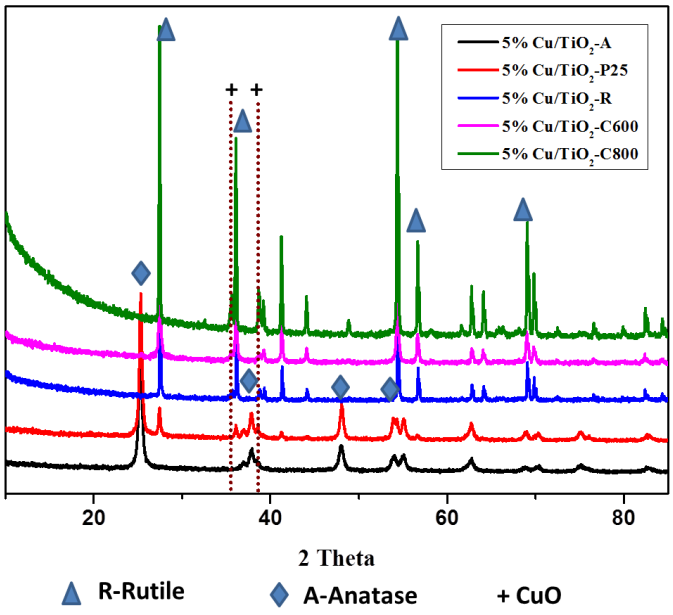

Figure 4-21: XRD patterns of Cu-based catalysts supported on different TiO_2 phases and calcined at different temperatures

In order to determine the influence of the particle size, the 5% Cu/TiO_2-P25 catalyst was calcined at different temperatures (600 and 800°C). It is observed that with the increase of the

calcination temperature the intensity of CuO peak increased, suggesting that the copper particle size was increased progressively (41 nm and 56 nm respectively) by a sintering phenomenon. Nevertheless, this went hand in hand with the phase transition from anatase to rutile, whereby the effect of the particle size was not clearly measurable (Figure 4-21).

C. H_2-TPR study

As seen before the catalyst based on TiO_2 (P25) support was found the best in terms of catalytic activity. To investigate the effect of the TiO_2 phase (Anatase, P25 and Rutile) on the reduction properties of copper, TPR analysis was performed and the profiles are shown in Figure 4-22. One can see that the anatase phase exhibited two reduction peaks at around 200 °C for the reduction of well-dispersed copper particles and a small shoulder at around 261 °C for the bulk copper species. Nevertheless, the rutile phase showed a single reduction peak at high temperature (264 °C). This result suggests the formation of not well-dispersed – bulk-like – copper oxide species during the synthesis. The hydrogen consumptions for anatase and rutile-based catalysts were 0.69 and 0.72 mmol.g^{-1} respectively, which is close to the theoretical value. For P25-based catalyst the reduction of one part of the Cu species occurred at even lower temperature (<150 °C). As a conclusion, copper species over anatase and P25 phases are reduced at lower temperature than in case of rutile support. This could be one reason why a better catalytic performance is observed over these catalysts.

Concerning the 5 wt.% Cu/TiO_2 catalyst calcined at 800°C, initially synthesized to investigate the effect of particle size on the catalytic performance, the TPR profile (Figure 4-22) shows two reduction peaks at 328 °C and another at very high temperature of 576 °C. Both peaks correspond to the reduction of big particles of bulk copper oxide species, supposedly easily formed by sintering at high temperature treatment as suggested by XRD (*cf.* section 4.2.2 A). Thus one can conclude that both, rutile phase as well as the high calcination temperature, are not favorable for the catalytic activity.

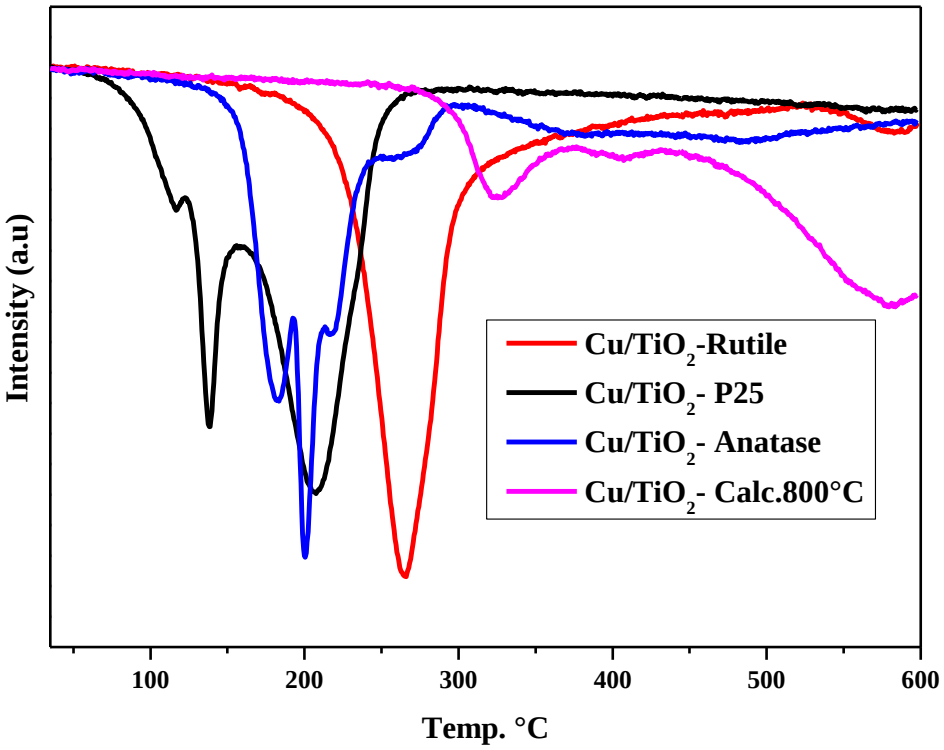

Figure 4-22: H_2-TPR profiles of Cu-based catalysts supported on different TiO_2 phases and calcined at different temperatures

4.2.3 Role of the support for copper-based catalysts

As we have seen in the previous sections the copper catalysts based on other kinds of supports than anatase-containing titania are not very efficient for ethylene oxide formation from ethanol. The following section is dedicated to the study of the influence of the nature of the support on the nature of the Cu species formed at the surface of the catalyst .

A. X-Ray Diffraction of the spent catalysts

The X-ray diffraction patterns of the spent copper catalysts based on different supports were recorded to determine the change in copper phases after reaction. Figure 4-23 A, B, C and D shows the XRD pattern of activated (i.e. pretreated under H_2 see Section 4.1.5) and non-activated spent catalysts based on Al_2O_3, SiO_2, ZrO_2 and activated carbon used as supports. For the Al_2O_3-based catalysts no characteristic peak of any copper species was observed, neither for the calcined nor for the spent (activated and non-activated) catalysts. Nevertheless, it is difficult to distinguish the CuO peaks because of the overlapping with the broad Al_2O_3 peaks. The SiO_2, ZrO_2 and carbon-based catalysts exhibited strong signals at 35.6° and 38.8° 2θ indicating the

presence of CuO phase in the calcined and spent catalysts. On the other hand, only for the SiO_2-based activated spent catalyst, the characteristic peaks at 36.2° for the Cu_2O phase was observed. Thus, one can conclude that SiO_2, ZrO_2 and carbon supported Cu catalysts were not reduced under reaction conditions.

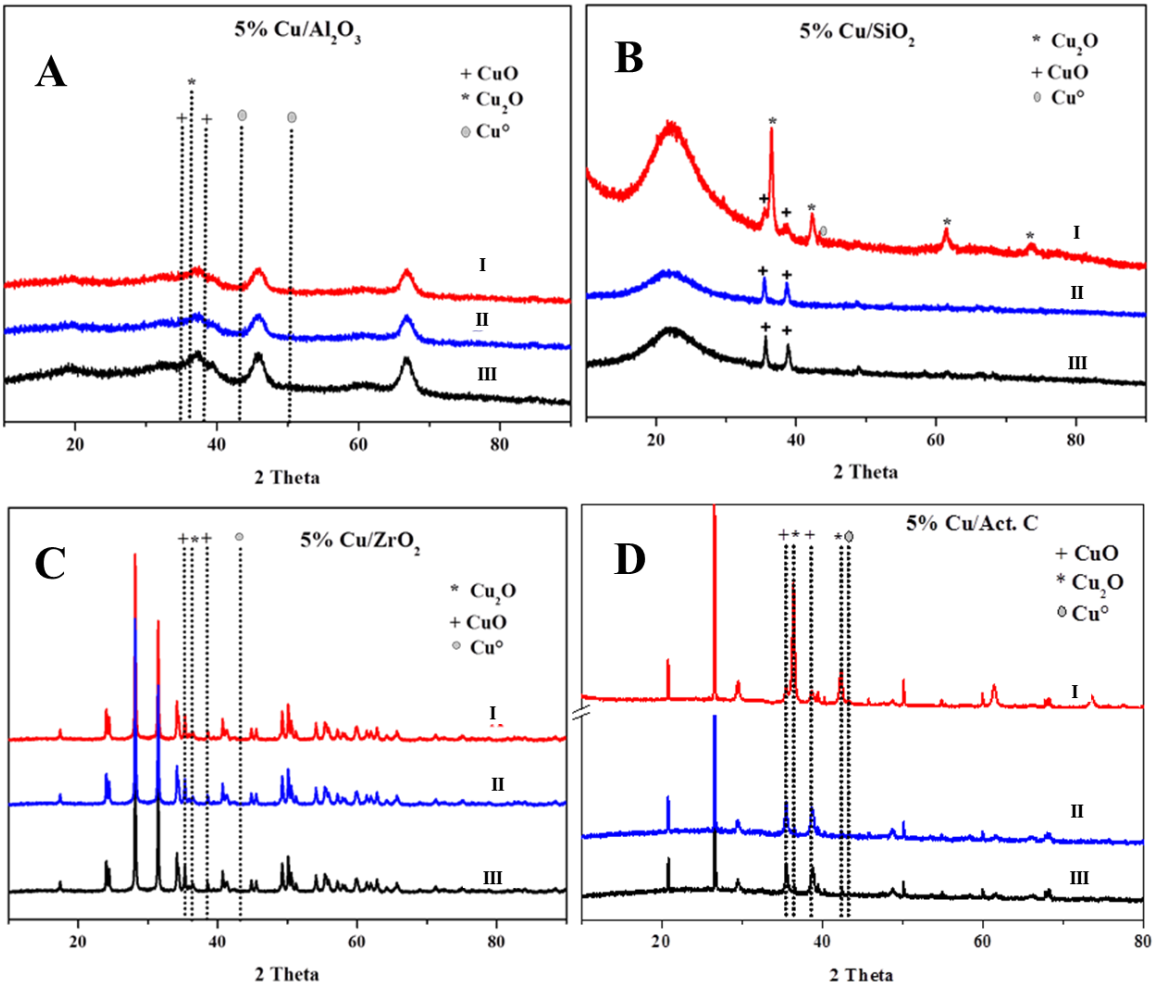

Figure 4-23: XRD patterns of A - 5 wt.% Cu/Al_2O_3, B – 5 wt.% Cu/SiO_2, C – 5 wt.% Cu/ZrO_2 and D – 5 Wt.% Cu/Act. Carbon

I - activated spent, II - non activated spent and III - calcined

Based on the numerous previous results, there is no doubt that the support has a pronounced effect on the performances of the catalysts and that it is due to the nature of the copper species formed at the surface of the solid. The support also plays a very important role on the dispersion of the copper species and on their reduction pattern. The XRD pattern of the TiO_2-P25 based

catalyst suggested a uniform dispersion of copper species, which was not the case for the other supports. Furthermore, highly dispersed copper species are found easily reducible under the reaction conditions. This was strongly evidenced by the characteristic peak of Cu° in the XRD pattern of used catalyst. For the SiO_2, activated carbon and ZrO_2-Ald based catalysts clear characteristic peaks of CuO species were observed showing the non-uniform distribution of the species. Finally, only copper catalysts supported on TiO_2 containing anatase phase shown excellent results for ethanol conversion to EO.

B. X-ray Photoelectron Spectroscopy (XPS)

The X-ray photoelectron spectroscopic analysis of the copper catalyst based on different supports was performed and the spectra obtained are depicted in Figure 4-24. The metal compositions determined by the XPS measurement are listed in Table 4-4. The Cu $2p_{3/2}$ peak was located near 334.2 eV and the $Cu2p_{1/2}$ near 953.3 eV for all catalysts.

The Al_2O_3-based catalyst showed the same features as the TiO_2-based catalysts with two kinds of surface copper species (Cu^{2+} and Cu^{+} - 89 and 11% resp.). Since the quantity of Cu^{+} (highly dispersed) is lower (11%) on the Al_2O_3 surface, one can conclude that most of the copper species are in the bulk type CuO form. Thus, the lower catalytic performance of the alumina-based catalyst compared to the titania one may be explained by the larger amount of bulk-type CuO, which are more difficult to reduce and therefore require a higher temperature. The other samples based on SiO_2, ZrO_2, and active carbon (Figure 4-24 F, G and H) exhibited a single peak at around 933 eV ascribed to Cu^{2+} (bulk type CuO). The amounts of copper present on the surface of the various catalysts were also determined and were 0.5, 7.1 and 4.9% for SiO_2, ZrO_2 and activated carbon respectively.

Table 4-4: Surface composition and oxidation states distribution of copper on different supports

Catalyst	Cu^{+2} (eV)	Cu^{+} (eV)	Cu^{+2} (%)	Cu^{+} (%)	Cu/Support
5% Cu/Al_2O_3	934.2	932.5	89	11	3.1
5% Cu/SiO_2	933.4	-	100	0	0.5
5% Cu/ZrO_2	933.7	-	100	0	7.1
5% Cu/C	934.9	-	100	0	4.9
5% Cu/TiO_2	933.6	932.3	29	71	5.3

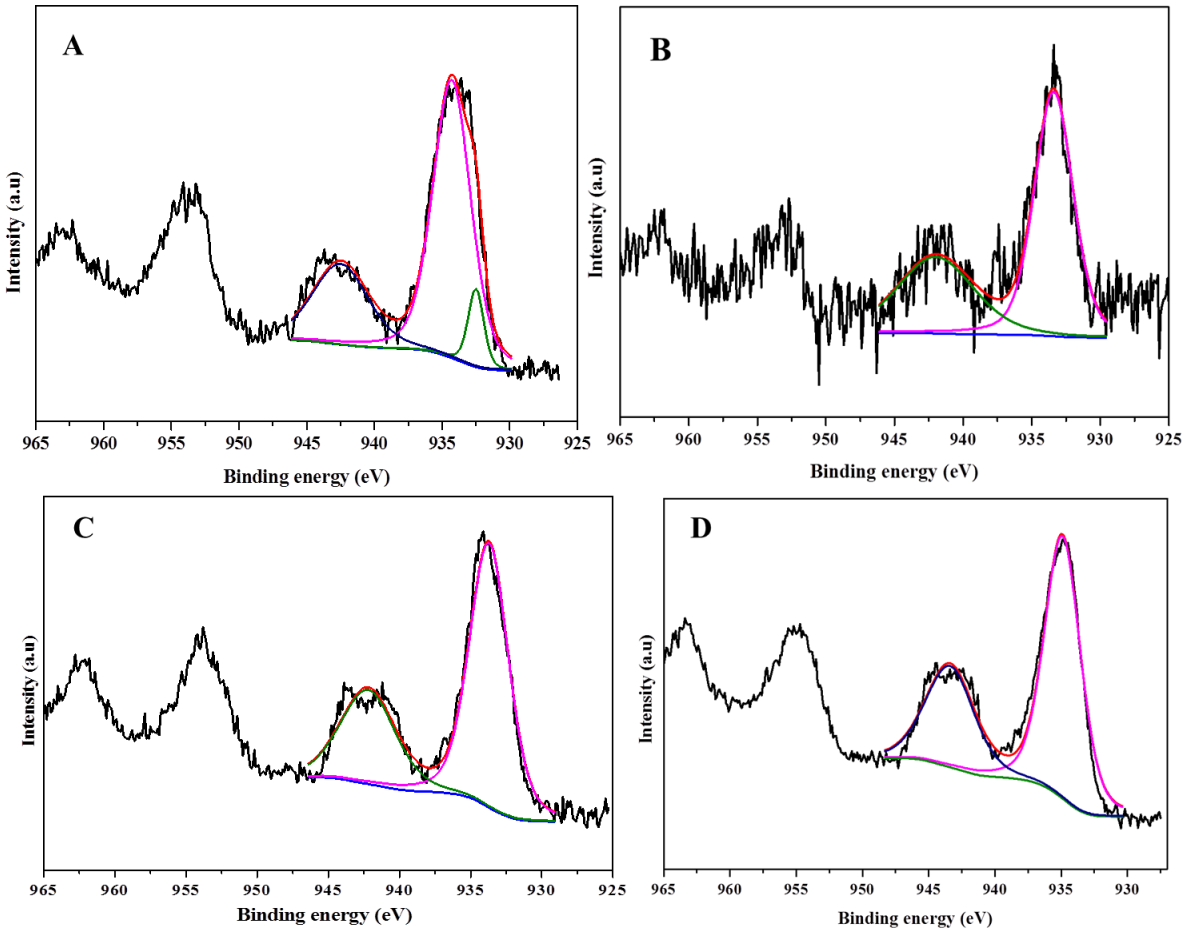

Figure 4-24: XPS spectra of A- 5% Cu/Al_2O_3, B- 5% Cu/SiO_2, C- 5% Cu/ZrO_2 and D-5% Cu/activated carbon

C. Temperature Programmed Reduction (TPR)

H_2-TPR of the copper catalysts based on different supports was performed in order to study the reducibility of the copper species. Figure 4-25 depicts the H_2-TPR profiles for Cu/Al_2O_3, Cu/SiO_2, Cu/ZrO_2 and Cu/activated carbon catalysts. The hydrogen consumption was calculated from the profiles and reported in the inserted table in Figure 4-25. From the profiles one can see that the silica-based catalyst exhibited two reduction peaks at 254 and 281 °C. The TPR peak at 254 °C was ascribed to well-dispersed and small particles of copper oxide species. The peak at 281 °C could be assigned to the reduction of bulk CuO or stepwise reduction of Cu^{2+} to Cu^{+} [16-19]. The hydrogen consumption of the SiO_2-based catalyst matched the theoretical value, meaning that all Cu was accessible to hydrogen. The Al_2O_3 TPR profile showed only one single peak for the copper reduction at 244 °C. In case of ZrO_2 and carbon-based catalyst peaks were

shifted to higher temperatures of 254 and 258 °C with hydrogen consumption of 0.61 and 1.95 mmol.g^{-1} respectively. Surprisingly, the hydrogen consumption for the carbon catalyst was found three times higher than the expected hydrogen consumption. The higher hydrogen uptake can be due to the presence of reducible functional group. With respect to the catalytic performance, we can conclude that the catalysts exhibiting a reduction temperature below 250 °C (reaction temperature) show activity for the formation of ethylene oxide. The better performance for the TiO_2-based catalyst compared to the Al_2O_3-based catalyst is in agreement with a decreased reduction temperature.

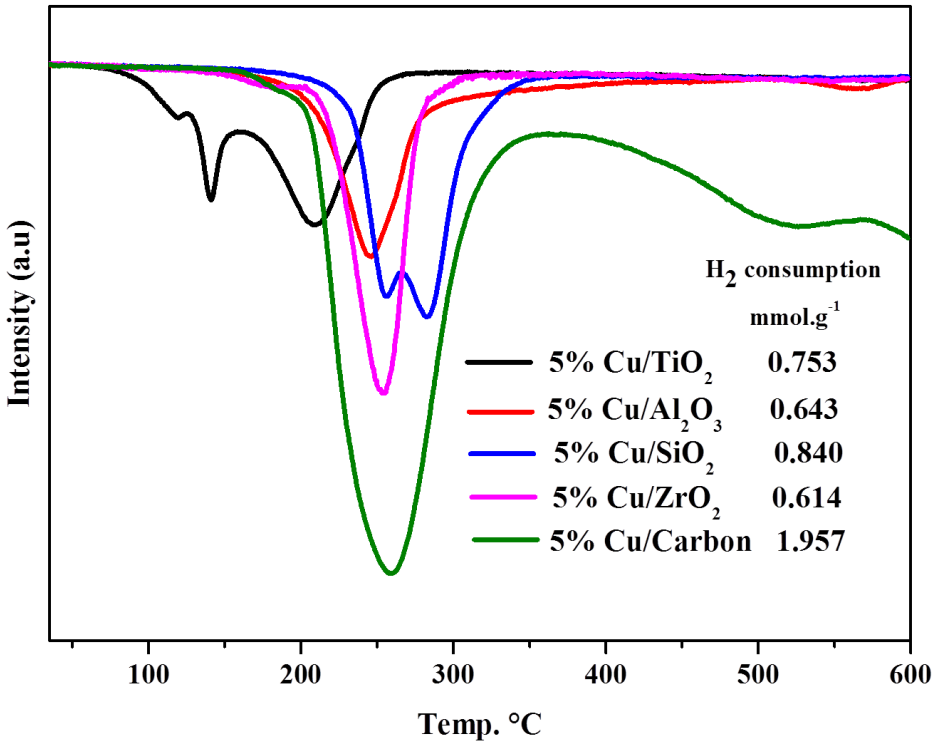

Figure 4-25: H_2-TPR profiles of Cu-based catalysts prepared with different supports

➢ Comparison of catalysts based on Aldrich and CLARIANT ZrO_2 supports

Figure 4-26 depicts the H_2-TPR profile of the Cu/ZrO_2-Ald and Cu/ZrO_2-CL catalysts. The obtained H_2-TPR profiles showed two reduction peaks for Cu/ZrO_2-CL, whereby the one at low temperature was ascribed to highly dispersed copper species and the second reduction peak to bulk CuO species. Concerning the reduction temperature, the copper catalyst based on CLARIANT- ZrO_2 reduced at lower temperature (200°C) compared to the catalyst based on the commercial Ald-ZrO_2 (254°C). The hydrogen consumption for the both catalysts are showing the

same value of 0.61 mmolg^{-1}. The significantly increased catalytic performance (*cf.* Section 4.1.4) in the case of the ZrO_2-CL-based catalyst could thus be correlated to the lower reduction temperature, allowing thus the reduction of the Cu species under the reaction conditions (250°C).

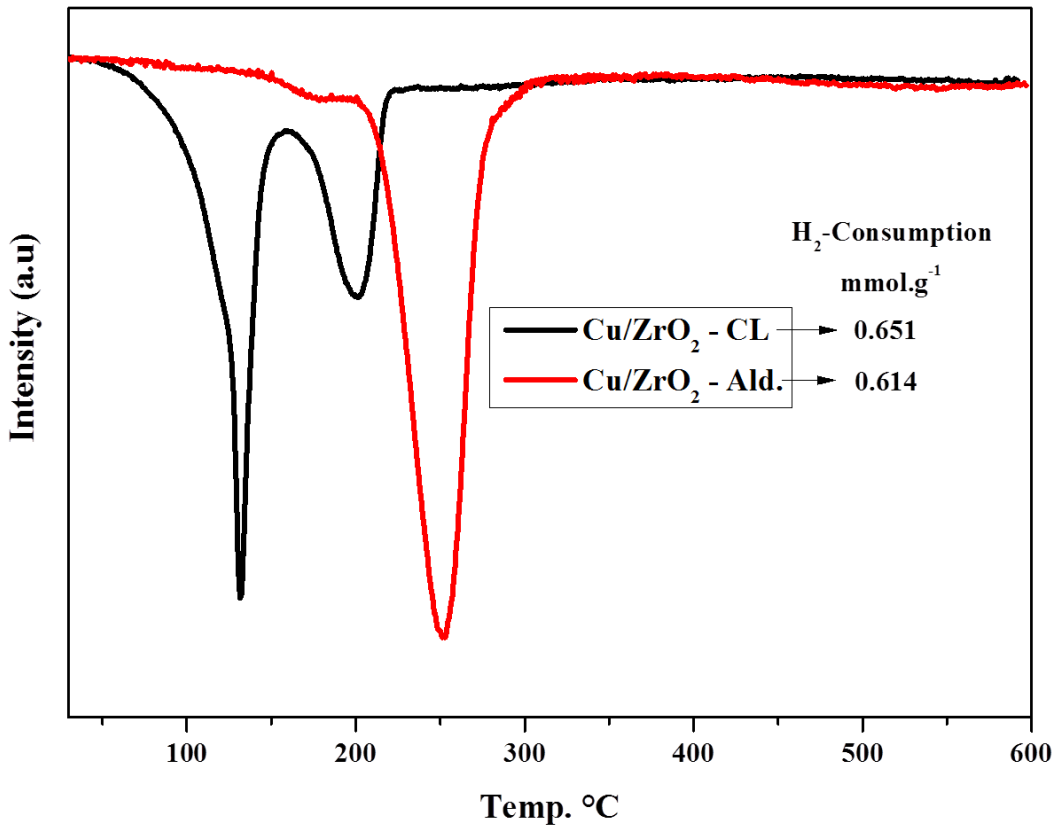

Figure 4-26: H_2-TPR for Cu/ZrO_2 based on Aldrich and CLARIANT provided zirconia

D. Transmittance Electron Microscopy (TEM)

The copper catalysts based on different supports were analyzed by TEM and the pictures are shown in Figure 4-27. The particle size and morphology of each support is different. Figure 4-27 E shows the distribution of copper over the Al_2O_3 support. It seems that the non-uniform distribution of copper was obtained, maybe due to the agglomeration of the copper particles. In case of the SiO_2-supported catalyst (Figure 4-27 F), the copper is uniformly distributed over the support, whereby the surface of the support is saturated with copper particles. Surprisingly, in contrast, the XPS analysis of this sample has shown very low amount of copper on the surface of the catalyst. Figure 4-27 G and H show the samples based on different ZrO_2 supports.

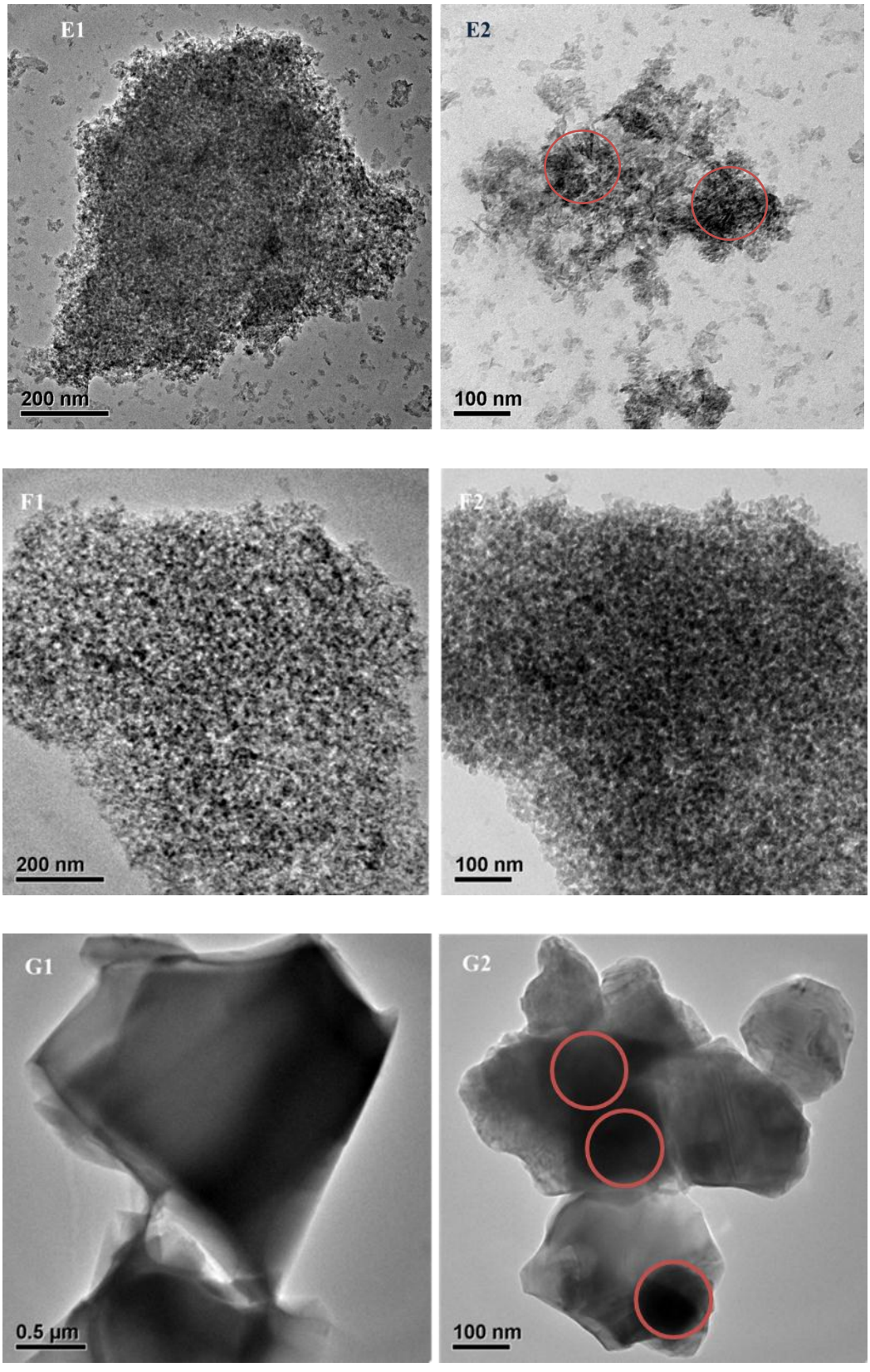

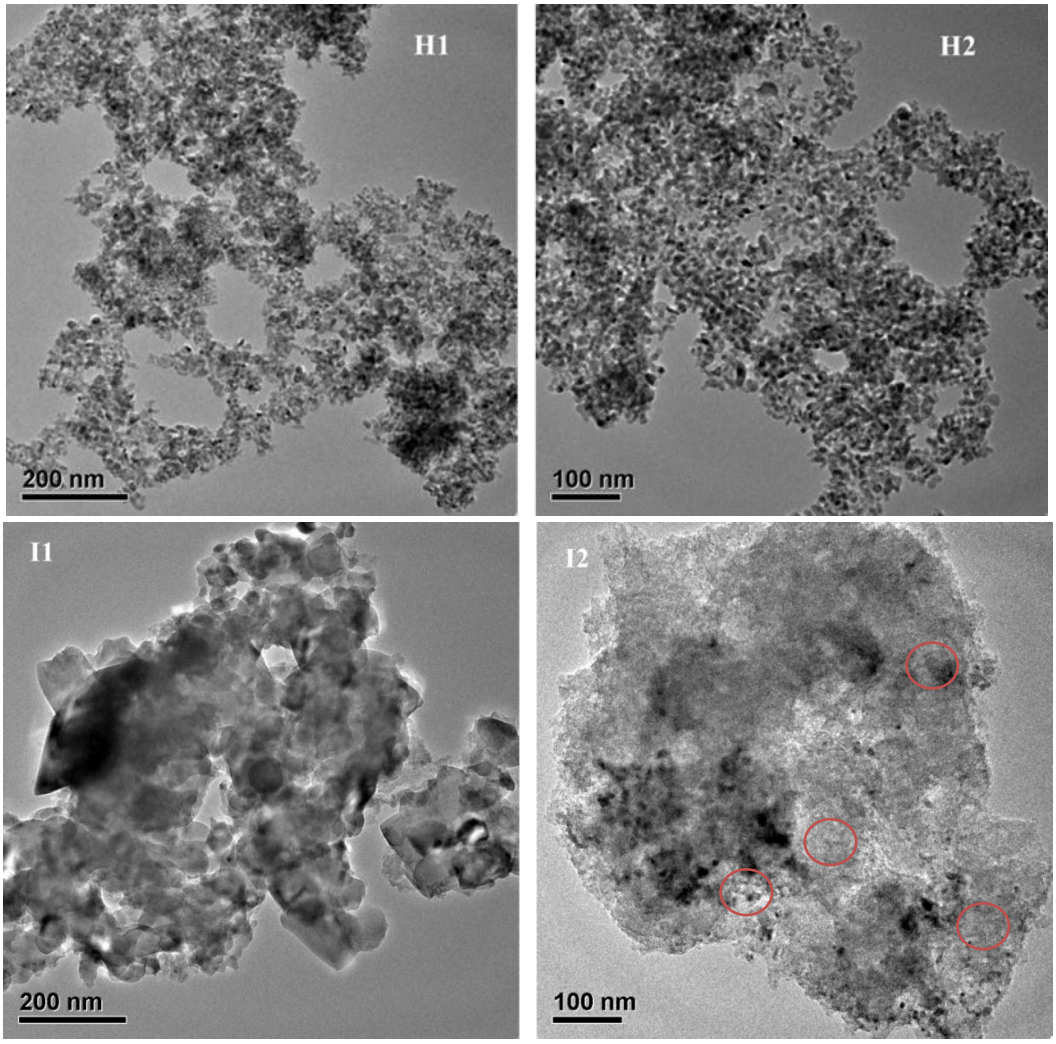

Figure 4-27: TEM images of E- 5wt.% Cu/Al_2O_3, F- 5 wt.% Cu/SiO_2, G- 5wt.% Cu/ZrO_2-Ald, H-5wt.%Cu/ZrO_2-CL and I-5 wt.% Cu/Act. carbon

The Aldrich provided ZrO_2 support having less surface area (*cf.* Section 3.1.3 B) exhibits a non-uniform distribution of Cu. On the other hand, for ZrO_2 from CLARIANT, a uniform distribution of the copper particle was observed with an average particle size in the range of 5-10 nm. The carbon catalyst (Figure 4-27I) also led to a bad distribution of Cu particles, as expected for a hydrophobic support after catalyst preparation in water. The particle sizes for Cu on silica, alumina, zirconia-Ald and carbon were difficult to calculate from the TEM images due to the low contrast.

E. Scanning Electron Microscopy (SEM) with EDX mapping

Scanning Electron Microscopy (SEM) with EDX mapping was performed to visualize the distribution of copper on the different supports. The SEM mapping images for all catalysts are shown in Figure 4-28. As discussed in the previous section, the red dots correspond to the copper particles in each catalyst. In case of the catalysts based on different supports, some agglomeration was observed. A careful look at the SEM images of SiO_2, ZrO_2-Ald and activated carbon-based catalysts (images F, G and H respectively) showed some inhomogeneity in the copper particles dispersion. However, SiO_2-based catalyst showed very fine dispersion in copper in the TEM analysis. Final conclusion from the SEM mapping images is that SiO_2, TiO_2 and Al_2O_3 supports are the best ones to finely disperse the copper metal particles using the impregnation method.

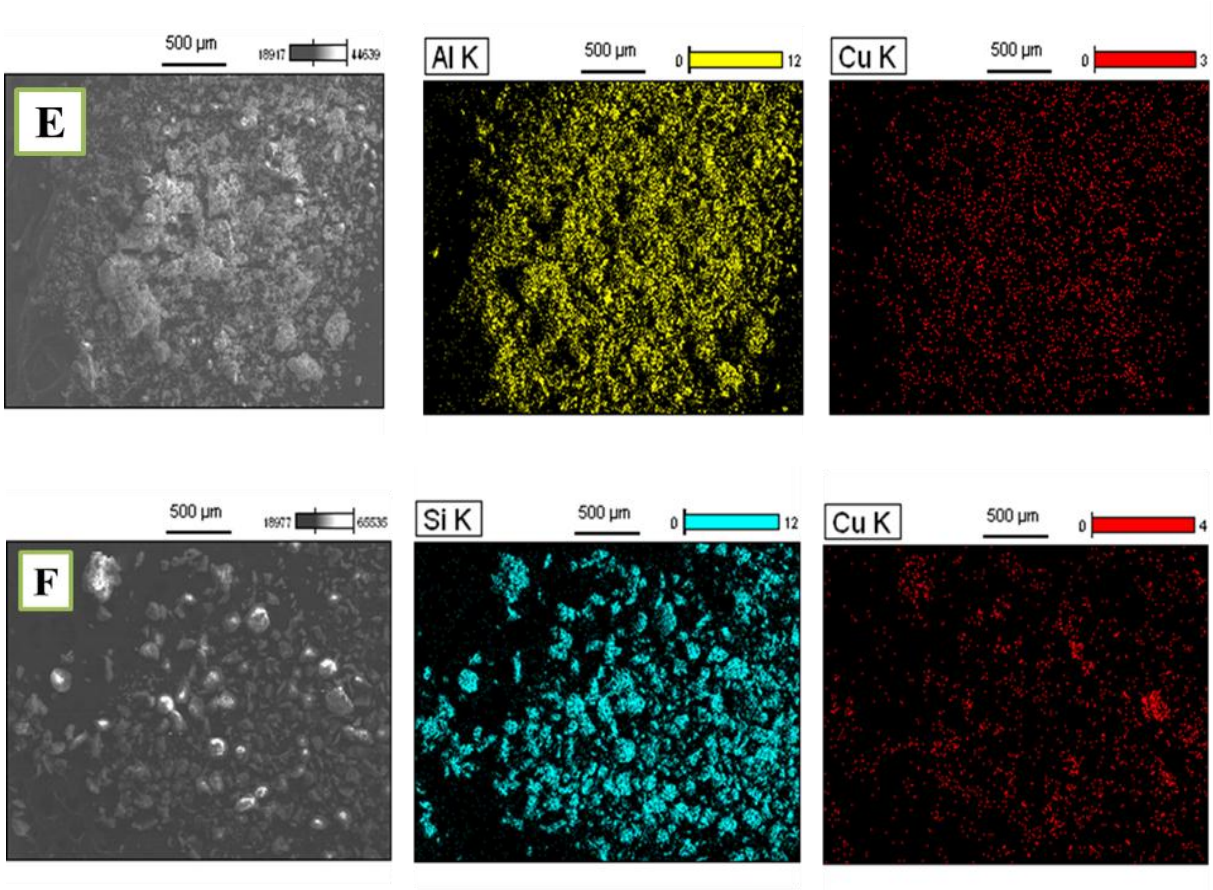

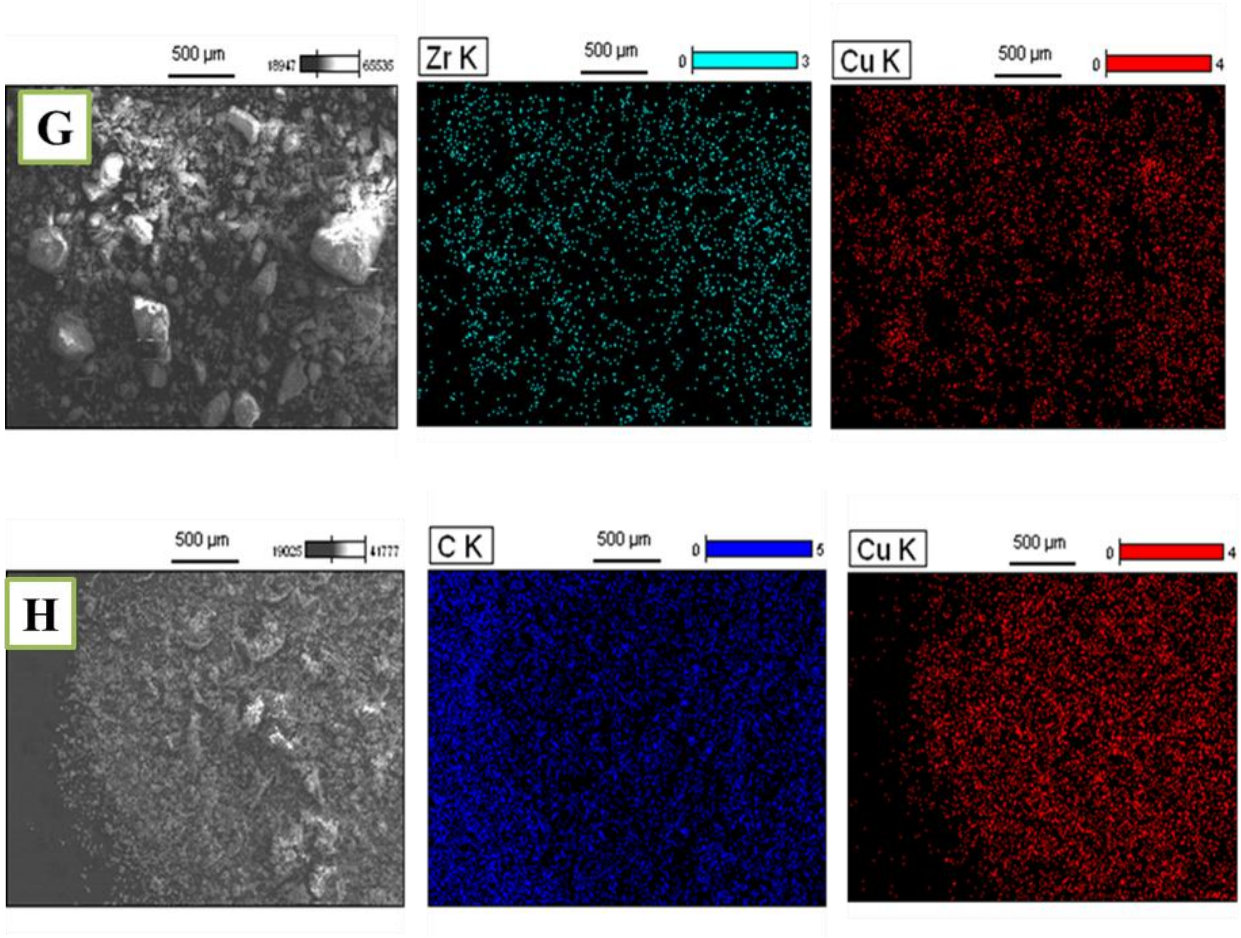

Figure 4-28: SEM images and element mapping for E- 5 wt.% Cu/Al_2O_3, F- 5 wt.% Cu/SiO_2, G- 5 wt.% Cu/ZrO_2-Ald, H-5 wt.% Cu/Act. carbon

4.3 Conclusion

In the first part of this chapter, the back optimization of TiO_2-P25-supported copper catalyst was performed to optimize the copper quantity in the catalyst. It was concluded that the 5 wt.% Cu/TiO_2–P25 catalyst was the best in terms of ethylene oxide formation. Furthermore, the activation of the catalyst by pre-reduction by H_2 was studied, showing no beneficial effect in terms of catalytic performance. Using catalysts based on different supports, we have seen that only the catalyst based on TiO_2 exhibited a Cu° phase after reaction. Furthermore, the catalysts based on different supports were characterized by a wide range of characterization techniques in order to establish a correlation between the chemical and physical properties of the catalysts and their catalytic performance.

The influence of the dispersion and particle size of copper over the different supports as well as with different loadings was studied. A good dispersion of the copper particles together with small particle size (around 15 nm) was observed over the TiO_2–P25 and ZrO_2-CL supports. The SEM mapping also gave supplementary information about the dispersion of copper species over the support. The bulk elemental composition determined by X-Ray Fluorescence technique showed that the catalyst synthesis was successful for all the samples. The characterization by XRD indirectly suggests the uniform dispersion or formation of small copper particles over TiO_2 and Al_2O_3 supports because there are no characteristic peaks for the copper. On the other hand SiO_2, ZrO_2-Ald and Act. carbon catalyst showed diffraction peaks for CuO, indirectly suggesting a non-uniform distribution of big copper particles. Furthermore, XRD analysis of spent catalyst showed a characteristic peak of Cu° which was supposedly explained by the copper species increased tendency to reduced under reaction conditions. Nevertheless, the reduction of copper species could not be observed in the catalysts with other supports than TiO_2 containing the anatase phase. On the other hand, the presence of Cu^{+2} and Cu^{+} species in the fresh catalyst as well as of Cu° and Cu^{+2} species in the spent catalyst was clearly demonstrated from XPS analysis of TiO_2-supported copper catalysts. The ratio of Cu^{+}/Cu^{+2} decreased with the increase in copper loading. The reduction phenomenon of the catalysts was also studied using H_2-TPR technique. The reduction of copper species over TiO_2 support containing the anatase phase was facilitated at a lower temperature compared to the catalysts based on the other supports. The higher dispersion and lower reduction temperature of the copper species clearly led to the best catalysts for converting efficiently ethanol to ethylene oxide.

4.4 References

1. M. Kevin, S. Agarwala, A. S. W. Wong, C. K. N. Peh, V. Thavasi, G. W. Ho, Applied Materials and Interfaces, **2010**, 2, 1844-1850.
2. N. Guan, G. Wu, L. Li, Catalysis Science & Technology **2011**, 1, 601-608.
3. P. Gheeka J. Trawczynski, J. Okalb, M. Zawadzkib, M. J. Ilan Gomez, Applied Catalysis A: General, **2011**, 409-410, 39-47.
4. S. R. González-Carrazán, C. M. Pedrero, M. A. Soria, P. Ruíz, Catalysis Today, **2013**, 203, 158-162.

5. Z. Wang, H. Q. Wan, J. Zhu, X. W. Li, B. Liu, F. Gao, L. Dong, Y. Chen, Applied Catalysis B: Environmental, **2008**, 79, 254.
6. Y. Wang, J. L. Cao, T. Y. Zhang, S. H. Wu, Z. Y. Yuan, Applied Catalysis B: Environmental, **2008**, 78, 120.
7. M. Flytzani-Stephanopoulos, L. Kundakovic, Applied Catalysis A: General, **1998**, 171, 13-29.
8. R. X. Zhou, X. M. Zheng Z. G. Liu, Catalysis Communications, **2008**, 9, 2183-2186.
9. F. Cui, Z. W. Huang, H. X. Kang, J. Chen, X. Z. Zhang, C. G. Xia, Chemistry of Materials, **2008**, 20, 5090-5099.
10. B. C. Zhang, X. L. Tang, Y. Li, Y. D. Xu, Q. Xin, W. J. Shen, Applied Catalysis A: General, **2005**, 288, 116-125.
11. H. J. Choi, M. Kang, International Journal of Hydrogen Energy, **2007**, 32, 3841.
12. N. Mettlach, S. Y. Lee, N. Nguyen, Y. M. Sun, J. M. White, Applied Surface Science, **2003**, 206, 102.
13. K. Suzuki, S. Velu, C. S. Gopinath, H. Yoshida, T. Hattori, Physical Chemistry Chemical Physics, **2002**, 4, 1990-1999.
14. M. Miyauchi, X.Q. Qiu, K. Sunada, M. Minoshima, M. Liu, Y. Lu, D. Li, Y. Shimodaira, Y. Hosogi, Y. Kuroda, K. Hashimoto, ACS Nano **2012**, 6, 1609-1618.
15. A. Carrero,]. A. Calles, A. J. Vizcanio, L. Garcia-Moreno, Catalysis Today, **2014**, 227, 198-206.
16. N. Takezavwa, M. Shimokawabe, H. Kobayashi, Bulletin of the Chemical Society of Japan, **1983**, 56, 1337-1340.
17. A. A. Greish, E. A. Redina, I. V. Mishin, G. I. Kapustin,O. P. Tkachenko, O. A. Kirichenko, L. M. Kustov, Catalysis Today, **2015**, 241, 246-254.
18. D. P. Volanti, A. G. Sato, C. Isabel, C. D. Freitas, E. Longo, J. Maria, C. Bueno, Catalysis Communications, **2012**, 26, 122-126.
19. A. Salnikov, S. Yashnik, N. Vasenin, V. Anufrienko, Z. Ismagilov, Catalysis Today, **2012**, 197, 214-227.

Chapter 5

General conclusion and perspectives

5.1 General Conclusion

In this work, the selective oxidation of ethanol to ethylene oxide was studied over catalysts based on various metals (Cu, Ag and Au) dispersed on different types of supports (Al_2O_3, two different ZrO_2, activated carbon, SiO_2 and several TiO_2). The catalytic as well as the physical and chemical properties – such as redox properties, crystal phases, textural properties, elemental composition and oxidation state of the metals used as active phases – were studied using a wide range of techniques in order to establish a correlation between the latter and the catalytic performance for the desired reaction.

In the first part of this work it was tried to reproduce the results reported previously by Lippits *et al.* [1, 2]. It was however unsuccessful probably because of too many differences in the catalyst synthesis procedure and the way of performing the catalytic tests. However, it was found that the copper-based catalysts could led to very promising results and it opened the way for a cheap and alternative catalyst to the expensive silver and gold-based catalysts.

Several supports and methods of preparation were used to prepare copper-based catalysts. For the Al_2O_3-based catalysts the co-precipitation method proved to be more efficient than the impregnation method for the copper dispersion and for the formation of small size particles. In that case the selectivity in ethylene oxide increased with the loading of copper.

Among the different supports tested (TiO_2-P25, ZrO_2, SiO_2, activated carbon and several phases of TiO_2) TiO_2 containing anatase phase was found to be the best one. The characterization study showed that the catalyst based on this TiO_2-P25 support had completely different characteristics compared to the other supported catalysts. The XRD, XPS and TEM confirmed the uniform distribution and small particle size of the copper species formed at the surface of the TiO_2-P25 support. Considering the porosity of all the supported catalysts, only TiO_2-based catalysts had a moderate surface area and well-defined, uniform and broad pores in the mesoporous region. Formation of big Cu particles or non-homogeneous dispersion was found for the catalysts based on ZrO_2 and activated carbon. On the other hand TPR showed that the TiO_2-P25 support allowed an easy reduction of the copper species (i.e. at lower temperature than for the other supports-based catalysts) which can be ascribed to the small size of the Cu particles. XPS of Cu/TiO_2–P25-based catalyst showed that the copper particles can even be reduced (from Cu^{2+} to Cu^{+}) by the simple bombardment effect of X-ray radiations.

The calcination temperature of the TiO_2–P25-based catalysts strongly affected the performance, due to the formation of big Cu particles at higher temperatures than 400 °C which was found optimal.

During the optimization of the reaction conditions, it was observed that temperatures below 230 °C were not favorable for the ethylene oxide formation. As too high temperature may cause the decomposition of ethylene oxide, the optimum was found around 250 °C. The use of an excess of oxygen led to higher yield in ethylene oxide but then the experimental conditions were in the explosive range and this can be a problem for scaling-up the process in the industry. One possibility could be to implement the reaction in microreactors to avoid the safety issues even within flammability limits. The excess of oxygen also helped in regulating the coke formation and hence in stabilizing the catalytic performance vs. time.

After reaction the copper in the TiO_2-P25-based catalysts was in reduced state even in presence of an excess of oxygen in the gas phase. It has also been showed that a pre-reduction of the catalysts before test had no significant impact on the catalytic performance. This means that the reduction of the copper particles occurred under stream probably by the action of ethanol.

With regard to these observations, we concluded that the optimum catalyst – in terms of performance – should exhibit easily reducible metal species. The reducibility of the copper species was correlated to its dispersion on the support surface and to its particle size [3]. In case of the titania-supported copper catalyst, the facilitated reduction was ascribed to the aforementioned observed high dispersion of the metal over the support [4]. Furthermore, the presence of interactions between the support and the metal cannot be ruled out [5]. The constant high performance for Cu on titania support containing the anatase phase was ascribed to the continuous oxidation of the amorphous carbon under stream because of the excess of oxygen in the feed.

Based on our results, we postulate the following mechanism (Figure 5-1):

Metallic copper (Cu°) was formed during the reaction and built a redox-couple with Cu^{2+}/Cu^{+} due to the dehydrogenation of ethanol to ethylene oxide. Molecular oxygen is involved in the re-oxidation of Cu° to Cu^{2+}/Cu^{+} as well as in the limitation of coke formation on the catalyst's

surface. The XPS, XRD and TPR results strongly suggest that more than 50% of the copper species are in the metallic form (Cu°) in the spent Cu/TiO_2-P25 catalyst.

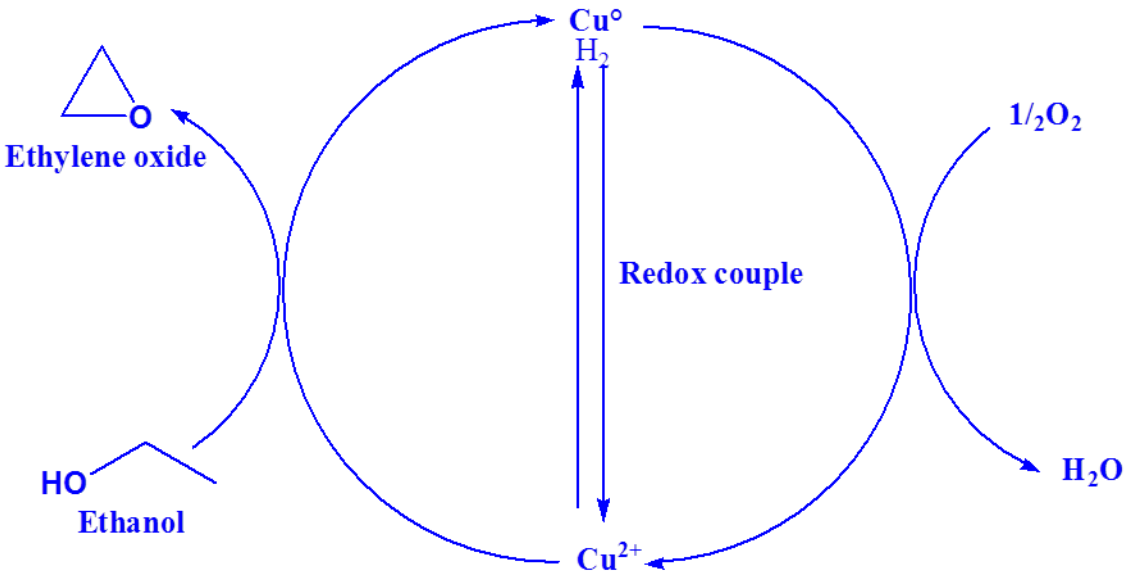

Figure 5-1: Possible way of dehydrogenation of ethanol and catalyst reduction

With respect to the observed in-situ reduction of copper, one can also understand why the hydrogen pre-treatment of the catalyst had no positive impact on the catalytic performance, since it does not enable to maintain the redox-couple Cu° to Cu^{2+}/Cu^{+} during the reaction.

Ethylene oxide formation could also proceed by oxidative dehydrogenation of ethanol whereby atomic oxygen takes direct part in the reaction with ethanol over the catalyst surface. Some indication for this mechanism may be derived from the observation that the selectivity to ethylene oxide increased with the oxygen concentration in the reaction feed. Nevertheless, this influence of oxygen can be explained by both mechanisms: in the first proposed mechanism oxygen is required to maintain the redox couple between Cu^{2+}/Cu° and in the second, the oxygen plays an important role in the formation of ethylene oxide by oxidative dehydrogenation (Figure 5-2). A more detailed kinetic study would be necessary to determine which mechanism is the good one.

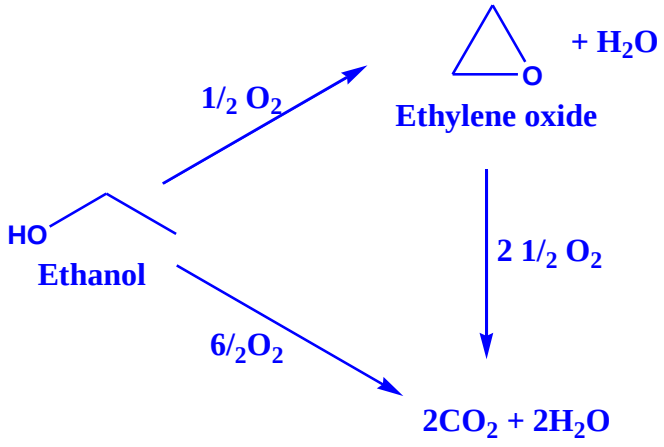

Figure 5-2: Possible way for oxidative dehydrogenation of ethanol

5.2 Perspectives

We have seen that Cu/TiO_2–P25 is the best catalytic system for the direct conversion of ethanol into ethylene oxide. This direct conversion of ethanol to ethylene oxide is a completely new approach and has never been described before. It is of high interest as it opens the door to the production of biosourced ethylene oxide. However, even if the conditions necessary to get an efficient and stable catalyst are now better understood it is still impossible on the basis of the data issued from this thesis to conclude on the mechanism. Additional work is required to do so. As one example, one may perform a detailed study on the interaction of ethanol and oxygen with the catalyst surface by *in-situ* spectroscopic techniques. Furthermore, as oxygen plays a very important role in the formation of ethylene oxide, it could directly allow concluding on the mechanism. Actually, the use of ^{18}O labeled ethanol could be a way to determine if the molecular oxygen is involved in the formation of ethylene oxide, or if it only acts in the re-oxidation of the catalyst.

With respect to the catalyst optimization, one may focus on the reducibility. As we have seen, the catalytic performance depends on their ability to be easily reduced, whereby the optimization of the catalyst should focus on the decrease of the reduction temperature. One may enlarge the study to other kinds of supports, which may allow this behavior (i.e. ZnO). Furthermore, we only focused on gold, silver and copper-based catalysts for the direct conversion

of ethanol to ethylene oxide, thus leaving much space to develop new catalytic systems with the doping of the copper catalysts to enhance its reducibility or stabilize its small particle size.

Finally, as the best results were obtained in the flammability limits which are not applicable at the commercial scale, it could be of interest to try to implement the reaction in a microreactor to avoid these safety issues.

5.3 References

1. M.J. Lippits, B.E. Nieuwenhuys, Catalysis Today, **2010**, 154, 127-132.
2. M.J. Lippits, B.E. Nieuwenhuys, Journal of Catalysis, **2010**, 274, 142-149.
3. D. P. Volanti A. G. Sato, D. M. Meira, S. Damyanova, E. Longo, J. M. C. Bueno, Journal of Catalysis, **2013**, 307, 1-17.
4. H. Jin, Y. Mi, Y. Kang, S. Yu, W. Kim, N. D. Kim, J. Yi, Journal of Molecular Catalysis A: Chemical, **2013**, 368-369, 72-77.
5. F. Yubero, A. Barranco, J. A. Mejias, J.P. Espinos, A.R. Gonzalez-Elipe, Surface Science **2001**, 482-485, 680-686.

Chapter 6

Annex

6.1 Procedure for leak-testing

In order to verify that the gas circuit of the catalytic test rig was leak-tight, the pressure loss method was employed. Therefore the whole gas circuit was pressurized at 2000 mbar and the loss of pressure was monitored during 10 minutes. When the loss of pressure was less than 1%, the catalytic test rig was supposed leak-tight. In the following the whole procedure is described in detailed based on Figure 2-1 (Chapter 2).

1) In the first step, the reactor containing the catalyst was installed and connected to the tubing.
2) In the second step, an air-flow of 20 mL/min was started via the mass-flow controller (labelled **MFC 1**) whereas the flow of the second mass-flow controller (labelled **MFC 2**) was completely stopped.
3) The by-pass valve (labelled **V-4**) was switched to the reactor, meaning that the latter was alimented by air.
4) The two valves connecting the ethanol saturator (labelled **V-2** and **V-2b**) were closed, meaning that the saturator was isolated. In fact, as the saturator is made from glass it must not be pressurized.
5) Finally the outlet valve (labelled **V-6**) was closed. With regard to the applied air flow via **MFC 1**, the pressure in the whole setup increased and could be monitored by the pressure indicator (labelled **P**).
6) When the pressure reached 2000 mbars (twice the pressure under reaction conditions), the inlet valve (labelled **V-1**) was closed, whereby the pressurized circuit between **V-1** and **V-6** (via **V-3**; **V-4**; reactor; again **V-4** and **V-5**) was isolated. In this configuration, the pressure loss indicated by the pressure indicator (labelled **P**) was monitored during 15 minutes. The loss must not overpass 1% (20 mbar) in order to attest leak tightness.

6.2 Safety consideration

In order to proceed experiments in safe environment, an ethylene oxide detector was installed in the reactor setup. The minimum (first) level for the ethylene oxide detection was fixed at 5 ppm as per legal limits indicated in the INRS form. The ethylene oxide detector was connected to the oxygen mass flow controller in order to cut the oxygen flow and thus stop the

reaction and ethylene oxide formation when the concentration overpasses the aforementioned limit. In case of a leak, the following procedure was applied. The second level of ethylene oxide detection was fixed at 7.5 ppm. The first level actionate a simple flashlight whereas the second level actionate an alarm as described below.

Safety Procedure for Alert on ethylene oxide in C004 lab

First alarm level: FLASHLIGHT

Measure to be taken:

- Inform the responsables:
  - Samadhan LOMATE (6089)
  - Benjamin KATRYNIOK (5438)
  - Sébastien PAUL (5457)
- Follow the instructions of the responsibles
- Under no circumstances open the doors of the vented hood

Second alarm level: SIREN

Measure to be taken:

- Leave the laboratory room immediately
- Inform the responsibles:
  - Samadhan LOMATE (6089)
  - Benjamin KATRYNIOK (5438)
  - Sébastien PAUL (5457)
- Follow the instructions of the responsibles. In case of absence of the latters, make evacuate the laboratory
- Do not enter to the laboratory room under any circumstances until siren is over. Only in case of emergency, you are allow to enter provided of a respiratory protection – gas mask (located outside the laboratory room in a dedicated box)

Automatic counter-measures:

The feed is automatically cut-off whereby the ethylene oxide concentration will decrease immediately.

A 4 ways electric valve has been installed in order to allow by-passing the reactor without opening the hood. Thus, if during the reaction any problem occurs we can turn the valve to bypass from outside of the safety hood. The switch, which is placed outside the hood, is shown in Figure 1.

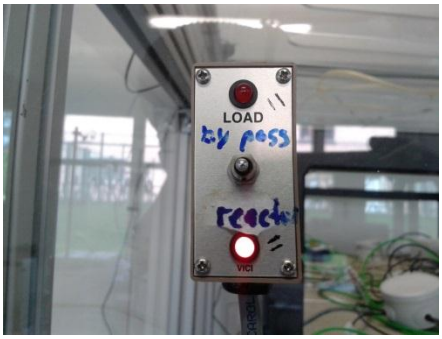

Figure 1 : Safety electric valve switch

On the other hand, to reinforce the safety, an electric flow-meter measuring the exhaust flow of the vented hood was installed.

6.3 Flammability limits

Ethylene oxide is a flammable, explosive chemical. The limits of flammability and explosion are as follows:

1. The minimum value cited for the lower flammable limit of ethylene oxide in air is 2.6 vol.% [1].

2. The upper flammable limit is typically stated to be 100% because pure EO can violently decompose with a significant release of heat in the absence of air or oxygen.
3. Accordingly, the flammable range of EO-air mixtures is 2.6-100 vol.% (Figure 2).
4. The auto ignition temperature of EO in air at atmospheric pressure is 445°C [2]. This temperature can be lower in presence of certain impurities such as water, acetaldehyde and rust.

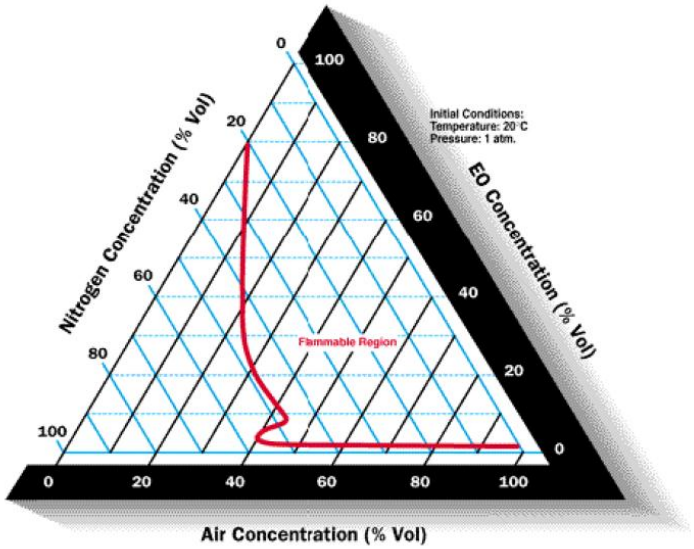

Figure 2 : Flammable region of EO/N_2/Air mixtures [1]

❖ **Experimental conditions used in this study**

According to the Antoine equation [3] and using an inert flow in the saturator we have calculated the appropriate temperature to get the desired partial pressure of EtOH in the feed at atmospheric pressure. The molar composition of the feed was as follows: Ethanol- 20%, O_2- 7.5%, Inert gas- 77.5% balance

At these experimental conditions we will always be out of the flammable limits.

As a matter of fact for 100 moles of the feed:

1. Assuming full conversion we consume 20 moles of ethanol and 10 moles of oxygen (O_2) forming 20 moles ethylene oxide and 20 moles water (inert). This results in a composition of EO/O_2/other of 18/0/82.
2. Assuming 75% conversion we consume 15 moles of ethanol and 7.5 moles of O_2 forming 15 moles of ethylene oxide and 15 moles of water (inert). This results in a composition (%) of EO/O_2/other of 13.9/2.3/83.8
3. Assuming half conversion we consume 10 moles of ethanol and 5 moles of O_2 forming 10 moles of ethylene oxide and 10 moles of water (inert). This results in a composition (%) of EO/O_2/other of 9.52/4.76/85.71

4. Assuming 40% conversion we consume 4 moles of ethanol and 2 moles of O_2 forming 4 moles of ethylene oxide and 4 moles of water (inert). This results in a composition of EO/O_2/other of 3.9/7.84/88.22

All these scenario are reported in Figure 3. It can be seen that in any case we stay out of the flammability region.

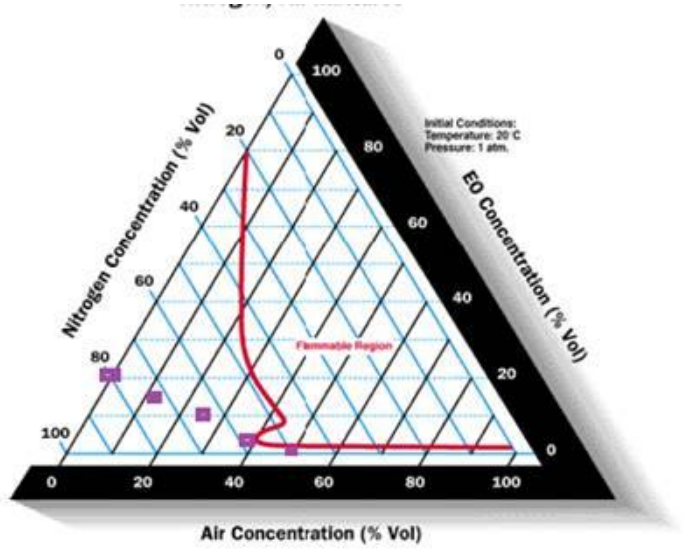

Figure 3 : Flammability range with preliminary experimental conditions

In the optimized experimental conditios, following are the concentrations in the feed.

Ethanol- 15%, O_2- 30%, Inert gas- 55% balance

At these experimental conditions we will be in the flammability range, as shown in Figure 4.

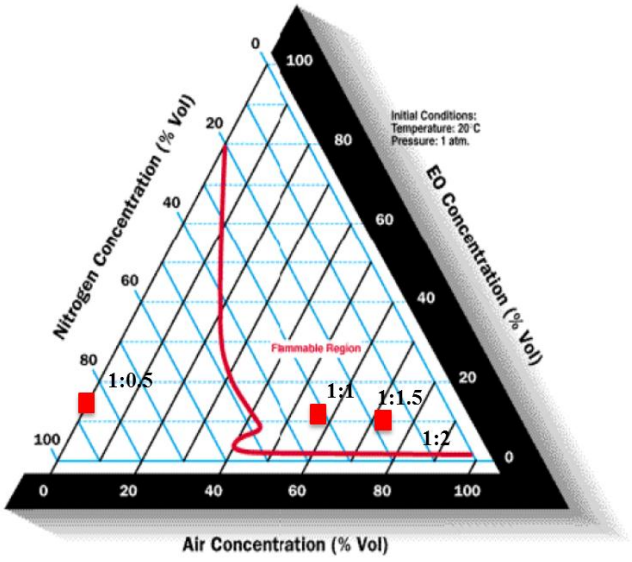

Figure 4 : Flamability region of current experimental conditions

The flammability limits of ethanol and air mixture are shown in Figure 5. The reaction conditions we used are therefore always out of flammability limits of the ethanol/air mixtures.

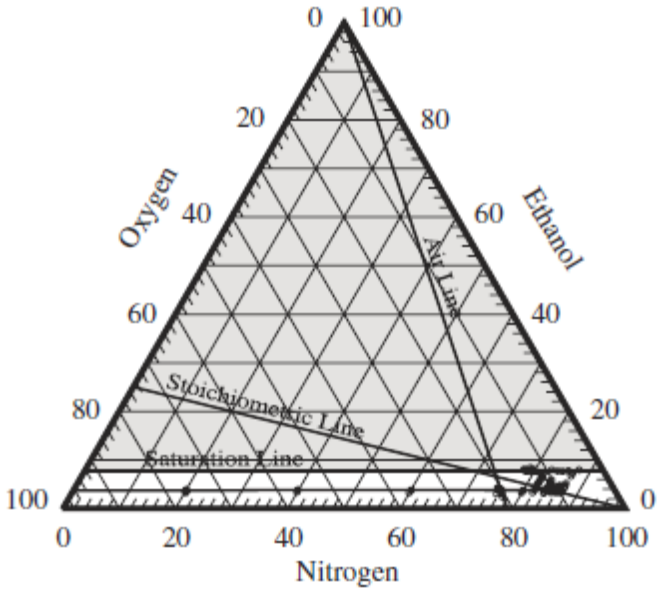

Figure 5 : Flammability envelope for ethanol [4]

6.4 References

1. D. Conrad, Bundesgesundheitsblatt, **1963**, 9, 139-141.

2. W. H. Perkin, Journal of the Chemical Society, **1893**, 63, 488.

3. http://webbook.nist.gov/cgi/cbook.cgi?ID=C64175&Mask=4&Type=ANTOINE&Plot=on.

4. D. A. Crowl M. R. Brooks, Journal of Loss Prevention in the Process Industries, **2007**, 144-150.